



**REMOVAL OF INORGANIC CONTAMINANTS IN  
AQUEOUS ENVIRONMENT BY BIO-BASED  
MATERIALS**

**BY**

**MR. JAKKAPON PHANTHUWONGPAKDEE**

**A DISSERTATION SUBMITTED IN PARTIAL FULFILLMENT  
OF THE REQUIREMENTS FOR THE DEGREE OF DOCTOR  
OF PHILOSOPHY (ENGINEERING AND TECHNOLOGY)  
SIRINDHORN INTERNATIONAL INSTITUTE OF TECHNOLOGY  
THAMMASAT UNIVERSITY  
ACADEMIC YEAR 2020  
COPYRIGHT OF THAMMASAT UNIVERSITY**

**REMOVAL OF INORGANIC CONTAMINANTS IN  
AQUEOUS ENVIRONMENT BY BIO-BASED  
MATERIALS**

**BY**

**MR. JAKKAPON PHANTHUWONGPAKDEE**

**A DISSERTATION SUBMITTED IN PARTIAL FULFILLMENT  
OF THE REQUIREMENTS FOR THE DEGREE OF DOCTOR  
OF PHILOSOPHY (ENGINEERING AND TECHNOLOGY)  
SIRINDHORN INTERNATIONAL INSTITUTE OF TECHNOLOGY  
THAMMASAT UNIVERSITY  
ACADEMIC YEAR 2020  
COPYRIGHT OF THAMMASAT UNIVERSITY**

THAMMASAT UNIVERSITY  
SIRINDHORN INTERNATIONAL INSTITUTE OF TECHNOLOGY

DISSERTATION

BY

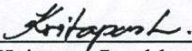
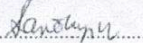

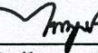
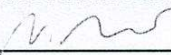
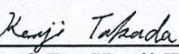

MR. JAKKAPON PHANTHUWONGPAKDEE

ENTITLED

REMOVAL OF INORGANIC CONTAMINANTS IN AQUEOUS ENVIRONMENT  
BY BIO-BASED MATERIALS

was approved as partial fulfillment of the requirements for  
the degree of Doctor of Philosophy (Engineering and Technology)

on May 6, 2021

Chairperson	 _____ (Dr. Kritanae Laohasurayotin, Ph.D.)
Member and Advisor	 _____ (Professor Dr Sandhya Babel, Ph.D.)
Member and Co-advisor	 _____ (Professor Dr Tatsuo Kaneko, Ph.D.)
Member	 _____ (Associate Professor Dr Paiboon Sreearunothai, Ph.D.)
Member	 _____ (Assistant Professor Dr Khanin Nueangnoraj, Ph.D.)
Member	 _____ (Research Asst. Prof. Dr. Kenji Takada, Ph.D.)
Director	 _____ (Professor Pruettha Nanakorn, D.Eng.)

Title	REMOVAL OF INORGANIC CONTAMINANTS IN AQUEOUS ENVIRONMENT BY BIO-BASED MATERIALS
Author	Mr. Jakkapon Phanthuwongpakdee
Degree	Doctor of Philosophy (Engineering and Technology)
Faculty/University	Sirindhorn International Institute of Technology/ Thammasat University
Thesis Advisor	Professor Sandhya Babel, Ph.D.
Thesis Co-Advisor	Professor Tatsuo Kaneko, Ph.D.
Academic Years	2020

## ABSTRACT

Bio-based materials (agriculture waste with minimal modification and newly synthesized materials) were employed to remove ionic inorganic pollutants such as iodide ( $I^-$ ), iodate ( $IO_3^-$ ), aluminium ( $Al^{3+}$ ), and copper ( $Cu^{2+}$ ) in an aqueous environment. They were tested for their efficiency as well as studied for their underlying removal mechanism.  $I^-$  and  $IO_3^-$  can exist as radioactive iodine (I-131 and I-129).  $Al^{3+}$  and  $Cu^{2+}$  are heavy metals. These ions create adverse effects on the human and other living organisms. For the anion removal,  $I^-$  was the main target in this study as this is the main form existing in nuclear power plants. Several wastes and bio-based materials were screened and selected. Among these materials, iron-alginate (Fe-Alg), sacha inchi kernels and hazelnuts shells exhibited  $I^-$  adsorption capacities of 139, 18.9, and 45.1 mg/g, respectively. They were characterized as bio-based cationic-containing adsorbents and were able to attract  $I^-$  through physisorption. The fruit wastes containing anthocyanin were another group of adsorbents considered for  $I^-$  and  $IO_3^-$  removal. Through the isotherm fittings, the  $I^-$  adsorption behavior of mangosteen pericarps and

red onion peels was better explained by the Langmuir model (than the Freundlich model), and the predicted adsorption capacity was over 70 mg/g, similar to that of the experimental one. The characterization techniques revealed that O<sup>+</sup>, as part of the flavylum cation in anthocyanin, attracted I<sup>-</sup> via electrostatic force, and the adsorption was controlled by ion-exchange. The computational radial distance between O<sup>+</sup> and I<sup>-</sup> was calculated to be ~3.28 Å. Further characterization by UV-visible spectrometry, FTIR, EDX, XPS, and XAS supported the involvement of flavylum cation in anthocyanin as the main I<sup>-</sup> adsorbing functional group. The IO<sub>3</sub><sup>-</sup> adsorption was proposed with a similar mechanism, but lower adsorption capacity values were observed in mangosteen pericarps and pomegranate peels. High-performance cationic biopolyamides bearing quaternary ammonium (PA-R1, PA-R2, PA-R3 and PA-R4) were also used for I<sup>-</sup> adsorption. PA-R4, with 120 min equilibrium time, achieved more than 80% adsorption of 10 mg/L initial I<sup>-</sup> concentration at 90 °C. The carboxylic acid-containing biopolyimide in the form of potassium salt (BPI-COOK) was used to remove Al<sup>3+</sup> and Cu<sup>2+</sup> from the water. The complexation occurred by an exchange of K<sup>+</sup> into the targeted multivalent heavy metal. The process created the complexation of BPI-COOAl and BPI-COOCu, with removal of heavy metal ions from the water at the same time. The successful removal of inorganic ions by bio-based materials provides potential water remediation systems that can be used in the nuclear power plants accidents, in industries and real environment. This study has provided a new opportunity for sustainable waste removal from aqueous environment.

**Keywords:** Adsorption, Anthocyanin, Biopolymer, Inorganic pollution, Radioactive iodine

## ACKNOWLEDGEMENTS

I, the author of this dissertation, would like to express the deepest gratitude to *Prof. Sandhya Babel* (SIIT main supervisor) for her supervision and words of encouragement throughout the course of this thesis completion. I strongly believe that the knowledge and wisdom that she has offered will become tremendous assets for my future endeavors.

For Japan Advanced Institute of Science and Technology (JAIST), I would like to express my gratefulness to *Prof. Tatsuo Kaneko* (JAIST main supervisor) for his advice and support from Japan. Indeed, his assistance has greatly contributed to the completion of this work.

I would also like to extend my appreciation to the other committee members of this dissertation defense; *Prof. Paiboon Sreearunothai* (committee, SIIT), *Prof. Khanin Nueangnoraj* (committee, SIIT), *Prof. Kenji Takada* (committee, JAIST), *Prof. Kritapas Laohhasurayotin* (committee, NANOTEC, NSTDA), and *Prof. Akhilendra Bhushan Gupta* (external examiner, M.N.I.T of Jaipur). A special acknowledgement to the *dual degree doctoral program* arranged by the following institutions: JAIST (Japan), SIIT (Thailand), and National Science and Technology Development Agency (NSTDA, Thailand).

Lastly, I would like to thank my family and friends for their moral support, and their reassurance has made this PhD journey in SIIT less difficult.

Mr. Jakkapon Phanthuwongpakdee

## TABLE OF CONTENTS

	Page
ABSTRACT	(1)
ACKNOWLEDGEMENTS	(3)
LIST OF TABLES	(8)
LIST OF FIGURES	(10)
CHAPTER 1 INTRODUCTION	1
1.1 Problem statement	1
1.2 Objectives of the Study	4
1.3 Scope of study	4
CHAPTER 2 REVIEW OF LITERATURE	6
2.1 Sources of iodine in the environment	6
2.1.1 Natural sources of radioactive iodine	7
2.1.2 Anthropogenic sources of radioactive iodine	8
2.1.3 Effects of radioactive iodine on environment and human	13
2.2 Chemistry of Iodide and Iodate	14
2.3 Iodine removal technology	16
2.3.1 Membrane separation technology	16
2.3.2 Coagulation-flocculation-sedimentation	19
2.3.3 Electrolysis	21
2.3.4 Ionic liquid	21

	(5)
2.3.5 Bioaccumulation by algae	23
2.4 Adsorbents for removal of iodine in the water	24
2.4.1 Activated carbon	24
2.4.2 Soil and clay	29
2.4.3 Mineral	34
2.4.4 Anion-exchange resin	38
2.4.5 Cementitious materials	39
2.4.6 Polysaccharide	41
2.5 Sources and effects of copper and aluminium in the water	42
2.5.1 Copper	42
2.5.2 Aluminium	43
2.6 Copper and aluminium removal technology	44
2.6.1 Membrane separation technology	44
2.6.2 Chemical precipitation, coagulation, and flocculation	44
2.6.3 Adsorption	45
2.7 Principle of Adsorption	45
2.8 Characterization Techniques	50
2.8.1 Nitrogen adsorption-desorption surface area analysis	50
2.8.2 Scanning electron microscopy with energy dispersive X-ray analysis	51
2.8.3 Fourier-transform infrared spectroscopy	52
2.8.4 Ultraviolet–visible spectroscopy	53
2.8.5 Carbon-13 nuclear magnetic resonance	54
2.8.6 Particle size analyzer for zeta-potential	54
2.8.7 X-ray photoelectron spectroscopy	55
2.8.8 X-ray absorption spectroscopy (XAS)	56



	(6)
2.8.9 Inductively coupled plasma optical emission spectrometry	57
<b>CHAPTER 3 METHODS</b>	<b>58</b>
3.1 Methodology Overview	58
3.2 Reagents	58
3.3 Bio-based adsorbents preparation	59
3.4 Screening test and adsorbent dose	61
3.5 Bio-based adsorbent characterizations	63
3.6 Adsorption experiments for iodide	63
3.7 Investigation of functional groups involved in iodide adsorption	65
3.7.1 Functional groups in Fe-Alg, hazelnut shells and sacha inchi shells	65
3.7.2 Functional groups in anthocyanin-containing adsorbents	66
3.8 Adsorption experiments for iodate	69
3.9 Removal of copper and aluminium by BPI-metal complexation	70
3.9.1 BPI-metal complexation kinetics and thermodynamic	70
3.9.2 BPI-metal complex characterization	72
<b>CHAPTER 4 RESULTS AND DISCUSSION</b>	<b>74</b>
4.1 Screening test and adsorbent doses for iodide adsorption	74
4.2 Material characterization for iodide adsorption	76
4.2.1 Surface morphology	76
4.2.2 Chemical composition	78
4.3 Iodide adsorption study	80
4.3.1 Adsorption kinetics and pseudo-order reactions	80
4.3.2 Isotherms	85

	(7)
4.3.3 Effects of temperature and thermodynamics	88
4.3.4 Effects of pH and zeta potential, competitive anions, and regeneration	92
4.4 Mechanism of iodide adsorption by bio-based adsorbents	95
4.4.1 Cationic metal species as iodide adsorption functional group	95
4.4.2 Investigation of anthocyanin involvement in iodide adsorption	97
4.5 Comparative study of adsorbents for iodide removal	107
4.6 Iodate adsorption by anthocyanin-containing adsorbents	110
4.7 Complexation of polyimide with copper and aluminium	114
CHAPTER 5 Conclusions and recommendations	122
REFERENCES	125
APPENDICES	152
APPENDIX A	153
APPENDIX B	154
BIOGRAPHY	155

## LIST OF TABLES

Tables	Page
2.1 The iodine concentration in different types of environments; terrestrial, aquatic, atmospheric and biotic. Information is adopted from a literature (Whitehead, 1984)	7
2.2 Estimated production of I-129 in the natural environment. The information is derived from a literature (Fabryka-Martin, 1984)	8
2.3 Summary of half-life and activities of iodine isotopes in the fuel of conventional pressurized power reactor. The information is derived from a literature (International Atomic Energy Agency, 2006)	9
2.4 Anthropogenic sources of radioactive iodine contaminant	11
2.5 Coefficient number for lifetime cancer mortality risk of I-129 and I-131. The information is adopted from a literature (Peterson et al., 2007)	14
2.6 Ionic properties of iodide and iodate	15
2.7 Overview of the characteristics and iodine removal efficiency for different kinds of pressure-driven membranes	18
2.8 Comparison of maximum removal efficiency for UF and RO system	18
2.9 Comparison of iodine adsorption with different types of activated carbon	27
2.10 Comparison of iodine adsorption in the collected soil, natural clay and modified clay	32
2.11 Comparison of iodine adsorption on various kinds of minerals	35
2.12 Removal of metal by membrane separation technology	44
3.1 Different types of bio-based adsorbents used in the screening test with their dose and contact time	61
4.1 Comparison of surface and pore characteristics for the anthocyanin-containing adsorbents	76
4.2 EDX analysis showing the elemental composition of the virgin and I <sup>-</sup> saturated bio-based adsorbents	79
4.3 Summary of I <sup>-</sup> adsorption experiment values, 8-day efficiency, and experimental adsorption capacity	82

4.4 Derived parameters of the linear fitting pseudo-order reactions	84
4.5 Derived parameters of the linear fitting isotherm models	87
4.6 Thermodynamic parameters of the I <sup>-</sup> adsorption by bio-based adsorbents at 5 – 65 °C	90
4.7 Total anthocyanin content (TAC) from the anthocyanin quantification, using the ultrasound-assisted extraction method, and the leaching experiment, using 10 mg/L I <sup>-</sup> solution with 2 h contact time.	98
4.8 Comparison of FTIR peaks corresponding to the dominant functional groups in anthocyanin of virgin and saturated anthocyanin-containing adsorbents	101
4.9 EXAFS quick-first shell fit	103
4.10 Partial charge of the atoms in the optimized cyanidin	105
4.11 Comparison with other adsorbents in term of experimental I <sup>-</sup> adsorption capacity and proposed mechanism	108
4.12 Derived parameters of the linear fitting isotherm models	112
4.13 Thermodynamic parameters for the complexation of BPI-COOAl and BPI-COOCu	116
4.14 BPI-COOCu EXAFS fit with the model structure of CuH <sub>2</sub> (CO <sub>2</sub> ) <sub>2</sub>	118

## LIST OF FIGURES

Figures	Page
2.1 Stability of different iodine species across different pH and electrical potential (Eh) conditions [adapted from a previous study (Medrano-Macías et al., 2016)]	16
2.2 Basic components of SEM and EDX adopted from a technical webpage (Nanakoudis, 2019). (a) creation of backscattered and secondary electrons for SEM and X-ray for EDX, (b) detailed scheme of X-ray emission by primary electron beam	52
2.3 Emission of electron from the sample by the X-ray excitation. Emitted electrons are captured and measured for their kinetic energy by a detector	55
3.1 Flow chart displaying overall methodology in this study	58
3.2 Structure of cationic polyamides used in this study	61
3.3 BPI-COOAl and BPI-COOCu syntheses	71
4.1 Screening test for various adsorbent doses with 10 mg/L I <sup>-</sup> initial concentration for 2 h at room temperature (a) seed shells and husks, (b) bio-based and metal-based synthetic materials, (c) anthocyanin-containing adsorbents, (d) cationic biopolyamides, (e) commercial adsorbents, (f) living plants	76
4.2 SEM images of bio-based adsorbents. (a) Fe-Alg, (b) hazelnut shells, (c) sachu inchi shells, (d) mangosteen pericarps, (e) red onion peels, (f) red dragon fruit peels, (g) passion fruit rinds (1 – virgin adsorbent, and 2 – saturated adsorbent)	77
4.3 SEM-EDX analysis showing the elemental composition on different parts of the passion fruit peels	78
4.4 Kinetic study showing I <sup>-</sup> removal efficiency (%) for 180 min with optimum adsorbent dose and 10 mg/L I <sup>-</sup> initial concentration at room temperature. (a) Fe-Alg, hazelnut shells, and sachu inchi shells, (b) anthocyanin-containing adsorbents, (c) cation biopolyamides	81

- 4.5 Batch experiment showing adsorption capacity,  $q$  (mg/g) over final  $I^-$  concentration,  $C_e$  (mg/L) with optimum adsorbent dose and equilibrium time. (a) Fe-Alg, hazelnut shells, and sachu inchi shells (2 – 200 mg/L initial  $I^-$  concentration), (b) anthocyanin-containing adsorbents (2 – 200 mg/L initial  $I^-$  concentration), (c) cation biopolyamides (5 – 1000 mg/L initial  $I^-$  concentration) 82
- 4.6 Linear fits of pseudo-order-reaction. (a) Fe-Alg, hazelnut shells, and sachu inchi shells, (b) anthocyanin-containing adsorbents, (c) cation biopolyamides 84
- 4.7 Linear fits of isothermal models. (a) Fe-Alg, hazelnut shells, and sachu inchi shells, (b) anthocyanin-containing adsorbents, (c) cation biopolyamides 87
- 4.8 Effects of temperature on  $I^-$  adsorption. (a) overall effects on adsorption capacity, (b) concentration-dependent adsorption of Fe-Alg, (c) concentration-dependent adsorption of hazelnut shells, (d) concentration-dependent adsorption of sachu inchi shells, (e) concentration-dependent adsorption of mangosteen pericarps, (f) concentration-dependent adsorption of red onion peels, (g)  $I^-$  removal efficiency of cationic biopolyamides with 10 mg/L  $I^-$  initial concentration 90
- 4.9 Linear fits of the Arrhenius model. (a) Fe-Alg, hazelnut shells, and sachu inchi shells, (b) mangosteen pericarps and red onion peels (insets - Arrhenius activation energy,  $E_a$ ) 91
- 4.10  $I^-$  adsorption efficiency at various pH (a) Fe-Alg, hazelnut shells, and sachu inchi shells, (b) anthocyanin-containing adsorbents, (c) cation biopolyamides at 10 mg/L initial  $I^-$  concentration, (d) zeta potential of Fe-Alg and sachu inchi shells 93
- 4.11  $I^-$  adsorption efficiency in the presence of competitive anions and regeneration cycle at 10 mg/L initial  $I^-$  concentration. (a) Fe-Alg, hazelnut shells, sachu inchi shells, and PA-R4 in the presence of competitive anions (b) anthocyanin-containing adsorbents in the presence of competitive anions, (c) Fe-Alg and PA-R4 efficiency of 5-cycle regeneration 94

- 4.12 Normalized iodine LIII-edge XANES spectra of the saturated Fe-Alg, hazelnut shells, and sacha inchi shells with KI (aq) and KIO<sub>3</sub> (aq) as references 95
- 4.13 FTIR spectra of the virgin and saturated bio-based adsorbents. (a) Fe-Alg, (b) hazelnut shells, (c) sacha inchi shells 97
- 4.14 Study of cyanidin ion-exchange properties. (a) cyanidin chloride solution, (b) cyanidin chloride in KI solution (equimolar ratio of cyanidin to I<sup>-</sup>) 99
- 4.15 UV-visible spectrum of anthocyanin in different I<sup>-</sup> concentrations. (a) cyanidin chloride, (b) anthocyanin extract of mangosteen pericarps, (c) anthocyanin extract of red onion peels 100
- 4.16 FTIR spectra of virgin and saturated anthocyanin-containing adsorbents. (a) mangosteen pericarps, (b) red onion peels, (c) red dragon fruit peels, (d) passion fruit rinds 101
- 4.17 Iodine oxidation state and local structure in the presence of anthocyanin. (a) I3d5 XPS spectra of mangosteen pericarps, (b) I3d5 XPS spectra of red onion peels (c) normalized iodine LIII-edge XANES spectra of the anthocyanin-based adsorbents, (d) graph of transformed K-space and R-space for potassium K-edge [1. mangosteen pericarps, 2. red onions peels, 3. cyanidin solution] 103
- 4.18 Optimized structure of cyanidin by Gaussian 09 with DFT method 105
- 4.19 Cyanidin-I<sup>-</sup> conformations with the lowest total estimated binding energy obtained from the program, AutoDock 4. (a) conformation 1 (b) conformation 2 (vdW – Van der Waals, Hbond – hydrogen bond, desolv – desolvation) 106
- 4.20 Removal of IO<sub>3</sub><sup>-</sup> by anthocyanin-containing adsorbents. (a) screening test with 1 g/L dose in 10 mg/L IO<sub>3</sub><sup>-</sup> solution for 2 h, (b) adsorbent dose of the selected adsorbents in 10 mg/L IO<sub>3</sub><sup>-</sup> solution for 2 h 111
- 4.21 Kinetic and batch experiment of IO<sub>3</sub><sup>-</sup> removal by anthocyanin-containing adsorbents. (a) Kinetic experiment for 720 min using 10 mg/L IO<sub>3</sub><sup>-</sup> initial concentration and optimum adsorbent doses at room temperature, (b) graph of concentration-dependent adsorption (q over C<sub>e</sub>) for 0 – 100 IO<sub>3</sub><sup>-</sup> initial

concentration, optimum adsorbent doses and equilibrium time of contact at room temperature, (c) linear fits of Langmuir model, (d) linear fits of Freundlich model	112
4.22 Effect of changing condition to $\text{IO}_3^-$ removal by anthocyanin-containing adsorbents using optimum dose and equilibrium contact time in 10 mg/L $\text{IO}_3^-$ initial concentration. (a) variation of pH, (b) variation of temperature	114
4.23 Kinetic study of metal complexation. (a) metal removal (%) calculated by Equation (3.7) over time for 0 – 120 min of BPI-COOK submerged in 1 mol/L $\text{Al}^{3+}$ and $\text{Cu}^{2+}$ solution, (b) batch experiment of BPI-COOK submerged in 0.5 – 6 mol/L $\text{Al}^{3+}$ and $\text{Cu}^{2+}$ solution for 30 min. $q$ is the amount of metal bound to a unit of BPI (mol/g), and $C_i$ is the initial metal ion concentration (mol/L).	115
4.24 BPI films made from 1 mol/L metal ion. (a) BPI-COOAl, (b) BPI-COOCu	115
4.25 Graphs for thermodynamic parameters. (a) $q$ (mol/g) over $C_e$ for BPI-COOAl, (b) $q$ over $C_e$ for BPI-COOCu	116
4.26 FTIR spectra in the fingerprint region of BPI-metal complex made from various metal ion concentrations with the spectra of BPI-COOH and BPI-COOK as references. (a) BPI-COOAl, (b) BPI-COOCu	117
4.27 XAS of BPI-COOCu at Cu k-edge. (a) XANES, (b) EXAFS K-space and R-space	118
4.28 Local structure at Cu atom of BPI-COOCu made from 1 mol/L $\text{Cu}^{2+}$ initial concentration	119
4.29 Proposed flame retardant mechanism of BPI-COOAl with Al2p XPS spectra and flame retardant mechanism diagram	120
4.30 Proposed flame retardant mechanism of BPI-COOCu with Cu2p3 with XPS spectra	121



## CHAPTER 1

### INTRODUCTION

The rise of the human population and activities have been leading to an increase of contaminants. The inorganic pollutants are released into the water environment via industry, mining, and agriculture. Above the permissible limit, these pollutants create adverse effects on the human and other living organisms. In the green society, there are needs for sustainable techniques for the removal of these inorganic pollutants from the water. In this study, bio-based materials (agriculture waste with minimal modification and newly synthesized materials) were employed to remove ionic inorganic pollutants such as iodide ( $I^-$ ), iodate ( $IO_3^-$ ), aluminium ( $Al^{3+}$ ), and copper ( $Cu^{2+}$ ) in an aqueous environment.

#### 1.1 Problem statement

Radioactive iodine species (I-131 and I-129) are considered to be some of the most dangerous substances released into the environment. Conventional uranium fission process in the nuclear power plants can create isotopic products of strontium, barium, caesium and iodine. Creating energy from the fission process in nuclear power plants seems to be one of the promising ways in securing electrical power in the future. However, since the first nuclear power plants were constructed, the safety concern relating to its waste products, that are being discharged into the environment, have been the issue to be dealt with (Ramana, 2009).

Although I-131 has a half-life of 8 days, its decay mechanism produces  $\beta$  particles with high specific activity (130,000 Ci/g) that can destroy the thyroid gland and causes thyroid cancer (Hall et al., 1992; Hieu et al., 2012; Peterson et al., 2007). I-129 emits  $\beta$  particles with a less specific energy of  $1.8 \times 10^{-4}$  Ci/g, but its 1.6 million-year half-life causes a problem of radioactive waste accumulation (Peterson et al., 2007). A recent study suggested that after three decades of Chernobyl incidents, 1.56 mBq/kg of highly water-soluble I-129 was still detected in the soil of the contaminated areas (Shaw et al., 2019). During the Fukushima Daiichi Nuclear Accident in Japan, up to 11 PBq total activity of I-131 and  $62 \times 10^7$  atoms/L of I-129 were discharged into the water environment (Hou et al., 2013; Kawamura et al., 2011). Leakages from nuclear

waste disposal sites and medical facilities also contributed to the discharge of the contaminants (Janardhan et al., 1990; Miyake et al., 2012; Ravichandran et al., 2011; S. Zhang et al., 2013).

In the water, iodide ( $I^-$ ) and iodate ( $IO_3^-$ ) are the main anionic forms of radioactive iodine. However,  $I^-$  is more common because cesium iodide (CsI) is the source of soluble radioactive substance in the nuclear facility, while iodide ( $I^-$ ) was found to be the iodine dominant species in the waste disposal sites (Konings et al., 2015; Lemma et al., 2015). Many kinds of technologies have been used to remove  $I^-$  from water. These include membrane separation, silver precipitation, and immobilization by cementitious materials (Bonhoure et al., 2002; Karkhanei et al., 2015; Y. Liu et al., 2016). Membrane separation requires high energy, while the silver precipitation method adds metallic silver directly to the water body. Both technologies are suitable only in closed-environment remediation. Cement production is poisonous to the environment because it produces by-products such as chlorine,  $SO_x$ ,  $NO_x$ , mercury, lead, chromium, and arsenic (Chen et al., 2010).

Adsorption processes have become an essential technology for the natural environment and industry effluent remediation. Several types of commercial polystyrene-based anion-exchange resins were reported to reduce  $I^-$  in groundwater. In a laboratory study, the  $I^-$  removal capacity of a silica-based ion-exchange resin was about 149 mg/g (Parker et al., 2014; Ye et al., 2019). However, these polystyrene-based resins, bearing cationic quaternary amines, relied on fossil fuel-based chemicals for their production. Other commercial adsorbents such as activated carbon and zeolite were considered as bio-derived materials. However, they were susceptible to a low adsorption efficiency of about 50% and 30%, respectively, at 50  $\mu\text{g/l}$  initial  $I^-$  concentration (Sato et al., 2011). There were attempts to improve the performance of the activated carbon by incorporating silver. An estimated maximum  $I^-$  adsorption capacity of 127 mg/g was reported (Hoskins and Karafil, 2002; Sánchez-Polo et al., 2006). The complexation of alginate by metal ions could also create potential adsorbents for anionic contaminant removal. With the reduction of  $I_2$  to  $I^-$ , Maghemite and titanium dioxide alginate beads yielded 19.5 mg/g adsorption capacity (Majidnia and Idris, 2015). The adsorption of arsenate by copper and iron alginate complexes was studied (Min and Hering, 1998). However, these adsorbents have not been used for the

direct adsorption of  $I^-$  in solution. Knowing that nuclear power is a crucial  $CO_2$ -free energy source, the first part of this study is dedicated to the removal of anionic iodine species by adsorption using bio-based adsorbents.

Copper is one of those heavy metals that can be emitted from metallurgist, automobile, and mining activities. It is considered to have low toxicity in human combining with body secrete mechanism and low availability in human food. However, it is one of the most toxic metals if present in aquatic ecosystems. High concentration of copper in water can be disruptive to fish organs functionality (Kantati et al., 2013; Malhotra et al., 2020). Aluminum in wastewater is generated from industrial wastes, especially wash water from drinking water treatment plants. It can bind to other agents and can become more toxic such as aluminum hydroxide. With acidic condition of water,  $Al^{3+}$  act as a toxic agent by causing failure of osmoregulatory function on gill-breathing organism like fish and invertebrate (Havens, 1993; Raddum and Fjellheim, 2002).

To solve this heavy metal pollution problem, adsorption has been used extensively to remove the heavy metal ions due to its capability, cost effective, and recyclability. Activated carbon is widely known as an adsorbent to remove heavy metal ions from water contamination because of its high porosity and large surface area. However, activated carbon has high cost and low selectivity. In order to obtain the selective property and cost effective, the adsorbents containing functional groups such as hydroxyl is needed. Other high-performance methods of metal removal are using sodium alginate or chitosan. Sodium alginate has high rate of heavy metal removal but when used in high quantity will result in viscous liquid on the surface and produce an unclear separation. Whilst chitosan when bonded with heavy metal will form a gel-like substance and the rate of removal can only reached a certain point despite the additional quantity of chitosan added afterward. A recent research had conducted on combining sodium alginate and chitosan to obtain metal removing with high removal rate and clear separation (Ablouh et al., 2019).

Polyimide (PI) is outstanding in thermal stability, chemical resistance, radiation resistance and mechanical properties. It can be used in wide range of applications from engineering plastics to biochemical implants. The polyimide in this study is synthesized

from the microbial organism which called bio-based PI (BPI) (Huang et al., 2016). This BPI has carboxyl groups and could help remove metals ions from contaminated water.

After the BPI metal complex (BPI-M<sub>x</sub>) is formed, it could be used for further diverse applications such as in magnetic data storage, micro-electronic devices, electromagnetic shielding materials, etc. Nonetheless, the optimization conditions for the bio-based polyimide adsorption have not been thoroughly studied. The removal of Al<sup>3+</sup> and Cu<sup>2+</sup> will be done by using BPI.

## 1.2 Objectives of the Study

The main aim of this study is to employ bio-based materials to remove inorganic pollutants such as I<sup>-</sup>, IO<sub>3</sub><sup>-</sup>, Al<sup>3+</sup>, and Cu<sup>2+</sup> from the water. The adsorption efficiency and capacity were investigated through kinetic and batch experiments. With the fittings of adsorption-related models, the adsorption behavior was predicted. The adsorbents were characterized to identify the functional group to understand the adsorption mechanism. The main focus of the study was the removal of I<sup>-</sup>, while IO<sub>3</sub><sup>-</sup>, Al<sup>3+</sup>, and Cu<sup>2+</sup> were briefly investigated. The objectives of the study include:

1. Searching for novel bio-based adsorbents for the removal of I<sup>-</sup>
2. Determine the optimum adsorption condition of I<sup>-</sup> removal by the selected bio-based adsorbents
3. Understand the functional groups and mechanism involved in the I<sup>-</sup> removal
4. Determine the IO<sub>3</sub><sup>-</sup> adsorption efficiency of anthocyanin-containing adsorbents
5. Investigate the efficiency of BPI to remove Al<sup>3+</sup> and Cu<sup>2+</sup> and the mechanism underlying BPI-metal complexation

## 1.3 Scope of study

The scope of this study is mainly concerning the removal of ionic pollutants such as I<sup>-</sup>, IO<sub>3</sub><sup>-</sup>, Al<sup>3+</sup>, and Cu<sup>2+</sup> from the aqueous environment by bio-based adsorbents. The detailed scope of study includes:

1. The experiments were conducted in the laboratory scale.
2. For safety reasons, stable I<sup>-</sup> and IO<sub>3</sub><sup>-</sup> were used. We assume isotopes of the same elements (in the same chemical form) possess the same chemical properties.

3. The quantifications of  $I^-$  and  $IO_3^-$  were done by colorimetric methods. All experiments were performed in triplicate.
4. The screening test was done for several bio-based adsorbents for removing  $I^-$ , and only the ones with high efficiency were selected for detailed adsorption experiments. To find optimum conditions for the adsorption, different parameters affecting the adsorption were varied. These include:
  - a. Variation in adsorbent dose
  - b. Contact time (explained by pseudo-order reactions)
  - c. Concentration-dependent adsorbents (explained by Langmuir and Freundlich isotherms)
  - d. Variation of temperature (explained by thermodynamic)
  - e. Variation of pH
  - f. Adsorption in the presence of other anions and water mediums
5. Regeneration studies for synthetic bio-based adsorbents were done to assess their reusability.
6. Characterization of the selected bio-based adsorbents to determine the functional groups and mechanism involved in the  $I^-$  removal
  - a. Nitrogen adsorption and Brunauer-Emmett-Teller (BET) surface area analysis (only for the anthocyanin-containing adsorbents)
  - b. Scanning Electron Microscope and Energy Dispersive X-ray Spectrometer
  - c. Fourier-transform infrared spectroscopy
  - d. X-ray photoelectron spectroscopy
  - e. X-ray absorption spectroscopy (only for the anthocyanin-containing adsorbents)
  - f. Nuclear magnetic resonance (only for the anthocyanin-containing adsorbents)
  - g. Computer simulation (only for the anthocyanin-containing adsorbents)
7. Only the anthocyanin-containing adsorbents were used for  $IO_3^-$  adsorption
8. Biopolymer such as BPI and cationic biopolyamides were synthesized in Japan Advanced Institute of Science and Technology. This dissertation does not contain information about synthetic routes nor polymer performance.

## CHAPTER 2

### REVIEW OF LITERATURE

#### 2.1 Sources of iodine in the environment

Iodine in the natural environment is less abundant than the other elements, but it is considered to be an important substance to many aquatic plants, bacteria and mammals, including the human (Christiansen and Lars, 1989). It plays a significant role in the world temperature regulation as well. Iodine from the ocean forms marine aerosols and cloud condensation nuclei that contribute to the cooling effects of the global budget of radiation (O'Dowd et al., 2002). However, some studies claimed that the ocean emission of iodine to the troposphere could trigger a reaction of hypoiodous acid (HOI) with Br and Cl, and ultimately destroy the ozone layer (Carpenter et al. 1999; Carpenter et al. 2000; Prados-Roman et al. 2015)

Iodine naturally exists in oxidation states. In water, the dissociation form of iodine are mainly iodide ( $I^-$ ) and iodate ( $IO_3^-$ ). In the marine and soil environment,  $IO_3^-$  dominates in most condition (Tsunogai and Henmi, 1971). In the ocean,  $IO_3^-$  is observed to outnumber  $I^-$  in different ocean depth, flat profile, and location (Tsunogai and Henmi 1971). Besides, the mentioned ion from, the species of volatile organic iodine, also known as organoiodine, existed in the natural environment. The examples of organoiodine are  $CH_3I$ ,  $C_2H_5I$ ,  $CH_2I_2$ ,  $CH_2IBr$ , and  $CH_2I_2$ . These are mostly produced by phytoplankton and seaweed metabolic system (Fielman et al., 1999). The main organoiodine released from the brown algae is  $CH_2I_2$  (Carpenter et al., 2000).

Iodine can be found in various kinds of environment. **Table 2.1** shows the concentration of iodine in the natural environment. In the ocean, the seawater concentrates a small amount of iodine while the substance is found mostly concentrated in the marine sediment and algae. Aquatic plants have an ability to accumulate high amount of iodine. The brown algae species named *Laminaria digitate* (known commonly as horsetail kelp) can accumulate up to 3134 mg of  $I^-$  per kilogram of its biomass (Martinelango et al., 2006). Soils and rocks contain a moderate quantity of iodine, as well as both organic and mineral contents in soils, has an ability to adsorb iodine (Refer to the Soil and Mineral section under the sorption heading for more information).

**Table 2.1** The iodine concentration in different types of environments; terrestrial, aquatic, atmospheric and biotic. Information is adopted from a literature (Whitehead, 1984)

Types of Environments		Average Iodine Concentration	
Terrestrial	Soils	0.50 – 20.0	mg/kg
	Igneous rocks	0.08 – 0.50	mg/kg
	Sedimentary rocks	0.20 – 10.0	mg/kg
	Metamorphic rocks	1.61	µg/kg
	Coal	1.0 – 15.0	mg/kg
Aquatic	Seawater	45.0 – 60.0	µg/L
	Marine Sediment	3.0 – 40.0	mg/kg
	River and Lake water	0.50 – 20.0	µg/L
Atmospheric	Atmosphere	10.0 – 20.0	ng/m <sup>3</sup>
	Rainwater	0.50 – 5.0	µg/L
Biotic	Mammalian tissues (excluding thyroids)	0.05 – 0.50	mg/kg
	Marine fish	0.50 – 6.00	mg/kg
	Freshwater fish	0.06 – 0.20	mg/kg
	Higher plants	0.05 – 0.50	mg/kg
	Marine algae	90.0 – 2500	mg/kg

### 2.1.1 Natural sources of radioactive iodine

Today, there are 37 known isotopes of iodine comprising of iodine-108 (I-108) to iodine-144 (I-144). Iodine-127 (I-127) is the only stable isotope of iodine. Iodine-129 (I-129) is the only isotope, out of a few radionuclides, that occurs naturally and can be detected by human. It is considered to be a cosmogenic nuclide which produced from the fission of uranium and by the interaction of cosmic ray particles with stable xenon in the atmosphere (Schmidt et al., 1998). Natural production of I-129 is summarized in **Table 2.2**. Most of the production comes from cosmic ray and solar wind activities in the upper atmosphere. The natural I-129 production per year in the environment is

minimal. Most of the radioactive iodine production came from anthropogenic activities. The information on human-made radioactive iodine is presented in the next section.

**Table 2.2** Estimated production of I-129 in the natural environment. The information is derived from a literature (Fabryka-Martin, 1984)

Source of I-129		Amount of I-129
Production in upper atmosphere	cosmic ray	$550 \times 10^{24}$ atoms
	solar wind	$9 \times 10^{24}$ atoms
Total production by fission of uranium-238 in geosphere compartment	ocean mixed layer	$1.2 \times 10^{-6}$ g/year
	deep ocean	$5.4 \times 10^{-5}$ g/year
	ocean sediment	$5.6 \times 10^{-4}$ g/year
	shallow groundwater	$9.7 \times 10^{-8}$ g/year
	deep groundwater	$<7.6 \times 10^{-8}$ g/year
	sediments	$9.3 \times 10^{-2}$ g/year
	igneous activity	2.2 g/year

### 2.1.2 Anthropogenic sources of radioactive iodine

Anthropogenic sources of radioactive iodine are nuclear power plants, weapon testing and medical procedures. Especially in the nuclear power plants, several isotopes of radioactive iodine are produced. **Table 2.3** shows iodine nuclides, their half-life and activity in a pressurized power reactor. Only two isotopes of iodine, I-129 and I-131, are concerned contaminants in the natural environment. In a pressurized reactor, I-129 might have a low radioactive activity of  $3.8 \times 10^{-2}$  Ci per tons of fuel, but the isotope can pose a long-term environmental problem with a half-life of 16 million years. For I-131, it is one of the most active radioactive nuclides of iodine found in the reactor ( $1.0 \times 10^6$  Ci per tons of fuel). It poses a short-term problem with a higher risk of to the human health and environment. Cesium iodide (CsI) is regarded as the source of soluble radioactive substance in the nuclear facility, while  $I^-$  was found to be the iodine dominant species in the waste disposal sites.



**Table 2.3** Summary of half-life and activities of iodine isotopes in the fuel of conventional pressurized power reactor. The information is derived from a literature (International Atomic Energy Agency, 2006)

Nuclide	Half-life	Activities (Ci per tons of fuel)
I-127	Stable	-
I-128	25 min	$1.3 \times 10^4$
I-129	$1.6 \times 10^7$ year	$3.8 \times 10^{-2}$
I-130	12.4 hours	$4.1 \times 10^4$
I-131	8.05 days	$1.0 \times 10^6$
I-132	2.3 hours	$1.4 \times 10^6$
I-133	21 hours	$1.8 \times 10^6$
I-134	52.8 minutes	$2.1 \times 10^6$
I-135	6.7 hours	$1.6 \times 10^6$
I-136	83 seconds	$6.4 \times 10^5$
I-137	23 seconds	$1.7 \times 10^6$
I-138	5.9 seconds	$1.6 \times 10^6$
I-139	2.0 seconds	$1.3 \times 10^6$

The anthropogenic activities have released amounts of I-129 and I-131 into the atmosphere (**Table 2.4**). There are specific nuclear-activity-related sites and incidents that had been prominently adding the radioactive iodine into the environment. These sites include Savannah River, Hanford, Nevada Nuclear Testing Site and nuclear reprocessing plants in Europe and Asia. In short, Hanford site, located in south-central Washington, near the Columbia river, was used extensively for nuclear weapon testing and production. For the Savannah River site, it is located in South Carolina. The place is also home to many nuclear reactors that are still in operation today.

The disastrous events that released the radioactive iodine into the environment are Chernobyl and Fukushima accident. Chernobyl disaster occurred in 1986 with the explosion of reactors in Chernobyl power plant located in Propyat, Ukraine. Following

the Earthquake near Japan in March 2011, the tsunami destroyed parts of Fukushima Nuclear power plants, releasing the substance from the reactors into the environment.

When comparing the natural production of I-129 in **Table 2.3** to those the quantity released by of human actions in **Table 2.4**, human have been contributing to a much higher amount of I-129 in the environment. In the aqueous environment, a high concentration of 1500 Bq/L and  $62 \times 10^7$  atoms/L of I-131 and I-129 were released during the accident at Fukushima. The unexpected events are more fatal to human's health and environment because of its high contaminant flux in a shorter amount of time. The extent of radioactivity of radioactive iodine produced in the daily nuclear reprocessing activities and hospital procedures might be far smaller than that of the accidental release. However, in the long run, the waste substances accumulate, and tentative attention is still needed for these sources.

In the natural environment, iodine is stored mostly in the atmosphere, marine sediment, aquatic plants and soil. I-129 can be produced, in a minimal quantity, by natural sources such as cosmic ray and uranium fission. Nevertheless, with anthropogenic activities like weapon testing, nuclear power plants and medical procedures, high amount of radioactive iodine is added to the environment. The accident of Chernobyl and Fukushima deteriorate the matter with an even greater release of contaminants within a short period. Humanly is concerned about I-129 and I-131 because of their effects on the environment and human's health. The next section in this report will summarize the adverse effects of radioactive iodine.

**Table 2.4** Anthropogenic sources of radioactive iodine contaminant

Source/ Incident	Environment Affected	Radioactive Iodine	Concentration/ Discharge	Total Activity	Ref.
Chernobyl, 1986	soil and atmosphere	I-129	-	0.04 TBq	(United Nations Scientific Committee on the Effects of Atomic Radiation, 2000)
Chernobyl, 1986	soil and atmosphere	I-131	-	$1.76 \times 10^6$ TBq	
Fukushima, 2011	air	I-131	-	153 - 160 PBq	(Kawamura et al., 2011)
Fukushima, 2011	ocean	I-131	300 – 4000 Bq/L	3.0 – 11.0 PBq	
Fukushima, 2011	ocean	I-129	$14.0 \times 10^7 - 62.0 \times 10^7$ atoms/L	-	(Hou et al., 2013)
Savannah River Site	groundwater	I-129	2.10 - 59.9 Bq/L	-	(Daniel I. Kaplan et al., 2014)
Nevada Testing Site	groundwater	I-129	0.777 Bq/L	-	(Smith et al., 2003)
Harford Testing Site	groundwater	I-129	2.20 - 42.5 pCi/L	-	(S. Zhang et al., 2013)

Reprocessing Plants	Baltic sea and rivers nearby	I-129	0.710 – 13.8 atoms/L	-	(Aldahan et al., 2006; Keogh et al., 2007)
Royal Hospital, Muscat, Oman (2006-2009)	liquid waste in the hospital	I-131	-	3777 MBq	(Ravichandran et al., 2011)
Medical institutes, Japan	Tap water	I-131	13.0 – 15.0 Bq/kg	-	(Kamei et al., 2012)

### 2.1.3 Effects of radioactive iodine on environment and human

I-131 can destroy thyroid gland and increase the risk for hypothyroidism, thyroid nodules, and cancer (Agency for Toxic Substances and Disease Registry, 2004). Human's thyroid gland, naturally, adsorb iodine for the purpose of hormonal growth and metabolic regulation. It can contain up to 30 to 40 times of iodine concentration than that of in the blood stream (Braverman MD and Cooper, 2005). Moreover, the pathway of iodine includes the adsorption from the gastrointestinal tract and lungs which the substance eventually end up in the bloodstream (Agency for Toxic Substances and Disease Registry, 2004). Iodine can also be found in other parts of human body including gastric mucosa, salivary glands, mammary glands, choroid plexus, ovaries, placenta, breast tissues, breast milk and skin (Jhiang et al., 1994; National Academy of Science, 1999). The exposure pathway of radioactive iodine to human includes the ingestion of cow milk, fruits, vegetable, fish, water and inhalation (National Academy of Science, 1999; Peterson et al., 2007)

I-131 can be used to treat hyperthyroidism, but the substance itself can cause thyroid and other kinds of cancer. The effects of radioactive iodine can also be studied from the increasing mortality of the patients diagnosed with I-131 therapy. Some patients have developed a higher mortality due of the development of cancers of other organs such as breast, lung, stomach, kidney and brain (Hall et al., 1992; Hieu et al., 2012). The coefficient of lifetime cancer mortality risk is presented in the radiological and chemical fact sheets (**Table 2.5**). In 1990-1994, 8-9 years old children were found to have thyroid cancer in Ukraine and Belarus (Pacini et al., 1997; Williams and Tronko, 1996). The cases were claimed to be associated with I-131 radiation because naturally, thyroid cancer only develops in the children of age 14 and above (National Academy of Science, 1999). The patients, living in Belarus, Russia and Ukraine, with thyroid cancer diagnosed in 1992–2002 were adolescents during the Chernobyl incidents, and radioactive iodine exposure contributes to these thyroid cancer cases (International Atomic Energy Agency, 2006; Morita et al., 2010)

I-129 poses a higher risk per pCi adopted for both inhalation and ingestion since it has a much longer half-life time beyond the human lifetime. If the co-efficient is to be calculated per atom, I-131, which emits higher activity (Ci/atom), should have a much higher mortality risk. However, with high abundant and long decaying time of I-

129, it poses another problem, especially to the environment. Permissible amount of I-131 used in the hospital patients is 50-100 mCi ( $1.85 \times 10^9$  and  $3.7 \times 10^9$  Bq) and 200 mCi is considered to be an extreme case (National Academy of Science, 1999).

**Table 2.5** Coefficient number for lifetime cancer mortality risk of I-129 and I-131. The information is adopted from a literature (Peterson et al., 2007)

Isotope	Specific Activity (Bq/g)	Lifetime Cancer Mortality Risk Co-efficient	
		Inhalation ( $pCi^{-1}$ )	Ingestion ( $pCi^{-1}$ )
I-129	0.00018	$6.20 \times 10^{-12}$	$3.30 \times 10^{-11}$
I-131	130,000	$2.10 \times 10^{-12}$	$1.40 \times 10^{-11}$

A large amount of iodine in the ocean can create negative feedback to the Earth's ozone layer. The iodine in the sea and marine aerosol are important aspects of the Earth's temperature and sun radiation regulation (O'Dowd et al., 2002). However, human's activities release iodine into the ocean which results in the increase of iodine in the natural cycle. The ocean emits iodine in the form of inorganic HOI. The substance can react with Br and Cl where the products can destroy the ozone layer in the troposphere (Carpenter et al., 1999; Fielman et al., 1999). Above the ocean 25% of ozone chemical had been lost due to the emission of iodine and 70% increase in ozone depletion due to iodine is estimated from that of in pre-industrial era (Prados-Roman et al., 2015). High I-129 released into the ocean can contribute to this adverse effect in the ozone layer.

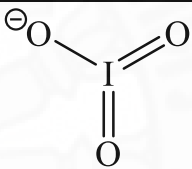
Radioactive iodine can adversely affect the environment and human's health. With all these impacts that it can create, there are needs to search and develop for suitable technologies to remove and immobilize the iodine. The next part of this report, the past and present studies of different kinds of iodine-removal technologies will be presented.

## 2.2 Chemistry of Iodide and Iodate

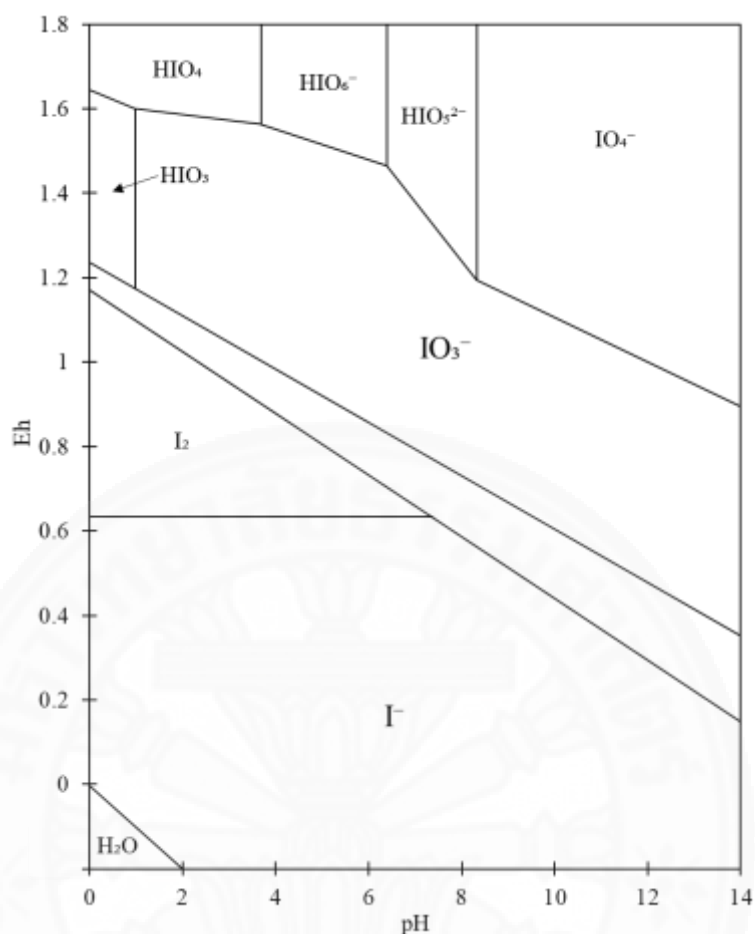
Ionic properties are important in the study of adsorption. The basic ionic properties of  $I^-$  and  $IO_3^-$  are depicted in **Table 2.6**. In term of ionic radius,  $I^-$ , to a small

extent, was calculated to contain a higher value. A high ionic radius of an adsorbate may create steric hindrance to prevent further adsorption due to saturation effects and overcrowding of anion (Faur-Brasquet et al., 2002). Nevertheless, the chemical structure of  $\text{IO}_3^-$  exhibits covalent bonds of I and O atom, which may also create steric effect, preventing the adsorption. It is reported in previous studies that in its salt form,  $\text{IO}_3^-$  is less soluble, and the ion is more stable than that of  $\text{I}^-$  (Bürigi et al., 2001). This is because  $\text{I}^-$  tends to be oxidized into  $\text{I}_2$  (Bürigi et al., 2001). The stability of  $\text{IO}_3^-$  may impede the ion from being adsorbed by the process of chemisorption.

**Table 2.6** Ionic properties of iodide and iodate

Ion species	Iodide	Iodate
Chemical formula	$\text{I}^-$	$\text{IO}_3^-$
Chemical structure	$\text{I}^\ominus$	
Molar mass (g/mol)	126.904	174.903
Ionic radius ( $\text{\AA}$ ) <sup>a</sup>	2.20	2.08

According to the stability diagram in **Figure 2.1**, we can deduce  $\text{I}^-$  and  $\text{IO}_3^-$  as dominant species in the natural environment. This is because both species can exist in most of the pH conditions. While  $\text{I}^-$  is found in a lower electrical potential (Eh) environment (approximately 0 – 0.6),  $\text{IO}_3^-$  can be found in a higher Eh environment (approximately 0.4 – 1 in base and 1.2 – 1.6 in acid).  $\text{I}^-$  is still more concerned due to it being the main anthropogenic source of radioactive iodine (Lemma et al., 2015). Nevertheless, through a biological pathway,  $\text{I}^-$  could also turn into  $\text{IO}_3^-$  (Moreno et al., 2020). In a laboratory condition,  $\text{I}^-$  can be oxidized to  $\text{IO}_3^-$  through method such as photochemistry, electrochemistry or oxidation by hypochlorite (Takayanagi and Wong, 1986; Vitt and Johnson, 1994).



**Figure 2.1** Stability of different iodine species across different pH and electrical potential (Eh) conditions [adapted from a previous study (Medrano-Macías et al., 2016)]

## 2.3 Iodine removal technology

### 2.3.1 Membrane separation technology

Pressure-driven membrane has been involved in the industrial separation of liquid waste since 1960, when Loeb and Sourirajan could successfully obtain pure water from a salt solution using an asymmetric cellulose acetate (Arnal et al., 2000). Van Der Bruggen et al. 2003 defines the technology as the process of splitting an inlet stream by a membrane into concentrate and permeate. By creating pressure, usually by motor, the water is driven through the membrane. Permeate is the water that passes through the membrane while concentrate is the waste water, usually containing the contents that do not pass through the membrane. Some fraction of concentrate can be recycled for another separation and is referred as percent recovery.



The membrane separation can achieve up to 10:1 contaminant reduction coefficient and has substituted technology such as evaporation and ion-exchange in many applications (Arnal et al., 2000). It is also suitable for a small scale management found in the private sectors (Arnal et al., 2000). This is supported by the successful removal of radioactive waste, including iodine, by using membrane separation for the waste effluents in hospital and steel industries (Kamei et al., 2012; Sancho et al., 2006).

There are different kinds of membranes with different rate of driven pressure. They are capable of removing different kinds of particles, which are categorized according to their sizes. An overview of pressure-driven membranes, their characteristics, and total iodine removal is shown in **Table 2.7**. The pore size has an inverse relationship to pressure. Higher pressure and energy are required to drive the water when the membrane has smaller pore size. The microfilter (MF) has the pore size of about 100-10,000 nm. It is suitable for removing suspended solid, colloids and bacteria (Van Der Bruggen et al., 2003). MF is usually utilised for pre-filter of the membrane separation series as it can protect clog and damage on the other membranes (Van Der Bruggen et al., 2003). The ultrafiltration (UF) is capable of removing large-size dissolved molecules like those of natural organic matter (Van Der Bruggen et al., 2003). While sieving is the main mechanism of MF and UF membrane separation, NF employs charge effects mechanism, in addition to sieving. This is because the polymeric NF contains the functional group such as the carboxylic or sulfonic acid (Van Der Bruggen et al., 2003). The nanofiltration is capable of removing charged particles and small organic matters. On a reverse osmosis (RO) membrane, the pores are less than 0.5 nm. The water permeates through it very slowly, and the passing of water through the membrane is called solution diffusion (Van Der Bruggen et al., 2003). As a result, a high pressure (up to 120 bar) is needed for the RO separation process. Although high energy is required, RO yields the permeate that is ultrapure and possess less than 1% of the original iodine concentration. Sometimes, the quality of the permeate is similar to the product water of desalination system. The removal of iodine in the water by pressure-driven membranes has been successfully observed for stable and radioactive iodine (Chae and Kin, 2014).

The survey reporting the removal of iodine in the hospital wastewater was conducted, using RO and UF (**Table 2.8**). UF and RO can remove stable and radioactive

iodine. RO is capable of removing iodine in more iodine the water. The difference between stable and radioactive cannot be compared because one of the studies did not mention the initial concentration of the iodine in the waste stream (Arnal et al., 2000). The initial concentration of I-131 in the waste stream to 240 kBq/L and 360 kBq/L (Sancho et al., 2006). In the UF system, the removal efficiency was reduced when the concentration increase. The contaminant concentration governs the sieving mechanism. In RO membrane separation, removal efficiency is not affected by the initial iodine concentration. However, it is not conclusive if the concentration of iodine controls the efficiency of the membrane mechanism. More initial concentrations are needed for the experiment of all membrane types. Future studies also need to include the effect of temperature and pH in the testing of RO membranes.

**Table 2.7** Overview of the characteristics and iodine removal efficiency for different kinds of pressure-driven membranes

Membrane technology	Pore size (nm)/ driven pressure (bar) <sup>a</sup>	Separation mechanism <sup>a</sup>	Materials <sup>b</sup>	Feed water (m <sup>3</sup> /d) <sup>b</sup>	Total iodine removal efficiency <sup>b</sup>
microfiltration	100 - 10000/ 0.1 – 2	sieving	polyvinylidene fluoride (PVDF)	65.5 m <sup>3</sup> /d	13%
nanofiltration	0.5 – 2/ 3 – 20	sieving and charge effect	polyamide	86.4 m <sup>3</sup> /d	98%
reverse osmosis	< 0.5/ 5 – 120	diffusion	polyamide	86.4 m <sup>3</sup> /d	99%

<sup>a</sup>(Van Der Bruggen et al., 2003)

<sup>b</sup>(Chae and Kin, 2014)

**Table 2.8** Comparison of maximum removal efficiency for UF and RO system

Types of Membranes	Initial Iodine Concentration	Maximum iodine Removal Efficiency	Ref.

UF (1 pass)	N.A. (stable iodine) <sup>a</sup>	70%	(Arnal et al., 2000)
RO (1 pass)		97%	
UF (1 pass)	240 kBq/L (I-131)	80%	(Sancho et al., 2006)
	360 kBq/L (I-131)	75%	
RO (3 passes)	240 kBq/L (I-131)	95%	
	360 kBq/L (I-131)	98%	

N.A. – not available

<sup>a</sup>Initial iodine concentration is not reported

An ion-exchange membrane has been adopted for many applications including electro dialysis, diffusion dialysis, reverse osmosis, membrane electrolysis, and membrane fuel cells (Koter, 1999). The technology is being researched for the removal of radioactive iodine in radioactive waste products. The membrane is more selective for I<sup>-</sup> ( $1.50 \times 10^{-4}$  mol/m<sup>2</sup>/sec ion flux) over chloride ions (Cl<sup>-</sup>, about  $1.25 \times 10^{-4}$  mol/m<sup>2</sup>/sec ion flux) using the same initial concentration (Inoue, 2004). The membrane permeability for I<sup>-</sup> depends on transmembrane potentials, transport number and membrane conductance and ion flux (Inoue and Kagoshima, 2000). An earlier study also confirmed that the presence of glucose and urea in the solution can accelerate the migration of iodide through the membrane (Inoue and Kagoshima, 2000). The I<sup>-</sup> removal performance of anion-exchange paper membrane with ionic electrochemical is susceptible to large water flux (Inoue et al. 2004) and can be less efficient with the presence of other ions (Inoue 2004). The future study should contain the amount removal in term of percentage for the iodide presented in different kinds of mediums.

### 2.3.2 Coagulation-flocculation-sedimentation

Coagulation-flocculation-sedimentation is a standard process used for conventional water treatment. It is usually seen placed before the filtration in the water supply treatment system. It is the addition of the chemical to neutralize and stabilize the contaminant particles or colloidal suspension. During the flocculation process, given an amount of contact time, the additive forms solidified particles with the targeted

contaminant. The participated particles settle and are easily removed from the water, in the sedimentation phase.

The coagulation process (followed by sedimentation) with aluminium sulphate, activated silica and ferric sulphate as the additives, remove only a minimal amount of I-131 (Eden et al., 1952). Another study reported the same results of the water collected from water treatment plants (Kosaka et al., 2012). The water of river and pond contaminated with I-131 went through a conventional coagulation-flocculation-sedimentation system in the treatment plants, and the contaminant was not removed from the water (Kosaka et al., 2012).

However, with the addition of various concentration of silver to the same coagulation process mentioned above, the results yielded 55-95% removal of I-131 (Eden et al., 1952). Silver is one potential metal sorbent for iodine in the water environment because it can react with iodine (refer to sorption section for more details on silver). Contaminated sample water was acidified for the deposition of silver, and silver nitrate was used as the (Kosaka et al., 2012). The literature claimed that around 30% of I-131, which comprised mostly of  $I^-$ , was removed.  $IO_3^-$  and molecular form of I-131 was not effectively removed by the silver ions (Kosaka et al., 2012). With the additions of chlorine and powered activated carbon, more iodine removal was witnessed. The results show that for 10 and 25 mg/L PAC treatment, the addition of chlorination increases the removal of I-131 in the water (Kosaka et al., 2012). On the other hand, for the 50 mg/L powered activated carbon treatment, the addition of chlorination created no effects because of a high concentration of powered activated carbon in the last treatment (Kosaka et al., 2012). The experiment can be further tested for different concentrations of chlorine to see its effect on the treatment. Another study obtained a similar result which the addition of polyaluminium chloride (PAC) for pre-chlorination to improve the iodine removal efficiency (Kitada et al., 2015). In addition, an amount of chlorination that should be added is about 0.5 to 1 mg/g (Kitada et al., 2015). The removal percentage is increased but not significantly when more chlorine concentration is added.

Powered activated carbon, chlorine and silver ion can reduce I-131 in the water during coagulation-flocculation-sedimentation. The drawback of this system is that the treatment plant is generally large, and transportation of contaminated water is needed.

The technique is strictly ex-situ. Moreover, filtration using adsorbents is normally needed after the coagulation-flocculation-sedimentation. As a result, the research on an appropriate adsorbent is deemed highly as it can be applied to the post coagulation-flocculation-sedimentation system.

### **2.3.3 Electrolysis**

Water purification by electrolysis is described as the process of running an electric current, using electrode, through the water containing ionic contaminant. The technique creates the reaction in the water and separates undesirable ions from the water. Many times, when the technique is applied for water treatment, it is called electrocoagulation.

As iodine often exists in the natural environment in the form of ions, it is possible to employ electrolysis to remove it from the water. A literature showed the results of the iodine removal efficiency for a flow type electrolysis. With 100 and 4000 ppb ions concentration, the system was able to separate 91.7% and 84.6% of the contaminant (Hamasaki et al., 2014). A removal efficiency of 99.4% was obtained for the removal of high I-125 activity, 15000 Bq/kg (Hamasaki et al., 2014). The technology is proved to have an elevated performance in separating the iodine contaminant in the water, making it a suitable portable water technology.

On the other hand, the electrolysis is limited to only drinking water treatment. The pre-filter micro-carbon unit was necessarily installed prior to the electrolysis for the function of particulates elimination. Such system design infers that adsorption technology is an essential part for the electrolysis. Furthermore, passing electrical current through natural aqueous environment might not be a decent idea. Not only that electrical current can kill organisms, but the electrolysis has had a reputation of producing numbers of reactive oxygen species (ROS) which damage living cells (Ewing and Jones, 1987; Kong and Lin, 2010; Ward, 1988).

### **2.3.4 Ionic liquid**

An Ionic liquid is a liquefied form of the organic salt which can contain several types of ions. Some advantages of the ionic liquid including low vapour pressure, liquidus range as high as 200 °C, a low freezing point below 100 °C, high thermal

stability and moderate polarity (Johnson, 2007). Moreover, the liquid has the same conductivity as those of electrolyte and is suitable to be utilised for solvents, catalysts, organic reactions and electrodeposition (Johnson, 2007).

The ionic liquid comprising of 1-butyl-3-methyl-imidazolium ([Bmim]) cation was studied for its removal and storing ability of the iodine contaminant. The 5-hour sorption studies were conducted using 0.1g of ionic liquid in cyclohexane containing 5ml of iodine molecule ( $I_2$ ), with the concentration of 0.01 mol/L (Yan and Mu, 2014). Bmim-[NO<sub>3</sub>], [Ac], [Cl], [TfO], [I], and [Br] could remove 39, 84, 87, 90, 92 and 96%, respectively (Yan and Mu, 2014). Bmim-Br was further studied using 100 ml of the cyclohexane containing the same amount of  $I_2$  concentration. Within 7 hours, the ionic liquid can remove 82% of iodine with the capacity of iodine sorption of 2.1g/g. The literature also demonstrates the stability of ionic liquid can retain iodine with the study of iodine leachate from the ionic liquid, using the method of nitrogen sweeping. The results show that after 10 hours, about 11% of iodine is a loss from the Br-based ionic liquid. The structure of ionic liquid and  $I_2$  concentration in cyclohexane solution affects the  $I_2$  sorption efficiency (Chen et al., 2016). The ionic liquid compositions include alkyl chain, anion-base, C2 methylation, cation and functionalization.

Halogen bonding can explain the system of iodine removal using ionic liquid. The ionic liquid cation acts as an electron donor, while the anion forms complex with  $I_2$  (Yan and Mu, 2014). Such complex is formed because of the attractive nature of halogen atoms and electronegative species, and its occurrence can be confirmed by UV/vis spectrometry (Yan and Mu, 2014).

The advantage of the ionic liquid is its ability to removal high amount of  $I_2$ . It is more stable than conventional solvent and does not vaporize easily. It also stores  $I_2$  with low leachate, making it one potential substance to be used for iodine contaminant removal. However, in the natural environment, iodine exists mostly in ionic forms. The liquid might be able to remove some radioactive iodine that is  $I_2$ , but most of the ionic contaminant would remain in the water body. Further research and study on the ionic liquid are necessary to optimize its capability to remove radioactive iodine in the natural environment.

### 2.3.5 Bioaccumulation by algae

Iodine intake and sorption process in algae is not a new topic in science and engineering fields. The accumulation of iodine by algae was studied regarding bioaccumulation or in particular, iodine exchange process. Bioaccumulation, in general, refers to the process when a living organism accumulates or concentrate a particular chemical species into its living cell via chemical uptake. The concentration of the chemical in the body of living organism exceeds one in the aquatic environment. Iodine exchange process is a part of metabolism in the algae (Baily and Kelly, 1955). The dynamic process is involved in the uptake where there is an exchange between iodine in algae and surrounding medium. While it only occurs in living cells, iodine diffusion can happen in both living and non-living cells of brown algae even though the latter had shown only an insignificant amount of iodine diffused (Baily and Kelly, 1951).

The protein of *Sargassum kjellmanianum* contains the most iodine with 65.5% while algin and pigment only contain 0.185% and 1.57% iodine respectively (Hou et al., 1999). The mature form and juvenile plantlets of the species, *Laminaria digitata* can contain iodine up to 0.30% and 4.50% of its dry weight respectively (Ar Gall et al., 2004). The contents signify a 30,000 – 150,000-fold accumulation of this element from that of the amount in the seawater (Leblanc et al., 2006).

Algae can be adopted for a phytoremediation for radioactive iodine. It is considered to be part of the green technology that minimizes the used of synthesized chemical, can be obtained with low cost, readily available and yields high biomass when grown (Tien, 2002). In a previous study, 25 species of seaweed collected at the coasts near power facility and large cities in Japan showed a different amount of I-131 contents (Morita et al., 2010). I-131 was also found distributed and accumulated in the brown seaweed *Fucus*, collected from several places in the northern hemisphere, after the incident of Chernobyl (Druehl et al., 1988).

The samples of macro-algae were determine for their I<sup>-</sup> contents were determined using Ion Chromatography-Mass Spectrometry (IC-MS) (Martinelango et al., 2006). Compared to other species of algae, *Laminaria sp.* used in the study accumulate iodine the most. The information is confirmed in Leblanc 2006 which mentions that among all the sea aquatic living organism brown algae can accumulate

the highest amount of iodine. The high value of BCFI in all species confirms that algae, in general, is selective for iodine in its bioaccumulation.

A strain of green microalgae, *Parachlorella sp binos* (Binos) was isolated for the iodine bioaccumulation experiment under the laboratory condition (Shimura et al., 2012). Under the sunlight, Binos was able to accumulate iodine (Shimura et al., 2012). Iodine uptake by Binos is correlated to its number cells where the maximum iodine capacity that it can accumulate is 100 mg/ml of cells in 1 ml water (Shimura et al., 2012). About 38.71% of iodine was removed after 24 hours (Shimura et al., 2012). The results infer that Binos accumulate iodine as a part of photosynthesis (Shimura et al., 2012). Besides iodine, Binos is found to accumulate Sr and Cs as well (Shimura et al., 2012).

The bioaccumulation of iodine by algae is another possible technique for radioactive iodine removal that should be continuously researched. Algae are capable of removing a high amount of iodine, and it is a natural product that has minimal adverse effects on the environment. However, unlike the usage of materials like activated carbon or chitosan, having living algae to remove the contaminant means that it needs to be kept alive for its bioaccumulation to function. For instance, sunlight must be presented for Binos to start accumulating iodine. Proper seawater environment is needed to keep *Laminaria saccharina* or *Laminaria saccharina* living.

## **2.4 Adsorbents for removal of iodine in the water**

### **2.4.1 Activated carbon**

Iodine adsorption by activated carbon has been reported for several decades. The activated carbon is derived from the carbonaceous materials such as coconut, nutshell, wood, and lignin. Sometimes, it is made of coal and can be described as activated coal (for this report, the activated coal maybe refers as an activated carbon). The gaseous iodine adsorption capacity is typically used to characterize the commercial activated carbon in the form of “iodine number”, which refers to how much amount of iodine (mg<sup>2</sup>) is being adsorbed by a gram of activated carbon. The activated carbon is, therefore, regarded as a potential adsorbent for the radioactive iodine in the water. Activated carbon has been utilized and studied extensively for both air and water pollution adsorption because of its large surface area. Many studies have shown a



successful iodine adsorption of radioactive venting from the nuclear power plant exhaust pipe and that of polluting the air environment (Adams and Browning Jr, 1960; Jubin, 1979; Zhou et al., 2014). However, in this report, the only removal of iodine in the water is considered and summarized in detail.

The activated carbon adsorbs sorbates by London dispersion force. It consists of micro-, meso- and macropores structures, where the major adsorption of iodine occurs mostly at the micropores (Yang et al., 1993). As a result, it is critical how these pores are arranged depending on the form of the activated carbon (Barkauskas and Dervinyte, 2004). The comparison of activated carbon in different form is exhibited in **Table 2.9**. One study compared the ability of granular and fiber activated carbon to remove  $I_2$  (prepared by HI), in the acetic acid (Yang et al., 1993). Under acidic environment, the activated carbon fiber can absorb 305 mg/g  $I_2$  higher than the adsorption capacity of 195 mg/g  $I_2$  in the granular form of activated carbon (Yang et al., 1993). The outcome coincides with the BET surface area for activated carbon fiber which is two times higher than that of the granular form. In fiber form, micropores are exposed to the surface of the sorbate, creating a fast iodine binding and diffusion rate (Yang et al., 1993). On the other hand, in granular form of activated carbon, there is a sequence binding and diffusion of iodine from the mesopores at the surface to micropores within the bulk of the sorbate (Yang et al., 1993).

Besides the physical form of activated carbon, its activation processes involved are important aspects in the adsorption mechanism. In the production phase, biomaterials would go through pyrolysis or oxidation for its physical activation to produce an activated carbon. In the pyrolysis process of activated coal where the temperature is increased to about 400 °C, iodine adsorption sites in coal are enhanced with increasing oxygen cross-link, and this results in higher adsorption capacity (Rodriguez and Marsh, 1987). On the other hand, oxidation process decreases the size of micropores and reduce the adsorption capacity in the activated carbon (Rodriguez and Marsh, 1987).

In a laboratory experiment, the activated carbon can perhaps remove up to 87.50% of 2 mg/L iodide in the solution (Hoskins and Karafil, 2002). However, studies have shown that the removal of iodine in other types of water medium may yield lower iodine removal. Compared to the results of the batch experiment using distilled water,

the one with 50  $\mu\text{g/L}$   $\text{I}^-$  and  $\text{IO}_3^-$  in tap water showed 60 % and almost 0 % removal, respectively (Sato et al., 2011). On the other hand, the result of adsorption in ground water is the lowest with about 20% maximum adsorption at 9.77  $\mu\text{g/L}$  initial total iodine (Parker et al., 2014). The presence of other chemical species in ground water environment may cause a competition on available sorption site, resulting in less removal percentage (Parker et al., 2014).



**Table 2.9** Comparison of iodine adsorption with different types of activated carbon

Type of Activated Carbon	Maximum Iodine Adsorption (mg/g) <sup>a</sup>	Removal (%)	Equilibrium Time	Experimental Condition					Reference
				Iodine Species	Initial Iodine Concentration (mg/L)	Adsorbent Dosage (g/L)	Medium	pH	
carbon fiber	305	-	2 h	I <sub>2</sub>	800	-	acetic acid	-	(Yang et al., 1993)
granular	195	-	24 h	I <sub>2</sub>	800	-	acetic acid	-	(Yang et al., 1993)
granular	0.635	87.5	-	I <sup>-</sup>	1.02	1	DI water	8	(Hoskins and Karafil, 2002)
granular	1.68 x 10 <sup>-3</sup>	18.5	-	I <sup>-</sup> , IO <sub>3</sub> <sup>-</sup> , I <sub>2</sub>	9.19 x 10 <sup>-3</sup>	1	groundwater	8.2	(Parker et al., 2014)
granular	-	60.0	-	I <sup>-</sup>	40.0 x 10 <sup>-3</sup> – 50.0 x 10 <sup>-3</sup>	-	tap water	7	(Sato et al., 2011)
1.05wt% silver-impregnated carbon	~ 127	-	-	I <sup>-</sup>	~ 1.0 – 200	1	DI water	5	(Hoskins and Karafil, 2002)
silver-activated carbon aerogel	0.638	-	7 d	I <sup>-</sup>	0.150	~ 0.2 (2000 g/L/min)	DI water	7	(Sánchez-Polo et al., 2006)
copper-modified activated carbon	1.91	95.7	2 h	I <sup>-</sup>	2	1	DI water	1	(Zhang et al., 2017)

<sup>a</sup>The value is obtained from the experimental data and not from the mathematical model

The activated carbon possesses several O<sub>2</sub>-containing functional groups such as carbonyl, phenol, lactone and carboxyl group (Barkauskas and Dervinyte, 2004; Nwosu et al., 2009). It is still not certain which group, in particular, is responsible for the sorption of iodine. However, there was an attempt to find the relation between the number of these functional groups in the nutshell, quantified by the method of NaOH-tritable surface and iodine sorption capacity (Nwosu et al., 2009). The sorption of iodine was found to be dependent moderately on the quantity of functional groups with a linear statistical correlation of 0.6115 (Nwosu et al., 2009). Isolating each functional group for the model would provide an answer to which O<sub>2</sub>-containing functional group is responsible for this sorption process.

Many times, the porous carbon can be modified to contain the inorganic material such as silver and aluminium for different sorption specification. Silver-impregnated carbon is often used for iodine sorption, and it is proved to be able to adsorb more iodine. The sorption capacity value of 1.05 % silver impregnated activated carbon is nearly two times higher than that of virgin activated carbon (Hoskins and Karafil, 2002). However, with only 0.05 % of silver impregnation, there is no significant change in the value compared to that of virgin activated carbon (Hoskins and Karafil, 2002). The silver-activated carbon aerogel was also brought to study in the dynamic adsorption test, where the results exhibit about 0.251-0.638 mg/g sorption capacity, depending on pH and porous characteristics of the aerogel (Sánchez-Polo et al., 2006). The nano composite of Cu<sub>2</sub>O/Cu-activated carbon was synthesized with the ability to remove 95.7 % of 2 mg/L I<sup>-</sup> and has about 1.91 mg/g adsorption capacity.

The sorption of iodine to activated carbon is affected by pH. At higher pH, activated carbon adsorb iodine effectively as elevated amount of OH<sup>-</sup> compete for the positive adsorption sites (Hoskins and Karafil, 2002). The pH effect was demonstrated in the batch experiments of unmodified and copper-impregnated activated carbon. The results show that all kinds of the activated carbon experience a lower I<sup>-</sup> adsorption capacity as pH is increasing from 3 to 11, although the copper-impregnated activated carbon was shown to At higher pH, activated carbon adsorbs iodine less effectively as elevated amount of OH<sup>-</sup> competes for the positive adsorption sites (Hoskins and Karafil, 2002). be more stable across the pH range (Sánchez-Polo et al., 2006).

The activated carbon may not be the best selection for the aqueous iodine adsorption. It is maybe one of the most common domestic and industrial water filtration media, but its efficiency decreases drastically when it is used in the natural environment. However, the modification can help to improve its performance. The carbon fibre and silver-impregnated activated carbon are among the best adsorbent of this category. The silver-activated carbon aerogel was also shown to have the same capacity as the unmodified activated carbon with about 10 times reduced in its dosage. In addition, the activation of biomaterials has brought about the potential in finding alternative and innovative way of making activated carbon. Several waste products such as coffee residue (Boonamnuyvitaya et al., 2005, 2004), soy bean oil cake (Tay et al., 2009) and even cigarette butts (Sun et al., 2017) became possible raw materials for the activated carbon, and these ideas could be applied for iodine removal in the future.

#### 2.4.2 Soil and clay

Iodine is often found as a content of natural soil and clay. Many times the soil itself is contaminated by radioactive iodine (Miyake et al., 2012). However, based on the contamination occurrences, it can be a potential natural-derived and low-cost sorbent for the pollution removal in water.

Organic and inorganic matters in soil are both responsible for the sorption of iodine. The iodine content in soil was found to be highly correlated to the amount of oxylate-soluble Al in the near-neutral pH condition, and to the amount of oxylate-soluble Fe in the more acidic environment (Whitehead, 1978). Generally,  $I^-$  and  $IO_3^-$  are ionically attracted to the positive charge provided by the free hydroxides of Fe and Al (Whitehead, 1984). **Table 2.10** shows iodine adsorption capacity and  $K_D$  value of different types of soil and clay. In a batch experiment, the maximum  $I^-$  adsorption of  $6.59 \times 10^{-3}$  mg/g occurred in the soil with 4.81 % Fe oxide and 5.66% Al oxide, while the maximum  $IO_3^-$  adsorbed in the soil with 0.64 % Fe oxide and 0.60 % Al oxide was  $3.41 \times 10^{-3}$  mg/g (Dai et al., 2009). The experiment was set up with 100 g/L soil dosage at 25 °C for 40 h (Dai et al., 2009).

Nevertheless, in the natural organic constituents of soil, where positive charge is still scarce, the iodine can still covalently bond and form complexes with functional groups presented in the soil such as phenol, thiol and amine (D I Kaplan et al., 2014;

Sakuma and Marzukee, 1995; Whitehead, 1974). The soil samples with higher content of organic matter, organic carbon, calcium carbonate, nitrogen, phosphorus, potassium and sulphur were found to adsorb iodine (Fukui et al., 1996; Nath et al., 2010). A batch experiment revealed the ability of the collected sandy loam soils to adsorb  $1.3 \times 10^{-4}$  to  $1.60 \times 10^{-4}$  mg/g of  $I^-$  adsorption at its capacity (Nath et al., 2010).

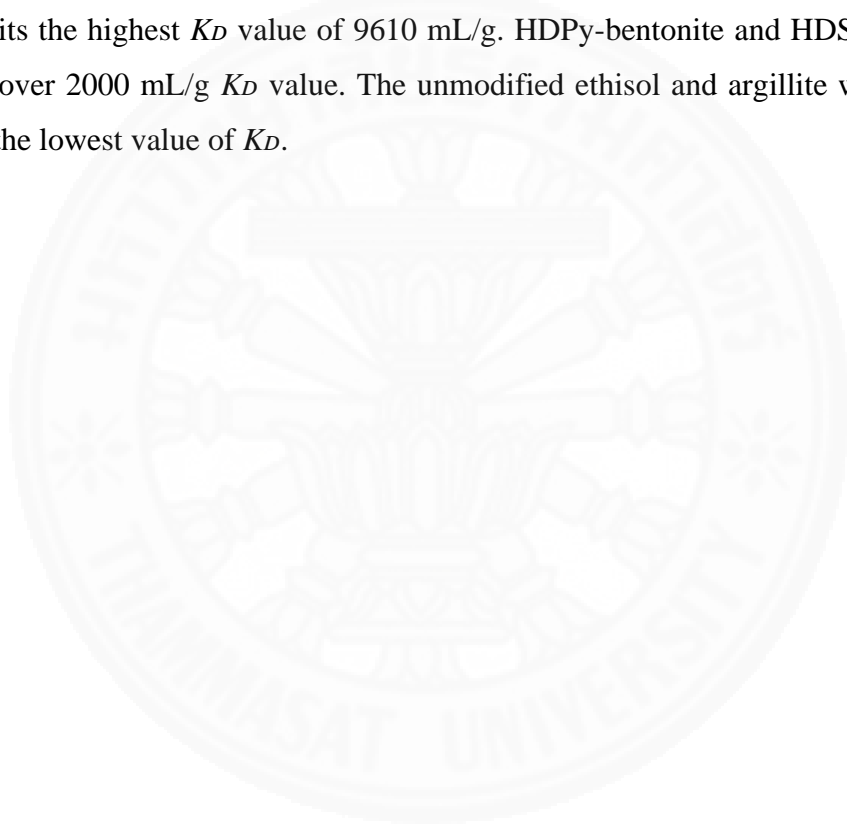
Nearly all the sorbate can be desorbed and recovered from the soil (Nath et al., 2010). However, this means that iodine sorption in the soil can be unstable under the condition where pH and temperature fluctuate. The adsorption of iodine may increase and reach its maximum at about 70 °C (Fukui et al., 1996; Hosseini et al., 2013). However, after that point, the adsorption was observed to decrease with the temperature. Higher pH condition decreases the sorption of iodine species in soil due to the  $OH^-$  presence, which compete for the adsorption sites (Fukui et al., 1996). The sorption of iodine is affected by the presence of other anions only when the pH value is below neutral (Fukui et al., 1996).

The increasing uptake of  $I^-$  and  $IO_3^-$  is dependent and independent on the time of contact, respectively (Fukui et al., 1996). Smaller soil grain size promotes a better iodine adsorption due to the increase in surface area (Fukui et al., 1996). However, unlike the activated carbon,  $IO_3^-$  is selected for soil instead of iodide. The adsorption of iodate is found to be higher than that of iodide in different temperature and pH condition (Dai et al., 2009; Fukui et al., 1996).

Besides natural soil, clay is another potential adsorbent that has been studied for the removal of iodine. Naturally, clay mineral is limited in its iodine adsorption ability but due to its high retention of cationic species. The non-modified clay, argillite and kaolinite have adsorption coefficient ( $K_D$ ) of 0.21 mL/g and 47.09 mL/g, respectively. However, by modifying the materials, iodine removal efficiency can improve significantly (Kaufhold et al., 2007). By placing inorganic interlayer cations into natural clay, organoclay is produced with the available sites for the iodine (Riebe et al., 2005). For instance, smectite, vermiculite and bentonite treated with hexa-decylpyridinium chloride ( $C_{21}H_{38}N^+ Cl^-$ ) has a  $K_D$  value of 297, 372 and 2800 mL/g, respectively (Riebe et al., 2005, 2001). More efficiency of 3600 mL/g was observed with the  $K_D$  value of 3600 mL/g after treating bentonite with hexadecyltrimethylammonium bromide ( $C_{19}H_{42}N^+ Br^-$ ). The commercial clay, ClayFloc™ 750, has the highest  $K_D$  value of

9610 mL/g (Li et al., 2014). The adsorbent was designed to contained cage-like structure aluminosilicate minerals, sulfur, iron, nitrogen-containing substitutions as well as quaternary amine functional group (Kaplan et al., 2015).

Although, most of the study regarding the iodine adsorption of soil and clay presented the efficiency in the form of coefficient,  $K_D$ , overall, the collected soil was found to have very low maximum iodine adsorption capacity. Nevertheless, like the activated carbon, modification clay was found to have higher efficiency than that of the unmodified adsorbent. In this category, the commercial product, ClayFloc™ 750, exhibits the highest  $K_D$  value of 9610 mL/g. HDPy-bentonite and HDSMB-bentonite have over 2000 mL/g  $K_D$  value. The unmodified ethisol and argillite were presented with the lowest value of  $K_D$ .



**Table 2.10** Comparison of iodine adsorption in the collected soil, natural clay and modified clay

Types of Soil or Clay	Method of Modification	Maximum Iodine Adsorption (mg/g) <sup>a</sup>	Equilibrium Time	$K_D$ (mL/g)	Experimental Condition				Ref.
					Iodine Species	Adsorbent Dose (g/L)	Temp. (°C)	pH	
orthic aridisols	not modified, collected from Xingjiang, China	$3.41 \times 10^{-2}$	-	57.60	$\text{IO}_3^-$	100	25	-	(Dai et al., 2009)
hydragric anthrosols	not modified, collected from Guangdong, China	$6.59 \times 10^{-2}$	-	1.97	$\text{I}^-$	100	25	-	(Dai et al., 2009)
sandy loam	not modified, collected from Zadenhan Iran	-	-	~ 200	$\text{I}^-$	55.56	9	-	(Hosseini et al., 2013)
entisol	not modified, collected from Varanasi, India	$1.60 \times 10^{-4}$	5 h	$2.50 \times 10^{-3}$	$\text{I}^-$	100	room	-	(Nath et al., 2010)
argillite	not modified	-	48 h	0.21	$\text{I}^-$	200	25	-	(Tournassat et al., 2007)
kaolinite	not modified	-	1 h	47.09	$\text{I}^-$	20	room	3.5	(Sakuma and Marzukee, 1995)



HDPy-smectite	treated with $C_{21}H_{38}N^+ Cl^-$	-	-	297	$I^-$	55.56	20	-	(Riebe et al., 2005)
HDPy-vermiculite	treated with $C_{21}H_{38}N^+ Cl^-$	-	-	372	$I^-$	55.56	20	-	(Riebe et al., 2005)
HDPy-bentonite	treated with $C_{21}H_{38}N^+ Cl^-$	-	-	2800	$I^-$	200	-	-	(Riebe et al., 2001)
HDSMB-bentonite	treated with $C_{19}H_{42}N^+ Br^-$	-	10 min	3600	$I^-$	20	25	7	(Choung et al., 2014)
ClayFloc™ 750	commercial bentonite containing quaternary amine	-	7 d	9610	$I^-$	10	22	5.5	(Kaplan et al., 2015; Li et al., 2014)

<sup>a</sup> Value obtained from the experimental data and not from the mathematical model

### 2.4.3 Mineral

Since it could be found in soil and clay, the inorganic matter or minerals adsorb iodine ions in various ways.  $\text{IO}_3^-$  and  $\text{I}^-$  are adsorbed to the mineral with the mechanism of specific adsorption (replacement of hydroxyl group) and electrostatic force, respectively (Evans and Hammad, 1995). Minerals containing metal ions adsorb iodine and form insoluble metal iodides, while anionic exchange process is also possible for those that contain other anions beside the ions of iodine (Sazarashi et al., 1994). Several researchers have studied the iodine sorption ability of different kinds of inorganic matters. **Table 2.11** shows the summary of iodide sorption capacity on minerals and rocks from various studies.

Zeolite is a group of hydrated aluminosilicate mineral. Examples of natural zeolite include clinoptilolite, mordenite and chabazite. Commercial zeolite is capable of removing a high amount of positive radioactive ions of strontium, barium and caesium (Lonin et al., 2015; Sato et al., 2011). However, it can absorb a minimal amount of iodine. With the initial iodine concentration of 40-50  $\mu\text{g/L}$ , the commercial zeolite can remove up to about 20 % of  $\text{I}^-$  and less than 10 % of  $\text{IO}_3^-$  (Sato et al., 2011). In a dynamic adsorption test, with a 4-day contact time, 0.1 g natural zeolite show the maximum  $K_D$  value for  $1.65 \times 10^5$ , which seems to be a huge number of the coefficient (Lonin et al., 2015). However, in the same research, the  $K_D$  value of zeolite for Nd(III) and Sm(III) are more than three times that of iodine at  $7.48 \times 10^5$  and  $5.47 \times 10^6$ , respectively (Lonin et al., 2015).

A modified form of zeolite might be more promising for the removal of iodine in water. Silver ion-exchange zeolite has been observed to remove iodine at the capacity of approximately 1.50 mol/g or 190 g/g in air stream (Choi et al., 2001). Modifying zeolite to include hydroxyapatite and hydroxyfluorapatite increases the stability of iodine captured by the sorbent from the air stream (Watanabe et al., 2009). Although methodologies in the mentioned literature are for the removal of radioactive in the gas phase, the same techniques and sorbent can be adapted for the removal contaminant from the aqueous phase, in the future

**Table 2.11** Comparison of iodine adsorption on various kinds of minerals

Mineral	Maximum Capacity (mg/g) <sup>a</sup>	Removal (%)	$K_D$ (mL/g)	Equilibrium time	Experimental Condition				Ref.
					Iodine Species	Initial Iodine Concentration (mg/L)	Adsorbent Dose (g/L)	pH	
zeolite	-	~ 20.0	-	30 min	I <sup>-</sup>	$4.0 \times 10^{-3} - 50.0 \times 10^{-3}$	-	7	(Sato et al., 2011)
chalcocite	0.713	56.0	1285	30 min	I <sup>-</sup>	1	1	5.81	(Anderson et al., 1995)
cuprite	N/A	75.0	1.50	-	I <sup>-</sup>	12.6	50	7.7	(Lefèvre et al., 2000)
argillite	N/A	N/A	1.70	14 d	I <sup>-</sup>	$3.78 \times 10^{-7} - 1260$	4	12.6	(Devivier et al., 2004)
cuprous sulphide	60.9	86.0	370	10 d	I <sup>-</sup>	-	20	8.5 – 9	(Lefèvre et al., 2003)
allophane	-	13.3	3.07	-	I <sup>-</sup>	$1.26 \times 10^{-4}$	50	6.3	(Sazarashi et al., 1994)
attapulgite	-	4.57	0.958	-	I <sup>-</sup>	$1.26 \times 10^{-4}$	50	6.3	(Sazarashi et al., 1994)

chalcopyrite	-	43.3	15.1	-	I <sup>-</sup>	$1.26 \times 10^{-4}$	50	6.3	(Sazarashi et al., 1994)
cinnabar	-	99.9	$2 \times 10^4$	-	I <sup>-</sup>	$1.26 \times 10^{-4}$	50	6.3	(Sazarashi et al., 1994)
hydrotalcites	193	95.1	-	1 d	I <sup>-</sup>	$1.68 \times 10^4$	10	-	(Paredes et al., 2006)
silver-hydrotalcites	496	> 90.0	-	-	I <sup>-</sup>	500	2	-	(Bo et al., 2016)
bismuth oxide	~ 70.0	-	$1.85 \times 10^4$	10 h	I <sup>-</sup>	20.0	0.2	7	(S. Liu et al., 2016)
bismuth oxide	~ 80.0	-	$1.34 \times 10^4$	10 h	IO <sub>3</sub> <sup>-</sup>	20.0	0.2	7	(S. Liu et al., 2016)
silica coated with magnetite and imidazole	130	98.0	-	40 min	I <sup>-</sup>	254	0.45	7	(Madrakian et al., 2012)

<sup>a</sup> Value obtained from the experimental data and not from the mathematical model

Cinnabar exhibits high  $K_D$  value as well as removal percentage (Sazarashi et al., 1994). The hydrotalcite yielded 192.5 mg/g iodine adsorption capacity (Paredes et al., 2006). When the adsorbent was doped with silver, to produce a silver-hydrotalcite, the iodine uptake capacity increased to 496 mg/g (Bo et al., 2016). On the other hand, at optimum conditions, allophane, attapulgite and chalcopyrite exhibit low  $K_D$  value and removal percentage (Sazarashi et al., 1994). For bismuth oxide, with 20 mg/L initial concentration, the adsorbent took 10 h to remove 70 and 80% of  $I^-$  and  $IO_3^-$ , respectively (S. Liu et al., 2016). The adsorbent may remove more  $IO_3^-$  than  $I^-$ , but the  $K_D$  values suggest that the bismuth oxide favor  $I^-$  removal (S. Liu et al., 2016).

The bismuth oxide is very stable in water at pH 7 as only 2.30% of iodine leaching was reported after a 12-hour leaching experiment (S. Liu et al., 2016). However, as pH increases, the sorption capacity decreases (S. Liu et al., 2016). With the anion competition experiment, the bismuth oxide has shown a strong  $I^-$  selectivity, but  $CO_3^{2-}$  or  $Cl^-$  could post a strong competition for the sorption sites (S. Liu et al., 2016). Lastly, the researchers studied the removal of iodine in the synthetic seawater, using Fukushima nuclear power plant as a reference. The bismuth oxide could remove 60.0 – 100% of the iodine in the seawater, depending on the initial concentration of iodine added (S. Liu et al., 2016).

The metallic mineral can be modified for iodine adsorption. The silica was coated with magnetite and imidazole. The sorbent was brought for the iodine removal, and the result was satisfactory with 98% iodine removal with about 130 mg/g maximum final sorption capacity (Madrakian et al., 2012). Up to 90.0% of iodine can also be recovered from the sorbent (Madrakian et al., 2012). ZIF 8 or (Zn(2-methylimidazolate)<sub>2</sub>), a type of metal organic framework (MOF) which contained zinc was studied for its ability to remove iodine in the vapour (Hughes et al., 2013). A gram of ZIF 8 can adsorb up to 0.660 g of iodine (Hughes et al., 2013). The research on this sorbent should be continued in the future with the sorption experiment in the water.

A natural material called gossypol can be modified to have zeolite morphology. The type is called gossypol P3 polymorph. The sorbent is described as a phenolic aldehyde pigment, extracted from cotton plants and seeds. It was investigated for its ability to remove iodine in the aqueous solution. The results confirm for iodine inclusion which iodine molecules enter the extended cavities of the channels within the

zeolite-like structure of the gossypol P3 polymorph (Talipov et al., 2007). The sorbent should be subjected to a batch experiment in the future.

Several kinds of mineral have shown promising results. The silver-hydroxalite has almost 500 mg/g iodide removal capacity and has been able to remove  $I^-$  in the seawater, so it becomes one of the best adsorbents in this category. The results of bismuth oxide also exhibited high  $K_D$  for both  $I^-$  and  $IO_3^-$ , and it is one of a few adsorbents that has been reported for the successful removal of  $IO_3^-$ . Consequently, the mineral is considered as one of the most essential adsorbents that contributes to the radioactive iodine removal and should be studied further for better results.

#### 2.4.4 Anion-exchange resin

Along with the activated carbon, the ion-exchange resin is another sorbent often used in conventional water softening and treatment. It is also a useful material for several other practices including medical procedure, food production and agriculture. Ion-exchange resins usually contain a cross-linked polymer matrix with ion-active sites throughout the structure. It has an ability to adsorb ions with a negligible effect on the chemical formation or change in the targeted ion forms (Wheaton and Lefevre, 2000). Ions can be recovered from the sorbent in the process called regeneration, which returns the resin to its initial state.

Cation-exchange is used to adsorb the cation presence in the water while anion-exchange targets for the anion. A commercial polystyrene-based anion-exchange resin, containing quaternary amines, was widely used for anion-contaminant removal from water. Therefore, the resin is one of the candidate adsorbents to be employed to remove the anionic-form radioactive iodine. The commercial anion-exchange resin is manufactured in various sizes of spheres or granules (Wheaton and Lefevre, 2000). Its existence started long back in the past, and there are different ways of synthesizing the resin (Bauman and Mckeller, 1952; Sussman and Mooretown, 1948).

Anion-exchange resin was used to extract I-129 in the study of iodine contamination of soil, seaweed and milk. The result shows that up to 2120 mg of iodine per a kilogram of seaweed can be extracted using the resin (Suzuki et al., 2007). Under a groundwater condition, a study shows that the conventional polystyrene-based cationic resin adsorption capacity peaked at 5.90  $\mu\text{g/g}$  (Parker et al., 2014).  $I^-$  is

observed to be a more desirable species for the adsorbent (Parker et al., 2014). In the Hanford site,  $\text{IO}_3^-$  is reported as a dominant iodine species (S. Zhang et al., 2013) so it is suggested that anion-exchange resin might not be suitable for the treatment of iodine on this site. The removal of  $\text{I}^-$  by a tannic-type resin was performed using seawater as a medium (Tachibana et al., 2015). The results in the literature exhibit a more favorable  $\text{I}^-$  removal at low pH with a maximum  $K_D$  value of about  $3.5 \times 10^{-3}$  L/mg (Tachibana et al., 2015). Consequently, the results cannot be used to show in this report visually. In a laboratory study, the  $\text{I}^-$  removal capacity of a silica-based ion-exchange resin was about 149 mg/g

Overall, the anion-exchange resin would continue to be a prominent commercial sorbent for industry and household water treatment. However, these polystyrene-based resins, bearing cationic quaternary amines, relied on fossil fuel-based chemicals for their production. Still, anion-exchange resin exists in many physical forms and chemical structure. There are gaps for its performance and sustainability improvement. Further study should be developed for its water treatment application.

#### 2.4.5 Cementitious materials

“Immobilization” and “encapsulation” are the terms that have been used very often for the study of cement properties related to waste management. These are phenomenon occurs due to adsorption, absorption, or the combination of both processes. In this report, adsorption, as a general term maybe refers to the cement properties to immobilize and encapsulate the waste products.

Cement material has been studied for its property to adsorb radioactive materials like strontium, uranium, cesium and iodine (Atkinson and Nickerson, 1988; Harfouche et al., 2006; Tits et al., 2011, 2006). Using solidified cement to immobilized radioactive waste containing I-129 is being utilized in the pressurized water reactor.

Several studies have found that different components in cement are responsible for iodine sorption. The hydrate group consists of calcium silicate hydrate and calcium aluminate sulphate hydrates (Bonhoure et al., 2002). The hydroxide content like calcium hydroxide, hydrotalcite and gibbsite (Toyohara et al., 2012). The cement component ratio can affect the adsorption process, so it is crucial to obtain the optimum cement mixture for iodine adsorption purposes. For instance, the ratio of  $\text{SO}_4/\text{Ca}$  and

SO<sup>4</sup>/Al in alumina cement were studied in a literature (Toyohara et al., 2012). The maximum  $K_D$  value (at 25 °C) of  $2 \times 10^{-1}$  m<sup>3</sup>/kg is obtained for 0.16 SO<sup>4</sup>/Ca mole ratio (Toyohara et al. 2000). Raising the temperature to 35°C the  $K_D$  value of the same SO<sup>4</sup>/Ca mole ratio increases to about 1 m<sup>3</sup>/kg (Toyohara et al. 2000). The maximum  $K_D$  value of  $1 \times 10^{-1}$  m<sup>3</sup>/kg for SO<sup>4</sup>/Al is found to be at the mole ratio of 1.4 to 1.9 (Toyohara et al. 2000). The method of X-ray diffraction is used to quantify iodine and the optimum mole ratio of SO<sup>4</sup>/Ca, monosulfate is formed in the cement (Toyohara et al. 2000).

Background condition was also studied for the cement sorption capacity. At higher pH, cement loses iodide concentration due to the presence of OH<sup>-</sup> (Toyohara et al. 2012). The literature set up the study of initial iodine concentration using the following concentration prepared from NaI:  $1.0 \times 10^{-8}$ ,  $1.0 \times 10^{-5}$ ,  $1.0 \times 10^{-4}$ ,  $1.0 \times 10^{-3}$ ,  $5.0 \times 10^{-3}$ ,  $1.0 \times 10^{-2}$ ,  $5.0 \times 10^{-2}$  and  $1.0 \times 10^{-1}$  mol/dm<sup>3</sup>. The results show that within this range of initial concentration, cement sorption capacity increases with the concentration (Toyohara et al. 2012).

X-ray absorption spectroscopy (XAS) was employed to determine the iodine ions stability in cement after the 28-day mobilization process (Bonhoure et al., 2002). The results show that iodine ions do not undergo significant modification during the sorption, and the sorbent is not affected by the redox state of iodine species (Bonhoure et al., 2002). Besides being stable in the sorbent, iodine can also be recovered from the solidified cement. Up to 70.0% of iodine can be recovered from 10.4 g of solidified cement sample, taken from the pressurized water reactor (Park et al., 2009).

From the properties mentioned about cement, it might be one of the most suitable adsorbents for the radioactive iodine. However, there is a concern about the production of cement because it can produce harmful substances like chlorine, SO<sub>x</sub>, NO<sub>x</sub>, mercury, lead, chromium and arsenic (Chen et al., 2010). Conclusively, cement is the material that has been used for the adsorption of radioactive iodine. Component mixtures and background condition are being researched to optimize the usage of cement in this application. The stable adsorbent also allows most of the iodine to be recovered. However, there is an environmental concern in its toxic wastes during the production phase.



#### 2.4.6 Polysaccharide

Starch and iodine have been known to react to form unique complex formation. Over a century, this reaction has often been employed in the field of analytical chemistry and food science (Szente et al., 1999). It was claimed that iodine can form a complex with both amylose and amylopectin in the presence of water (Saibene and Seetharaman, 2006). As a result, iodine can be used to determine amylose and amylopectin content in various kinds of starches such as those in corns and potatoes (Rendleman, 2003). Knowing that such complex formation exists, there were some attempts to use natural and synthetic polysaccharide in iodine sorption.

A natural polysaccharide called chitin was discovered in 1884. It is considered to be the most abundant natural polysaccharide, second to cellulose, found in the exoskeleton of arthropods such as insects, crabs, and shrimps. Chitin and its ability to bind iodine have been researched for the application of drug delivery (Takahashi, 1987). Chitin can be reacted with iodine and the results shows that 1 g and 3 g of chitin can bind up to 0.149 g and 0.350 g of iodine, respectively (Takahashi, 1987). A report presented the synthesis of chitin aerogel with silver impregnation (Gao et al., 2017). The porous adsorbent is capable of adsorbing I<sub>2</sub> from the vapor (Gao et al., 2017).

Chitosan is another kind of polysaccharide, which was made from chitin by the process of alkaline deacetylation. It is considered to be one of a few natural cationic polymers. It is soluble in aqueous solution and can be modified into many forms such as gel, films and fibre. In a batch experiment using 0.1 g chitosan beads in 50 ml ethanol solution of various iodine concentration, the highest adsorption capacity was determined to be about 0.2 g iodine per gram of chitosan (Chen and Wang, 2001). A *K<sub>D</sub>* value of 88.0 ml/g was presented in another study (Li et al., 2014).

Cyclodextrin is a sugar molecule that linked to form a ring. It is produced from starch, and like chitin and chitosan, it has been studied extensively for food and drug delivery system (Chen and Wang, 2001). A study exhibits a study of cyclodextrin for gaseous radioactive iodine entrapment in the nuclear waste management (Szente et al., 1999). Although the study was done for air contamination, it shows that cyclodextrin can adsorb iodine in the presence of water vapor. A complex of cyclodextrin-chitosan was found to have maximum iodine removal capacity of 1200 mg/g (Chen and Wang, 2001).

The alginate is another adsorbent that has been researched for the iodine adsorption. The mucilaginous layers on the surface of brown algae was proposed to play a crucial role in iodine adsorption (Loderio et al., 2005). The alginic acid is found within these mucilaginous layers, and it is the main ingredient of sodium alginate. Sodium alginate is a pharmaceutical and commercial product. It can be used as a chelator to eliminate I-131 and Sr-90 from bodies of affected consumers (Loderio et al., 2005; Sutton et al., 1971). However, the alginate is an anionic polysaccharide. As a result, some studies impregnated it with various kinds of metals, for iodine sorption in batch experiments. The iodine adsorption on calcium alginate–silver chloride composite yielded the adsorption capacity within the range of 133 to 152 mg/g across a set of initial iodine concentration and temperature (Zhang et al., 2011).

The alginate can also be taken to react with Polyvinyl alcohol (PVA), titania ( $\text{TiO}_2$ ) and maghemite ( $\gamma\text{-Fe}_2\text{O}_3$ ) to create a unique sorbent (Majidnia and Idris, 2015). The  $\text{TiO}_2\text{-Fe}_2\text{O}_3\text{-PVA}$  alginate beads is shown to adsorb iodine in an aqueous solution with about 20 mg/g maximum uptake (Majidnia and Idris, 2015). pH 8 provided the optimum condition for the sorption mechanism as the highest iodine percentage removal of about 98.0%, in 200 mg/L iodide initial concentration, was obtained (Majidnia and Idris, 2015). Additionally, it was shown that  $\text{TiO}_2\text{-Fe}_2\text{O}_3\text{-PVA}$  alginate beads can be reused for more than seven times with only 10.0% reduction of sorption efficiency is observed at the seventh usage (Majidnia and Idris, 2015).

Compared to those of the other categories, the research on polysaccharide was found to be limited. Still, the cyclodextrin-chitosan complex exhibited one of the most iodine uptake capacity across all the adsorbent categories. The complex was only studied for the binding of  $\text{I}_2$ , but, like the calcium alginate-silver chloride, it can possibly be modified for the removal of anionic species in the natural environment. Since, polysaccharide is widely available, more research should be focused on this category, so that more kinds of potential adsorbent are discovered.

## **2.5 Sources and effects of copper and aluminium in the water**

### **2.5.1 Copper**

According to the Environmental Protecting Agency, copper is regarded as one of the organic contaminants that poses risk to human, organisms, and ecology (US

Environmental Protection Agency, 2008). Throughout the world, there have been researches about copper monitoring in the water bodies (Harvey et al., 2016; Matthiessen et al., 1999; Yang et al., 2009). Copper can be discharged with wastewater from many sources such as fertilizers from agricultural activities, petroleum refining plants, and industries related to paints (Wittman, 1981). Its usual disassociation form in the water is divalent cationic metal,  $\text{Cu}^{2+}$ . The concentration of  $\text{Cu}^{2+}$  can be as high as 1800 mg/L in the wastewater (Kocasoy and Şahin, 2007). Particularly, in the copper plating industry wastewater, the concentration of  $\text{Cu}^{2+}$  was found to be 126 mg/L.

In many organism including human, copper is a required nutrient to maintain metabolic functions. However, excessive intake of the metal can lead to undesired symptoms. The lowest-observed-adverse-effects level (LOAEL) of Cu in adults is 6 mg per liter of purified water, and a no-observed-adverse-effects level (NOAEL) of Cu is 4 mg per liter of purified water (Araya et al., 2001). A more-than-necessary dose of copper could create symptoms like upsetting gastrointestinal tract and nausea (O'Donohue et al., 1993). A clinical case study of chronic copper exposure on a man showed a liver failure, which the removed organ showed extensive structural damage (O'Donohue et al., 1993).

### **2.5.2 Aluminium**

The sources of aluminium include automotive industries, cookware production, construction as well as aluminium sulphate widely used in drinking water treatment plants (Asrarian et al., 2014; Boaventura, A. R., Duarte, A. S. A. & Almeida, 2000). In the water, aluminium is disassociated into a trivalent cation,  $\text{Al}^{3+}$ . The cationic metal can range from 20 to 100 mg/L in the wastewater effluents (Goher et al., 2015; Pour et al., 2014).

In human, although  $\text{Al}^{3+}$  is not adsorbed the intestinal tract, the cationic metal can enter the metabolic system through inhalation and dermal contact (Perez-Granados and Vaquero, 2002). High concentration of aluminium can reduce bone formation and hinder the synthesis of hemoglobin cells (Ganchev et al., 1998; Goodman et al., 1984; Sedman et al., 1987).

## 2.6 Copper and aluminium removal technology

### 2.6.1 Membrane separation technology

Several types of membranes such as UF, NF and RO had been used to remove Cu from the water (**Table 2.12**). The UF can remove a high concentration of Cu (160 mg/L) with a removal efficiency of up to 99.5 % (Al-Saydeh et al., 2017). The removal of trace amount of Cu with more than 98.0% efficiency can be achieved for NF and RO (Al-Saydeh et al., 2017). In the RO system, 5 bars of pressure were required (Al-Saydeh et al., 2017). MF was shown to remove up to 98.0% of the initial Al concentration of 1.40 mg/L (Matsui et al., 2013). The membrane separation technology exhibited high removal but the pressure and electrical power were needed.

**Table 2.12** Removal of metal by membrane separation technology

Metal	Type of membrane	Initial concentration	Operating pressure (bar)	Removal efficiency (%)	Ref.
Cu	UF	160 mg/L	n.a.	98.0 – 99.5	(Al-Saydeh et al., 2017)
	NF	0.47 mol/L	2	96.0 – 98.0	
	RO	$7.86 \times 10^{-3}$ mol/L	5	98.0 – 99.5	
Al	MF (MCE-0.1 $\mu$ m)	1.40 mg/L	n.a.	Up to 98.0%	(Matsui et al., 2013)
	MF (PTFE-0.1 $\mu$ m)				

### 2.6.2 Chemical precipitation, coagulation, and flocculation

Chemical precipitation is regarded as one of the most common technique for the removal of heavy metal ions. In processes, heavy metals would react with ions such as hydroxide, phosphate, carbonate and sulfide to form insoluble precipitates. The coagulants and flocculation are included to increase the precipitates particle size. The insoluble particles containing heavy metal are separated from water through either sedimentation or filtration. Hydroxide is often used in the chemical precipitation method (Gunatilake, 2015). Flocculants added in the process can be polyacrylamide (PAM), and polyferric sulfate (PFS). A recent study reported that this method could remove 82.0% of copper in salted water with no initial concentration reported (Ayoub

et al., 2001). Water treated with coagulation and flocculation is generally followed by filtration to completely remove the trace metal contaminant.

### 2.6.3 Adsorption

Many types of adsorbents (unmodified or synthetic) can be employed to remove toxic heavy metal ions from water. These include, for instance, conventional adsorbents (activated carbon, zeolite, and ion-exchange resin), clay minerals, industrial solid waste, and biological materials. A study reported the increase in  $\text{Cu}^{2+}$  adsorption capacity from 133 mg/g to 148 mg/g by the zeolite derived by fly ash when the temperature increased from 18.9 to 36.9 °C (Mishra and Tiwari, 2006). Under microwave irradiation, chitosan could possess the  $\text{Cu}^{2+}$  adsorption capacity of up to 165 mg/g (Cao et al., 2001). Unconventional adsorbent like fish scale yielded  $\text{Cu}^{2+}$  adsorption capacity of about 80 mg/g (Huang, 2007). For  $\text{Al}^{3+}$ , the commercial activated carbon (granular form) and cation-exchange resin possessed 99.2 and 99.6% adsorption efficiency at 100 mg/L initial adsorbate concentration (Goher et al., 2015). More than 90 mg/g of  $\text{Al}^{3+}$  adsorption capacity was reported for chitosan-tannic acid modified biopolymers (Badawi et al., 2017).

It can be seen that the research on adsorption of  $\text{Cu}^{2+}$  and  $\text{Al}^{3+}$  has been done extensively. Many synthetic adsorbents were used. Some Al-incorporated materials can be used further to adsorb toxic anions such as fluoride, selenate and arsenate (Liu et al., 2012; Yamani et al., 2014). Further applications of the synthetic adsorbents or complexes containing  $\text{Cu}^{2+}$  and  $\text{Al}^{3+}$  should be explored after the pollutant removal.

### 2.7 Principle of Adsorption

Adsorption is the process of the association or/and adherence of fluid phase on the surface of the solid phase. This can happen in two ways, through physical and/or chemical interactions. The physical adsorption usually deals with London dispersion forces (as one of Van Der Waal forces). London dispersion force is an intermolecular attraction between uneven electrons and protons, creating temporary dipole. The interaction energy depends on surface contact area of the molecules, polarizability (based on molecule size) and the number of pi-bonding present. The chemical adsorption deals with ionic and covalent bonding between the target molecules and the

functional group of the adsorbent. The physical adsorption is usually weaker than the chemical adsorption. The binding process of adsorption is related to the thermodynamic Equation (2.1).

$$\Delta G = \Delta H - T\Delta S \quad (2.1)$$

where  $\Delta H$  and  $\Delta S$  are the change in enthalpy (kJ/K/mol) and entropy (kJ/mol), respectively.  $T$  represents the temperature (K) used in the experiment.  $\Delta G$  is the change in Gibbs free energy (kJ/mol), which is associated with adsorption process with the Equation (2.2).

$$\Delta G = -RT \ln K \quad (2.2)$$

where  $R$  is an ideal gas constant, which has a fixed value of 8.314 J/mol/K.  $\Delta G$  is related to the spontaneity of adsorption process where the higher in negative value of  $\Delta G$  reflects more energetically favorable adsorption (Plazinski, 2012). Substituting Equation (2.1) into (2.2) would yield Equation (2.3).

$$\ln K_L = -(\Delta H/RT) + \Delta S/R \quad (2.3)$$

For an experiment with changing in temperature is observed,  $\Delta H$  and  $\Delta S$  can be obtained from the slope and the intercept of the plot  $\ln K$  against  $1/T$ . If we are determining the equilibrium relationship between solid and aqueous solution, we can first equilibrate the known adsorptive solution and the sorbent at a fixed temperature and pressure. The equilibrium relationship, described by isotherms, will be obtained when adsorptive solution and the adsorbent are allowed to make contact for a period of time. The amount of adsorption or amount of mass of solute adsorbed per unit mass of adsorbent,  $q$  (expressed in mol/g or mg/g) can be calculated with the mass balance equation [Equation (2.4)]

$$q = [(C_i - C_e) \times V]/m \quad (2.4)$$

where  $C_i$  and  $C_e$  was previously defined as the adsorbate concentration in the water (mg/L) before and after the adsorption, respectively.  $V$  is the volume of solute (L) while  $m$  represents the mass of adsorbent used in the adsorption experiment (g). To determine the most suitable adsorption model, it is important to understand that adsorption isotherms exhibit many different shapes for different combination of sorbates and sorbents. By plotting  $q$  against  $C_e$ , if linear graph is obtained, the relationship between  $q/C_e$  can express as a ratio of solid-solution distribution coefficient  $K_D$  [Equation (2.5)].

$$K_D = q/C_e \quad (2.5)$$

Linear adsorption usually occurs at low solute concentration and low amount of sorbate (Delle Site, 2001). If the plot of  $q$  against  $C_e$  yields a non-linear graph, it indicates that after a period of time, the sites of sorbent become saturated and the degree of adsorption does not change anymore. Two kinds of models can be used for this particular case. The first model derived from the equation of the change in final concentration over time which expressed as:

$$\frac{\partial C_e}{\partial t} = -k_1 m \times C_e (q_{max} - q) + k_2 q m \quad (2.6)$$

where  $q_{max}$  is the adsorption capacity or adsorbed solutes concentration corresponding to the total number of surface sites.  $k_1$  and  $k_2$  are the rate constant for adsorption and desorption. The rate of adsorption is assumed to be proportional to  $C_e$  and to the difference in  $q_{max}$  and  $q$ . The equation can be reduced to express the relationship between  $q$  and  $C_e$  as shown in Equation (2.7).

$$q = (q_{max} K_L C_e) / (1 + K_L C_e) \quad (2.7)$$

where  $K_L$  is the Langmuir constant or coefficient related to the enthalpy of adsorption. Equation (2.8) depicts the linear relation between  $q$  and  $C_e$ .

$$C_e/q_e = 1/K_l q_{max} + C_e/q_{max} \quad (2.8)$$

In the Langmuir model, the relation between  $q$  and  $q_{max}$  can be described as when the solute concentration is increasing at low surface coverage with the available adsorption sites reaching saturation and  $q$  is increasing linearly to approach  $q_{max}$ . The model has  $q_{max}$  representing monolayer coverage and assumes that adsorption energy is independent of degree of surface coverage (Delle Site, 2001). It also assumes the energy to be equal for all sites, where only localized ones are involved in adsorption process without interaction between adjoining sorbed molecules (Delle Site, 2001).

The second model takes into account the degree of surface coverage and sorption energy for the sites. It is called Freundlich model where the relationship of  $q$  and  $C_e$  is expressed in Equation (2.9).

$$q = K_F C_e^n \quad (2.9)$$

where  $K_F$  is used as the Freundlich coefficient and  $n$  is the exponent relates to adsorption intensity and free energy. To get the linear plot for Freundlich Isotherms, natural log transformation is used as shown in Equation (2.10).

$$\ln q = (1/n) \ln C_e + \ln K_F \quad (2.10)$$

If  $n$  is 0, a constant adsorption free energy at all sorbate concentration is observed. On the other hand, a value of  $n$  more than 1 means the increase in the presence of sorbate enhances the free energies for further adsorption but when  $n$  is less than 1, weaker free energies with increasing sorbate is observed.

It is worthy to note that the linear, Langmuir or Freundlich isotherms equation cannot solely explain the sigmoidal isotherm relation. Instead, sigmoidal behavior signifies the combination of two different adsorption mechanisms, one after another. It occurred due to alternation in the functional groups, numerous components of a heterogeneous sorbates or diversity in free energies related to the adsorption process.

To explain the change of concentration over time, rate reaction can be used. The first-order-reaction is known to proceed at a rate that depends linearly on one



reactant concentration. However, in the adsorption, the pseudo first-order-reaction is used instead. This reaction is supposedly occurred at a higher order (higher than 1). However, it occurs by the first order because the concentration of one reactant used is very high and another reactant is very low and can be neglected. If we assume  $A$  and  $B$  as reactants (adsorbent and adsorbate), we can write Equation (2.11).

$$\text{Rate} = -d(A)/d(t) = k(A)(B) \quad (2.11)$$

In an adsorption system where  $B$  is neglected as excess, we can change Equation (2.11) to (2.12).

$$d(A_t)/d(t) = k(A_0 - A_t) \quad (2.12)$$

where  $A_0$  and  $A_t$  represents the concentration of  $A$  at the start and end of the reaction, respectively. We can change these into adsorption related parameters [Equation (2.13)].

$$d(q_t)/d(t) = k(q_e - q_t) \quad (2.13)$$

After integrating Equation (2.13) for the boundary conditions of  $t = 0$  to  $t = t$  and  $q_t = 0$  to  $q_t = q_t$ , linearized form can be obtain as the pseudo first-order-reaction in Equation (2.14).

$$\log(q_e - q_t) = \log q_e - (k_1/2.303)t \quad (2.14)$$

where  $k_1$  is the constant derived from pseudo-first-order reaction (L/min), while  $k_2$  represents the constant from pseudo-second-order reaction (g/mg/min). At a given experimental time ( $t$ , min),  $q_t$  represents the quantity of  $I^-$  removed from the water per quantity of bio-based adsorbent (mg/g).  $q_e$  represents amount of  $I^-$  adsorbed per weight of bio-based adsorbent at an equilibrium,  $e$  (mg/g). The calculation  $q_t$  and  $q_e$  follows the adsorption equilibrium in Equation (2.4).

The pseudo second-order-reaction takes into account both reactants (adsorbent and adsorbate) participate in the reaction to determine step in the rate reaction. Equation (2.15) shows the reaction of second order with adsorption parameters.

$$d(q_t)/d(t) = k(q_e - q_t)^2 \quad (2.15)$$

After the integration (boundary conditions:  $t = 0$  to  $t = t$  and  $q_t = 0$  to  $q_t = q_t$ ) and rearrangement, pseudo second-order-reaction is depicted as a linearized log-transformed equation in Equation (2.16).

$$t/q_t = 1/k_2q_e^2 + t/q_e \quad (2.16)$$

## 2.8 Characterization Techniques

### 2.8.1 Nitrogen adsorption-desorption surface area analysis

Surface area and porosity are crucial for the characterization of an adsorbent. Provided the interested functional groups exist, a high porous structure leads to an increase in surface area, which elevates the chance for interactions between functional groups and the adsorbate. To quantify the surface area, the relation between the amount of gas adsorbed and the relative pressure in a system of gas adsorption by an adsorbent is used.

Nitrogen is often used due to its availability, purity, and strong interaction with many solid adsorbents (Dąbrowski, 2001). The monolayer distribution of gas molecules on a porous structure was known to be proposed by Langmuir (Langmuir, 1918). However, Brunauer, Emmett, and Teller (BET) later proposed the multi-layer gas adsorption behavior on porous structure (Brunauer et al., 1938). The BET equation [Equation (2.17)] became widely used to determine a material surface area.

$$1/X[(p/p_0) - 1] = (1/X_m C) + [(C - 1)/(X_m C)](p/p_0) \quad (2.17)$$

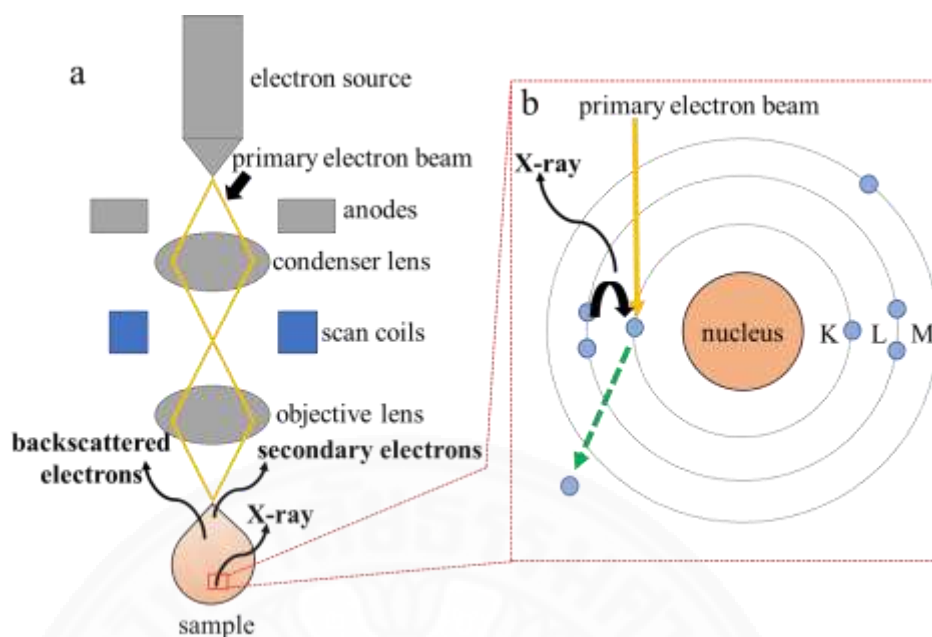
The pore volume can be calculated either by Barrett, Joyner, and Halenda (BJH) or density functional theory (DFT) method. BJH method relates the pressure to the pore size, taking into consideration the thickness of the adsorbed layer of adsorbate

(Thommes and Cychosz, 2014). On the other hand, the DFT method relies on the simulation of direct gas filling into the pores of adsorbates (Thommes and Cychosz, 2014). Lastly, the t-plot method is used to quantify the micropore volume (Galarneau et al., 2014).

### 2.8.2 Scanning electron microscopy with energy dispersive X-ray analysis

A scanning electron microscope is used to obtain images with the surface morphology and structural change of the adsorbents before and after the adsorption. At the top of a column, electrons are generated at the electron source. The positively charged anode attracts the electrons and sends them down the column. Electromagnetic lenses (condenser and objective), equipped with scanning coils, are used to control the path of electrons. The secondary and backscattered electrons coming out of the samples are detected and transformed into images. The backscattered electrons are reflected from elastic interactions of a deeper region of a sample. In an SEM image created by backscattered electrons, different parts of a sample exhibited different brightness. This infers a difference in atomic number in those parts. A part with higher atomic number appears brighter in the image (Nanakoudis, 2019). In contrast, an image created by secondary electrons appears contained more details as secondary electrons originate from the inelastic interaction at the sample surface (Nanakoudis, 2019).

Energy Dispersive X-ray (EDX) analysis technique is used with SEM. EDX can be used for the elemental composition analysis. Unlike creating SEM, the EDX analysis came from detections of X-ray. After the electrons beam hits the electron in an inner shell of an element, one of the outer shell electrons quickly fills the available place. This process creates an X-ray which can be detected. Different elements emit different wavelengths of X-ray. The data generated is the spectra of peaks corresponding to the elements emitting their respective X-ray. This becomes the elemental composition of a sample. **Figure 2.2** shows basic components of SEM and EDX.



**Figure 2.2** Basic components of SEM and EDX adopted from a technical webpage (Nanakoudis, 2019). (a) creation of backscattered and secondary electrons for SEM and X-ray for EDX, (b) detailed scheme of X-ray emission by primary electron beam

### 2.8.3 Fourier-transform infrared spectroscopy

Fourier-transform infrared spectroscopy (FTIR) is an effective analytical instrument for detecting functional groups and characterizing bonding information. It is the study of how molecules interact with infrared radiation (IR). As IR is introduced to the sample, some functional groups in the sample absorb IR. When IR is absorbed at a specific frequency, molecules vibrate and those with a dipole change can be detected. If the chemical bonds of the molecules in the functional groups are treated as spring, the frequency of vibration can be determined by Equation (2.18).

$$\text{frequency of vibration} = (1/2\pi)\sqrt{k/\mu} \quad (2.18)$$

where  $k$  is the strength of the bond or the spring, and  $\mu$  is the reduced mass of the atom involved in the chemical bonding. As the transmitted IR is detected, the results is calculated by a Fourier Transform that converts the output into a spectrum. A spectrum of FTIR is normally produced in the form of percent transmittance, % $T$  over

wavenumber ( $\text{cm}^{-1}$ ) of IR. These can be calculated according to Equation (2.19) and (2.20), respectively.

$$\%T = 100 \times (I/I_0) \quad (2.19)$$

$$\text{wavenumber} = 1/\lambda \quad (2.20)$$

where  $I$  and  $I_0$  are final and initial IR intensity.  $\lambda$  is the wavelength related to IR frequency and velocity. Absorbance can be calculated from  $T$  as shown in (2.21).

$$\text{absorbance} = -\log_{10} T \quad (2.21)$$

The spectrum of absorbance or  $\%T$  over  $400 - 4000 \text{ cm}^{-1}$  wavenumber is usually produced. At different wavenumbers, weak and strong bands are corresponding to different detected stretching or bending of molecules.

#### 2.8.4 Ultraviolet–visible spectroscopy

Ultraviolet-visible (UV-visible) spectroscopy can also be used to detect certain kinds of organic compounds such as benzene, naphthalene, and anthocyanin (Sugioka, 2009; Syukri et al., 2013). This is possible due to the UV absorbance of different forms of aromatic ring-containing-molecules. The absorbance can be calculated according to Equation (2.19) and (2.20). However, another application of the UV-visible spectroscopy is the concentration quantification of interested molecules. This can be done using the colorimetric analysis, which different colors of solution absorb different UV wavelength. Beer's law [Equation] is used in such quantification technique where absorbance is equal to the product of molar absorption coefficient,  $\epsilon$ , molar concentration,  $C$ , and cuvette pathlength,  $l$ .

$$\text{absorbance} = \epsilon Cl \quad (2.22)$$

### 2.8.5 Carbon-13 nuclear magnetic resonance

Carbon-13,  $^{13}\text{C}$  has nuclear spin due to an unequal number of protons and neutrons in the nucleus. Protons can spin to create their random magnetic fields. Placing these protons in an applied magnetic field,  $B_0$ , the proton spin can be arranged in two different ways. A proton can align its spin in the same direction of  $B_0$ ,  $\alpha$  state or it can align its spin in a completely opposite direction,  $\beta$  state. The energy taken for the  $\alpha$  state to flip to  $\beta$  state is  $\Delta E$ . By applying a radio frequency, protons can flip between the two states, and this is called the magnetic resonance. The carbon atom in different electronic environment will require a different amount of  $\Delta E$ , and this can be calculated by Equation (2.23).

$$\Delta E = h\nu = h \times [(\gamma/2\pi)B_0] \quad (2.23)$$

where  $\nu$  is the frequency (Hz), and  $\gamma$  is the gyromagnetic ratio ( $\gamma$  of  $^{13}\text{C}$  is 10.705 MHz/T). With an NMR machine that creates different spectrometer frequency (MHz), the data of  $^{13}\text{C}$  is shown in the unit of ppm according to

$$\text{vibration in ppm} = \nu/\text{spectrometer frequency} \quad (2.24)$$

With this, we can get a spectrum of NMR with various shifts of  $^{13}\text{C}$  at a different frequency. These shifts can combine to yield molecules structures. Changes in molecules structures due to adsorption can be detected by the absence or broadening of  $^{13}\text{C}$  shifts (Hartman and Kelusky, 1979).

### 2.8.6 Particle size analyzer for zeta-potential

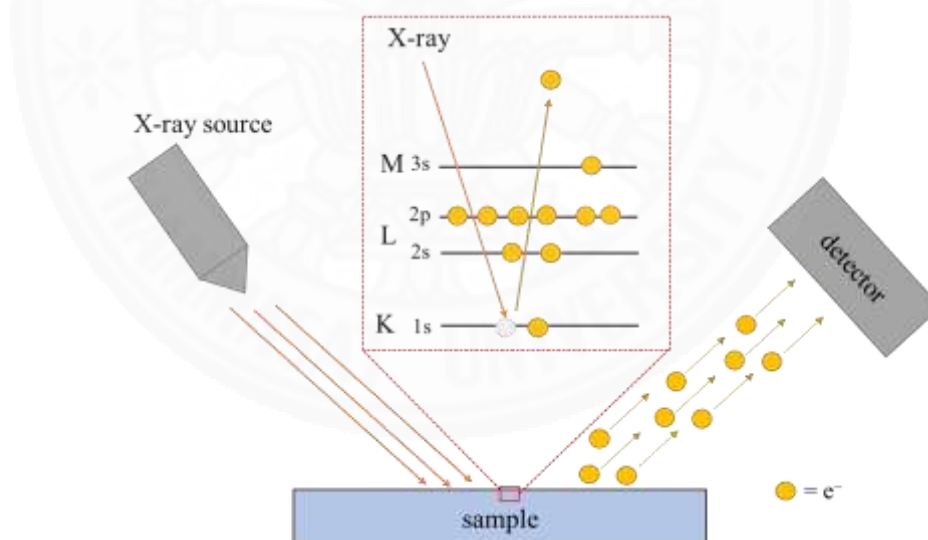
The study of zeta-potential can reveal the nature of the surface charge of an adsorbent. In an adsorption study, the zeta-potential is the measure of the potential difference between the colloidal form of adsorbent and its layer electrostatically attached to the dispersed ions. A particle size analyzer can measure the zeta-potential of a sample.

One way to introduce ions is to change the pH of the solute.  $\text{H}^+$  is predominant in an acidic condition, while  $\text{OH}^-$  is mostly found in the basic one. A graph of zeta

potential over pH is plotted. At 0 eV, the pH is said to be of the point of zero charge ( $\text{pH}_{\text{PZC}}$ ) when  $\text{H}^+$  or  $\text{OH}^-$  are attracted to the surface of adsorbent to the point that there is no potential between the adsorbent surface and disperse ions. In the pH environment with positive or negative zeta potential, attractive or repulsive are present. The zeta-potential analysis will help determine the nature of adsorbent, especially if electrostatic interaction is the main adsorption mechanism.

### 2.8.7 X-ray photoelectron spectroscopy

X-ray photoelectron spectroscopy (XPS) can be used to find chemical state and electronic state of the elements within an adsorbent. In the XPS, the X-ray excites electrons from a material surface. The schematic illustration of the excitation of electrons by X-ray is shown in **Figure 2.3**. The electron energy depends on the elemental electron orbital binding energies. Different binding energies are caused by different bonding and oxidation states of the atoms. These determined the shifts in XPS results as the emitted electrons have various kinetic energy.



**Figure 2.3** Emission of electron from the sample by the X-ray excitation. Emitted electrons are captured and measured for their kinetic energy by a detector

The XPS measures the kinetic energy (eV) of an electron while the binding energy (eV) can be calculated by Equation (2.25).

$$\text{binding energy} = h\nu - \text{kinetic energy} - \phi \quad (2.25)$$

where  $h\nu$  represents photo energy from the X-ray source and  $\phi$  is the spectrometer work function. The XPS spectrum presented various shifts (representing different elements and their forms) on a graph of intensity versus binding energy.

### 2.8.8 X-ray absorption spectroscopy (XAS)

X-ray absorption spectroscopy (XAS) is similar to XPS in the way that they utilize X-ray for exciting core electrons in the sample. However, the XAS is may be used to excite different core electrons at different energy levels. XAS edges or adsorption edges refer to the different transition of the excited electron at a different core level. For instance, K-edge is used to describe the excitation of 1s electrons, while L<sub>III</sub>-edge represents the excitation of 2p electrons ( $J = 3/2$ ).

XAS is separated into X-ray absorption near edge structure (XANES) and extended X-ray absorption fine structure (EXAFS). XANES can be used to determine an oxidation state of an interested element. It can be measured in two ways using X-ray transmittance or fluorescence mode. The transmittance mode measures an absorbance using the ratio of incoming and outgoing X-ray in intensity. These are represented by  $I_{x0}$  and  $I_x$ , respectively. Equation (2.26) is used to calculate the absorbance of the transmittance mode.

$$\text{absorbance of transmittance mode} = \ln(I_{x0}/I_x) \quad (2.26)$$

The fluorescence mode is used to measure the X-ray fluorescence emitted by a relaxation of an electron that filled the empty hole. The X-ray fluorescence is represented by  $I_F$ , and the calculation of the absorbance for this mode is shown in Equation (2.27).

$$\text{absorbance of fluorescence mode} = I_F/I_x \quad (2.27)$$

EXAFS takes into account the local environment. The wave interactions are created between the ejected photoelectron and electrons around the absorbing atom.



The wave hit neighbour atoms and return to the original atom. The phenomenon can be used to estimate the distance between neighbour atoms and the atom of our interest.

### **2.8.9 Inductively coupled plasma optical emission spectrometry**

The inductively coupled plasma optical emission spectroscopy (ICP-OES) is one of the techniques widely used for the quantification of the known inorganic element.

ICP is the part that creates high-temperature plasma (6000-10000 K) by the ionization of argon gas in the fluctuating magnetic field. As the collision of the ions and argon atoms occurs, the plasma is generated. The sample is sprayed at the top of the plasma tail, where different atoms are forced to its excited state by the plasma heat. As the atoms move back to its ground state, they emit light. Different atoms of different elements emit different wavelength. Initially, the sample with various elements produces polychromatic light, which include the mix of many wavelengths. Then the filter is used to separate these wavelengths into monochromatic light.

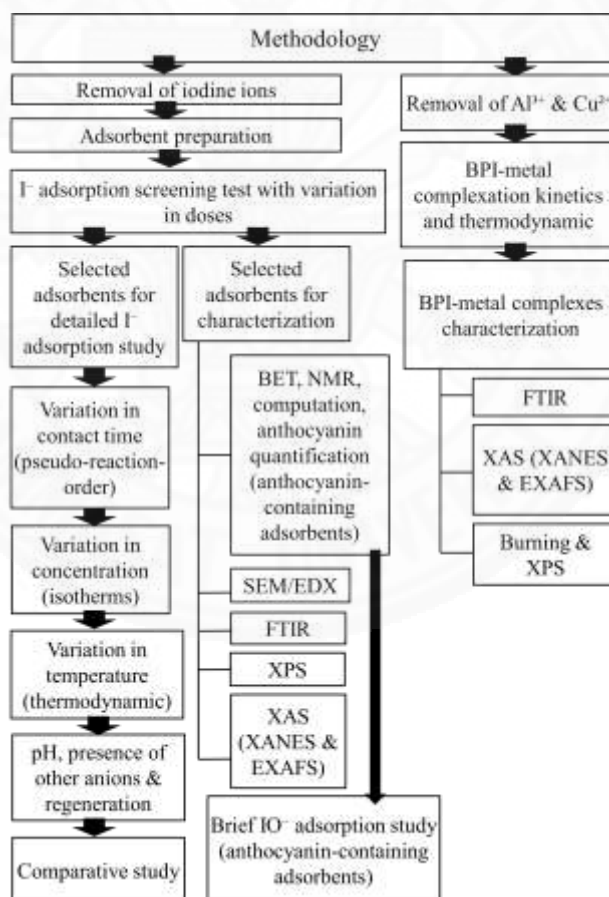
OES is employed to measure the monochromatic light wavelength of each respective element, where the intensity of light is proportional to the amount of element presented in the sample. In an optical system, the spectrometer separates the individual wavelengths of light and focus the desired wavelengths onto the detector.

## CHAPTER 3

### METHODS

#### 3.1 Methodology Overview

The study is composed of two main routes. The first contained the study of removal of iodine ions ( $I^-$  and  $IO_3^-$ ).  $I^-$  was the main focus as detailed adsorption experiments and extensive characterization were performed on the selected bio-adsorbents.  $IO_3^-$  adsorption was briefly studied using only the anthocyanin-containing adsorbents. The second route concerned the removal of  $Al^{3+}$  and  $Cu^{2+}$  by complexation with BPI. This contains a kinetic study of metal ion removal and BPI-metal characterization. **Figure 3.1** is the scheme showing overview of the study.



**Figure 3.1** Flow chart displaying overall methodology in this study

#### 3.2 Reagents

The source of  $I^-$  and  $IO_3^-$  potassium iodide (KI, TCI, Japan) were potassium iodate ( $KIO_3$ , Loba Chemie Pvt Ltd, India). The reagents for  $I^-$  quantification include

4,4',4''-methylidynetris[*N, N*-dimethylaniline] (Sigma Aldrich, USA), OXONE<sup>®</sup> potassium monopersulfate triple salt (Sigma Aldrich, USA), critic acid (C<sub>6</sub>H<sub>8</sub>O<sub>7</sub>·H<sub>2</sub>O, Sigma Aldrich, USA), conc. ammonium hydroxide (NH<sub>4</sub>OH, Sigma Aldrich, USA), ammonium phosphate monobasic (NH<sub>4</sub>H<sub>2</sub>PO<sub>4</sub>, Sigma Aldrich, USA), mercury(II) chloride (HgCl<sub>2</sub>, Sigma Aldrich, USA), and sulfuric acid (H<sub>2</sub>SO<sub>4</sub>, Kanto Chemical Co. Inc., Japan). Metal salts were bought from Tokyo Chemical Industry, Japan. These include copper(II) chloride (CuCl<sub>2</sub>), ferric chloride (FeCl<sub>3</sub>), calcium chloride (CaCl<sub>2</sub>), sodium chloride (NaCl), Sodium sulfate (NaSO<sub>4</sub><sup>2-</sup>), sodium bicarbonate (NaHCO<sub>3</sub>), potassium bromide (KBr), and potassium iodate (KIO<sub>3</sub>). Aluminum sulfate-18-hydrate (Al<sub>2</sub>(SO<sub>4</sub>)<sub>3</sub>·18H<sub>2</sub>O, Sigma-Aldrich, USA) was used as received. Sodium tripolyphosphate (STPP, Sigma Aldrich, USA), conc. hydrochloric acid (HCl, Kanto Chemical Co. Inc., Japan), and sodium hydroxide (NaOH, Kanto Chemical Co. Inc., Japan) were used as received. Sodium alginate (food grade) was bought from a baking supply shop, and chitosan flakes were bought from a local agricultural supply store. The laboratory-grade reagent was not preferred due to the high cost and less suitability for the adsorbent preparation.

### 3.3 Bio-based adsorbents preparation

The sodium alginate gel of 2% (w/v) was prepared and added dropwise into different 2% (v/v) metal solutions. These solutions were prepared separately with CaCl<sub>2</sub>, CuCl<sub>2</sub>, and FeCl<sub>3</sub>. A metering pump (DMI 1.1-16, Grundfos, Germany) was used and set up for 1 L/h to control the bead size. Swollen beads of calcium alginate (Ca-Alg), copper alginate (Cu-Alg), and iron alginate (Fe-Alg), were formed. The beads were allowed to settle in the solution for 24 h. After separation, the beads were washed 3 times with DI water and dried at 60 °C in an oven. A swollen bead was about 5 cm in diameter. When it was dried, the diameter was reduced to about 2 cm. Before being used, dried beads were kept in a closed container, while swollen beads were kept in DI water.

The chitosan flakes were crushed into pieces. They were weighted and added to the 2% (v/v) acetic acid solution to create 2% (w/v) chitosan gel. The solution was stirred until the flakes dissolved. The obtained chitosan gel was added dropwise to a

2% (w/v) STPP solution. The swollen beads were allowed to sit in the solution for 24 h. After drying in an oven at a temperature of 60 °C, the dried beads were kept in a closed container before being used, and the swollen ones were kept in DI water.

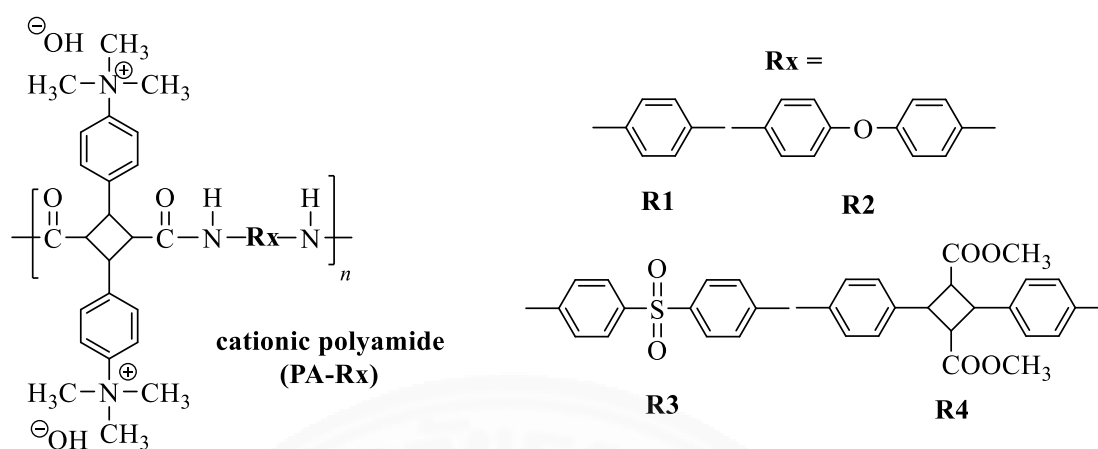
Pistachio shells, peanut shells, sacha inchi (*Plukenetia volubilis*) shells, and coconut husks, were obtained from a local market. At the same time, hazelnuts were bought from an online store, and only its shells were used. All plant wastes were washed with DI water before being dried in an oven. They were ground, sieved with standard sieves for 0.5 – 0.711 mm pieces, and stored in sealed containers until further use.

Mangosteen pericarps, red onion peels, red dragon fruit peels, passion fruit rinds, pomegranate skins, radish skins, beetroot skin, and purple corn cobs were obtained from a local farm and market. They were washed with DI water, cut into small pieces, and dried at 60°C for 24 h in a vacuum oven (France Etuves C3000, France). All the adsorbents were ground with a grinding machine and sieved with standard aluminum sieves for the selection of 0.5 – 0.711 mm pieces.

The living plants used in this screening test includes *Limnophila heterophylla*, Duckweeds (Genus: *Lemna*), Water fern (Genus: *Azolla pinnata*) and *Hydrilla verticillata*. They were collected from a nearby river. The plants are kept in the open container with tap water, under the sun. For duckweed and water fern, the roots are still intact, indicating that the plants are still living and growing.

Cationic biopolyamides was previously synthesized from a glucose-based monomer in Kaneko Laboratory, Japan Advanced Institute of Science and Technology. The synthesis procedure can be found in a published study (Phanthuwongpakdee et al., 2020). The four types of cationic biopolyamides used in this study were PA-R1, PA-R2, PA-R3 and PA-R4. Their structures can be found in **Figure 3.2**. The biopolyamides were treated with KOH so that they were in the form of OH<sup>-</sup>.

Two types of commercial grade anion-exchange resins were employed as references in the adsorption experiment. DOWEX-1 (DOWEX<sup>TM</sup>-1-chloride, Dow Chemical, USA) and DOWEX-550 (DOWEX<sup>TM</sup>-550-chloride, Dow Chemical, USA) were selected. The resins had a 50 – 100 mesh size and was used without further modification. Activated carbon (Iodine number 1000 mg/g, EUNICARB, Thailand) and anthracite (C&C, Australia) were washed with DI and dried at 60°C for 24 h in a vacuum oven.



**Figure 3.2** Structure of cationic polyamides used in this study

### 3.4 Screening test and adsorbent dose

The adsorbents were separated into categories for the screening test as shown in **Table 3.1**. The contact time and dose are also presented in the same table.

**Table 3.1** Different types of bio-based adsorbents used in the screening test with their dose and contact time

Category	Adsorbent	Contact time	Dose (g/L)
seed shells and husks	pistachio shells	2 h	0.05, 0.1, 0.5, 1, 2, 5
	peanut shells		
	hazelnut shells		
	sacha inchi shells		
	coconut husks		
bio-based and metal-based synthetic materials	Ca-Alg (swollen)	2 h	0.05, 0.1, 0.5, 1, 2, 5
	Ca-Alg		
	Cu-Alg (swollen)		
	Cu-Alg		
	Fe-Alg (swollen)		
	Fe-Alg		
	chitosan flakes		
chitosan beads (swollen)			

	chitosan beads		
anthocyanin-containing adsorbents	mangosteen pericarps red onion peels red dragon fruit peels passion fruit rinds		0.05, 0.1, 0.5, 1, 2, 5
cationic biopolyamides	PA-R1 PA-R2 PA-R3 PA-R4		0.01, 0.1, 1, 2, 5
commercial adsorbents	DOWEX-1 DOWEX-550 activated carbon anthracite		0.05, 0.1, 0.5, 1, 2, 5
living plants	<i>Limnophila heterophylla</i> <i>Lemna</i> <i>Azolla pinnata</i> <i>Hydrilla verticillata</i>	24 h	0.5, 1, 5

To quantify  $I^-$  in solution, the Leuco Crystal Violet (LCV) method was employed (Clesceri, 1999). The method created a violet solution in which the intensity was proportional to  $I^-$  concentration, quantified by the absorption of light (592 nm) produced by a UV-visible spectrometer (Lambda 25, Perkin-Elmer, USA) at room temperature. The adsorption experiments were performed in triplicate on an orbital shaker (150 rpm).

The screening test condition was set up with 10 mg/L initial  $I^-$  concentration. The removal efficiency was determined by the total percentage of  $I^-$  being adsorbed by the adsorbent, after a given contact time.  $I^-$  removal efficiency was calculated by Equation (3.1).

$$I^- \text{ removal efficiency (\%)} = [(C_i - C_e)/C_i] \times 100 \quad (3.1)$$

where  $C$  represents the adsorbate concentration in the water (mg/L). The subscript  $i$  and  $e$  denote initial and equilibrium, respectively. As a result,  $C_i$  and  $C_e$  are the concentration of the adsorbate (in this case  $I^-$ ) before and after the adsorption (mg/L), respectively. Only the selected adsorbents from the screening test were characterized and examined further for the adsorption mechanism.

### 3.5 Bio-based adsorbent characterizations

Before the nitrogen adsorption/desorption process, the adsorbents were subjected to degassing (Smart VacPrep, Micromeritics, USA) in a vacuum environment at 60°C for 24 h. A surface area analyzer (3Flex, Micromeritics, USA) was set up with pre-set values: 0.003 – 1 and 1 – 0.009 for the adsorption and desorption relative pressure ( $p/p_0$ ), respectively. Only the anthocyanin-containing adsorbents were analyzed for surface area using the nitrogen adsorption technique.

The  $I^-$  saturated adsorbents were prepared by conducting the adsorption at 100 mg/L  $I^-$  initial concentration. The optimum dose of adsorbents and equilibrium contact time were used. A scanning electron microscope (SEM, JOEL JCM-6000Plus, Japan) was employed to investigate the surface morphology alteration of the selected adsorbents. SEM images of the virgin and  $I^-$  saturated adsorbents were obtained for comparison. The energy-dispersive X-ray spectroscopy (EDX, JOEL JCM-6000Plus, Japan) was used to analyze the elemental composition in the virgin and saturated adsorbents.

### 3.6 Adsorption experiments for iodide

In an adsorption study, the adsorbent capacity is one of the most important parameters. The value of adsorbent capacity is denoted by  $q$  (mg/g), and the calculation is represented by Equation (2.4).

The appropriate doses of selected adsorbents were chosen for the kinetic experiment, which was conducted at 0 – 180 min, at room temperature. The initial  $I^-$  concentration was 10 mg/L. The pseudo-order-reactions were used to explain the behavior of the rate-limiting steps of the  $I^-$  adsorption. The adsorption results were fit to the linearized form of the pseudo-first-order and pseudo-second-order reactions, as displayed in Equation (2.14) and (2.16), respectively.

The stability for the adsorbents to retain the adsorbate was tested. The desorption of  $I^-$  was determined after leaving the adsorbents in contact with  $I^-$  for a duration equivalent to the half-life of I-131 (8 days or 192 h).

After the kinetic experiment, the obtained equilibrium time for the respective adsorbent was used to understand the adsorption efficiency at various  $I^-$  concentrations. The concentration range of 0 – 200 mg/L  $I^-$  was used for Fe-Alg, hazelnut shells, sacha inchi shells, and anthocyanin containing adsorbents. On the other hand, a range of 0 – 1000 mg/L  $I^-$  was used for the cationic biopolyamides. The optimum dose of adsorbent was used at room temperature. To comprehend the  $I^-$  adsorption through the saturation of  $I^-$ , the linear equations of the Langmuir isotherm model [Equation (2.8)] and Freundlich isotherm model [Equation(2.10)] were used.

To evaluate the effect of temperature, the  $I^-$  adsorption for 10 mg/L initial  $I^-$  concentration was performed at 5 – 90 °C. To evaluate the thermodynamic behavior, the adsorption experiment with various concentrations was repeated at 5, 15, 25, 45, and 65 °C. This was only repeated for Fe-Alg, hazelnut shells, sacha inchi shells, mangosteen pericarps, and red onion peels. The modified thermodynamic equation with  $K_L$  is depicted in Equation (3.2). Linear plot of Equation (2.3) and the calculation of Equation (2.1) were used to determine the thermodynamic parameters. The activation energy was also obtained from the fitting of the Arrhenius equation [Equation (3.3)].

$$\ln K_L = -(\Delta H/RT) + \Delta S/R \quad (3.2)$$

$$\ln K_L = \ln A - (E_a/RT) \quad (3.3)$$

$E_a$  is the calculated Arrhenius activation energy (kJ/mol), while  $A$  represents the Arrhenius factor.  $I^-$  solution has a weak charge so  $K_L$  (calculated from the Langmuir model) is used for a distribution coefficient as recommended by a previous study (Liu, 2009).

The effect of pH (2 – 12) on  $I^-$  adsorption was investigated. HCl (0.1 M) and NaOH (0.1 M) were added to the solute to adjust the pH. Fe-Alg, hazelnut shells, sacha inchi shells, and PA-R4 were examined for the anion selectivity. The adsorption



experiment was conducted with additions of competitive anions, such as  $\text{Cl}^-$ ,  $\text{SO}_4^{2-}$ ,  $\text{HCO}_3^-$ , and  $\text{Br}^-$ . These anions were prepared from  $\text{NaCl}$ ,  $\text{NaSO}_4$ ,  $\text{NaHCO}_3$ , and  $\text{KBr}$ , respectively, with the concentration of the seawater composition (Kester et al., 1967). Tap water and seawater were also used in the selectivity experiment. The seawater was taken from Chon Buri province, Thailand. For, the anthocyanin-containing adsorbents, only  $\text{Cl}^-$  was used as the anionic competition. With 10 mg/L  $\text{I}^-$  initial concentration, different iodide to chloride ( $\text{I}^-:\text{Cl}^-$ ) ratios were prepared: 1:20, 1:200, and 1:2000. Additionally, the adsorption of  $\text{I}^-$  was tested in tap water and seawater.

The adsorption-regeneration tests were performed for 5 cycles. Only Fe-Alg and PA-R4 were regenerated as they were considered as synthetic adsorbents that performed well. Each regeneration was done by submerging the bio-based adsorbents in excess of 1 M  $\text{NaCl}$  for 1 h. In the pH, anion selectivity, and adsorption-regeneration experiments, the optimum dose of adsorbent and equilibrium time were used with 10 mg/L initial  $\text{I}^-$  concentration, at room temperature.

### **3.7 Investigation of functional groups involved in iodide adsorption**

The possible functional groups and mechanism of adsorption was performed for Fe-Alg, hazelnut shells, sacha inchi shells, and anthocyanin-containing adsorbents. For the cationic biopolyamides, quaternary ammonium were confirmed to be responsible for attracting  $\text{I}^-$  via ion-exchange (Phanthuwongpakdee et al., 2020).

#### **3.7.1 Functional groups in Fe-Alg, hazelnut shells and sacha inchi shells**

Zeta-potential (mV) of Fe-Alg and sacha inchi shells were determined in different pH conditions (3, 5, 7, and 11).  $\text{HCl}$  (0.1 M) and  $\text{NaOH}$  (0.1 M) were used to adjust the pH of DI water. The adsorbents were ground into powder and added to pH adjusted water to create colloid. After 2 h, the colloid was transferred to a clear disposable zeta cell. Zeta potential was measured by a particle size analyzer (ZetaSizer Nano ZS, Malvern Instruments Ltd., UK) with the dynamic light Scattering method.

X-ray absorption spectroscopy (XAS) was used to determine the adsorbents local structure of and the adsorbed iodine oxidation state. Beamline 5.2 in Synchrotron Light Research Institute (Nakhon Ratchasima, Thailand) was employed for this. The XAS was equipped with electron energy of 1.2 GeV, iodine  $\text{L}_{III}$ -edge probe element

(4557 eV) of 0.2 eV energy step and germanium (220) double crystals monochromator. To obtain the X-ray absorption near edge structure (XANES) spectra, the fluorescence mode was applied during the analysis of I<sup>-</sup> saturated adsorbents. KI and KIO<sub>3</sub> were used as references.

The possible functional groups responsible for attracting I<sup>-</sup> was investigated by analyzing the adsorbents (virgin and saturated) with Fourier-transform infrared spectroscopy (FTIR, Thermo Fisher Scientific, Nicolet iS50, USA). The removal of moisture was done by leaving the adsorbents in a vacuum oven (40 °C) for 6 h.

### 3.7.2 Functional groups in anthocyanin-containing adsorbents

Since it is hypothesized that anthocyanin content influences the adsorption of I<sup>-</sup>, the amount of anthocyanin in the adsorbents was quantitatively analyzed. For this, the ultrasound-assisted extraction method described previously was slightly modified and adopted (Hiranrangsee et al., 2016). In brief, all adsorbents were ground into powder. Ethanol (50%) was used at a ratio of 1:8.5 w/v (adsorbent to solvent). The mixture was sonicated for 10 min. A colored liquid (anthocyanin extract) was separated from the solid. The extract (1 mL) was further buffered to pH 1 and 4.5 using 0.025 M potassium chloride (KCl) and 0.4 M sodium acetate (Sigma Aldrich, USA), respectively. The absorbance of the samples was measured, within 20 – 50 min of preparation, at 510 (A510) and 700 nm (A700) by using a UV-visible spectrophotometer (Thermo Fisher Scientific, Genesys 10, USA). The total anthocyanin content was expressed as mg of cyanidin-3-glucoside equivalents per 100 g of dry sample (mg/100g). The total anthocyanin content (*TAC*) was calculated by Equation (3.4).

$$TAC(mg/100g) = (Abs \times MW \times DF \times 1000)/(\epsilon \times L) \quad (3.4)$$

where *MW* is the molecular weight of anthocyanin (449.2 D), and  $\epsilon$  is the cyanidin-3-glucoside molar absorbance (26,900 L/mol/cm). *L* and *DF* stand for the cuvette path length (1 cm) and extract dilution factor (10), respectively. *Abs* is the absorbance calculated by Equation (3.5).

$$Abs = [(A510 - A700)_{pH1}] - [(A510 - A700)_{pH4.5}] \quad (3.5)$$

Depending on the nature of an adsorbent, anthocyanin can be highly soluble in water. It is likely that the functional groups were leached into water, causing low adsorption efficiency. Consequently, the anthocyanin leaching experiment was performed with 0.5 g of the prepared adsorbents, with 10 mg/L I<sup>-</sup> solution for 2 h. After separation, the solvent was subjected to pH differentiation, absorbance measurement, and TAC calculation, following the instructions mentioned. The color of the solvent after the anthocyanin quantification and leaching experiment was observed for each adsorbent.

Cyanidin chloride (Sigma Aldrich, USA) was used in the NMR experiment to check for possible I<sup>-</sup> and flavylum cation interactions in the liquid phase. The chemical was diluted to 5 mg/L for NMR analysis (<sup>13</sup>C NMR, Bruker Biospin Inc., 400 MHz, D<sub>2</sub>O). The same procedure was performed on a 1:1 molar ratio mixture of 5 mg/L cyanidin chloride and I<sup>-</sup> solution. After agitating for 6 h, the mixture was subjected to the NMR measurement.

Following the extraction of anthocyanin, the ethanol was removed with a rotary evaporator and vacuum oven at 40°C. The dried extract anthocyanin from mangosteen pericarps and red onion peels were diluted to be equal to 0.1 mg of cyanidin-3-glucoside to 1 L of water. The extract was reacted with 10, 100, and 1000 mg/L I<sup>-</sup> solution for 6 h. The shifts in peaks corresponding to the flavylum cation from increasing the I<sup>-</sup> concentration were investigated with UV-visible spectrometry. The same procedure was performed with 0.1 mg/L of cyanidin chloride.

To confirm the functional groups associated with I<sup>-</sup> adsorption, the virgin adsorbents and those that underwent 100 mg/L I<sup>-</sup> adsorption were analyzed by FTIR. Before FTIR analysis, the adsorbents were dried in the vacuum oven at 40°C for 6 h. The FTIR spectrums were compared by their peak shifts.

The X-ray photoelectron spectroscopy analysis (XPS, PHI5000 VersaProbe II, ULVAC-PHI, Japan, equipped with Al-K $\alpha$  radiation, 1486.6 eV), was performed to determine the form of iodine in the adsorbents after I<sup>-</sup> adsorption. XPS was conducted at Beamline 5.3 (BL5.3), Synchrotron Light Research Institute (Public Organization), Nakhon Ratchasima, Thailand. The adsorbents were left in contact with 100 mg/L I<sup>-</sup>

for 24 h. After separation and drying (6 h in a vacuum oven at 40°C), the adsorbents and their virgin forms were measured for C1s, O1s, and I3d5.

The saturated adsorbents were studied for the iodine oxidation state and local structure by XAS at Beamline 5.2 with 1.2 GeV electron energy. The XAS spectra were recorded by setting iodine as the probe element ( $L_{III}$ -edge at 4557 eV) and the energy step at 0.2 eV. Germanium (220) double crystals were utilized as a monochromator. Transmission and fluorescence modes were applied to collect the spectra of XANES and EXAFS, respectively. XANES spectra indicated the presence of iodine in the sample. Still, EXAFS fit was not possible due to the trace iodine concentration and the interference of  $L_{II}$  iodine absorption edge at 4852 eV (Shimamoto and Takahashi, 2008). Additionally, the X-ray energy for the iodine K-edge is unavailable in the facility. Therefore, EXAFS was analyzed for another element to study  $I^-$  local structure.

According to the EDX results (Section 4.2.2), other XAS-compatible-elements were observed (O, Cl, Mg and K). Consequently, XAS analyses were recorded in fluorescence mode by focusing on potassium (K-edge) as the probe element. The measurements were performed at 3609 eV using Si(111) DCM. Only mangosteen pericarps and onion peels underwent XAS analyses after 24 h of contact with 100 mg/L  $I^-$  solution, and then solute-adsorbent separation and oven-drying. Cyanidin chloride solution (0.1 mg/L) and 100 mg/L  $I^-$  solution were mixed at a 1:1 ratio and was used as a reference. The mixture was left for 24 h before being dropped onto a small piece of filter paper. After drying, the filter paper was used for XAS analyses.

The mechanism of anthocyanin attracting  $I^-$  was studied using the computational method. Cyanidin, in the form of flavylum cation, was used as a representation of the anthocyanin-based adsorbent active site. Its structure was drawn using the software, GaussView and optimized for the ground state by Gaussian 09 with the Density Functional Theory (DFT) method. The optimized structure of the molecules was transferred to the software, AutoDock 4, as host. The guest molecule of  $I^-$  was attached to an uncharged dummy (H atom) due to the molecular requirements of the program. The partial charge of  $O^+$  in the cyanidin molecule and  $I^-$  were manually assigned to be +1.000 and -1.000, respectively. The algorithm docking was set to run for 100 times with a grid box covering the molecules. After the completion of the

calculation program, the Cyanidin-I<sup>-</sup> conformations with the lowest binding energy were analyzed.

### 3.8 Adsorption experiments for iodate

The IO<sub>3</sub><sup>-</sup> quantification was done by a colorimetric method, which was adopted from a previous study (Afkhami et al., 2001). A yellow solution was developed by adding 1 mL of 2% v/v H<sub>2</sub>SO<sub>4</sub> and 1 mL of 2% w/v KI to 25 ml of the IO<sub>3</sub><sup>-</sup> solution. After a minute, an intense yellow solution was diluted with DI water to 100 ml. The solution was measured by a UV-visible spectrophotometer at a wavelength of 428 nm.

Only anthocyanin-containing adsorbents were used for IO<sub>3</sub><sup>-</sup> adsorption. Mangosteen pericarps and red onion peels were used due to their high I<sup>-</sup> adsorption capacity. Added to the list of anthocyanin adsorbents were pomegranate skin, radish skin, beetroot skin, and purple corn cobs. They were washed with DI water, cut into small pieces, and dried at 60°C for 24 h in a vacuum. The adsorbents were ground with a grinding machine and sieved with standard aluminum sieves for the selection of 0.5 – 0.711 mm pieces. The adsorption experiments were performed in triplicate on an orbital shaker (150 rpm). Dowex-550 was used as a reference when appropriate.

In the screening test, 1 g/L adsorbent dose was used in IO<sub>3</sub><sup>-</sup> solution of 10 mg/L. The adsorption was performed for 2 h under room temperature. The selected adsorbents were further examined for kinetic and batch experiment. I<sup>-</sup> removal efficiency was calculated by Equation (3.6), which the parameters and their definitions are the same as those of Equation (3.1). However, in the case, IO<sub>3</sub><sup>-</sup> is the adsorbate.

$$\text{IO}_3^- \text{ removal efficiency (\%)} = [(C_i - C_e)/C_i] \times 100 \quad (3.6)$$

To determine an optimum dose of the selected adsorbents, 0.5, 1, 2, 3, and 4 g/L adsorbents were tested in 10 mg/L IO<sub>3</sub><sup>-</sup> solution for 2 h under room temperature.

The optimum doses of adsorbents were used in the kinetic experiment with the contact time of 0 – 720 min. The initial IO<sub>3</sub><sup>-</sup> concentration was 10 mg/L, and the kinetic experiment was performed under room temperature.

With the equilibrium time and optimum doses, the batch experiments were performed to understand the effect of IO<sub>3</sub><sup>-</sup> concentration. The IO<sub>3</sub><sup>-</sup> concentration range

of 2 – 100 mg/L was used in this experiment under room temperature. In order to comprehend the isothermal behavior, the batch experiment results were used to fit Langmuir [Equation (2.8)] and Freundlich model [Equation (2.10)].

The effect of pH on  $\text{IO}_3^-$  adsorption by anthocyanin-based adsorbents was investigated. The pH was varied from 3 to 10. The temperature variation experiment was also performed at 20 – 50 °C. These experiments were done with 10 mg/L  $\text{IO}_3^-$ , adsorbent optimum dose and equilibrium time.

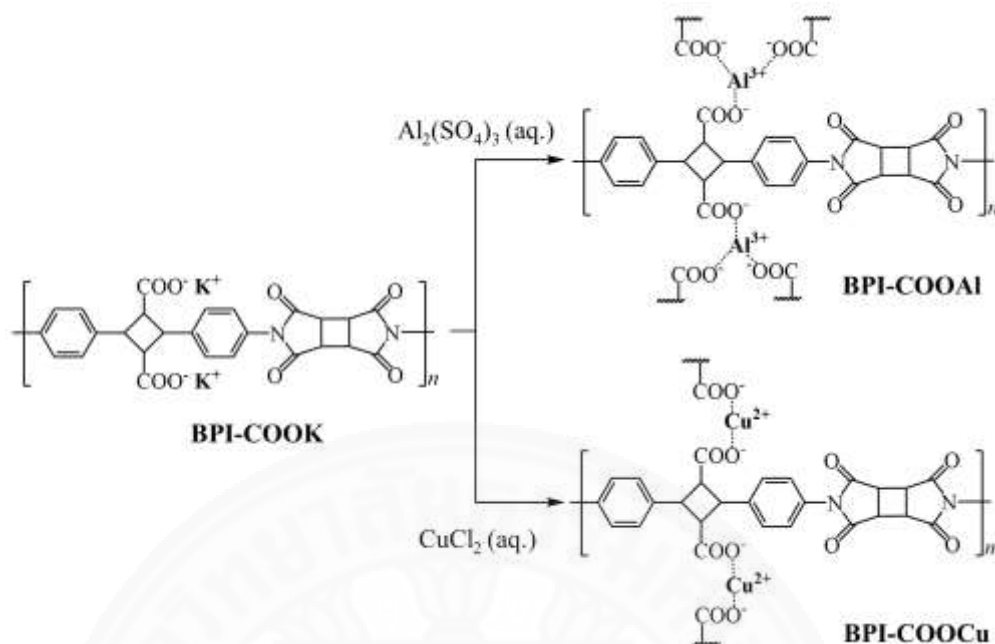
### 3.9 Removal of copper and aluminium by BPI-metal complexation

#### 3.9.1 BPI-metal complexation kinetics and thermodynamic

A glucose-based biopolyimide (BPI) was synthesized and bought from Japan Advanced Institute of Science and Technology. The BPI was synthesized to be fibril with potassium attached (BPI-COOK). The BPI-metal complexation scheme is shown in **Figure 3.3**. The BPI-COOK fibril was dissolved in water to produce a viscous 50 g/L solution. The solution was cast onto a glass substrate and dried at 40 °C on a hot plate. The resulting film had a thickness of  $0.13 \pm 1$  mm. A BPI-COOK film sample was cut to have dimensions of 200 × 500 mm. The metal solutions were prepared with  $\text{Al}_2(\text{SO}_4)_3 \cdot 18\text{H}_2\text{O}$  and  $\text{CuCl}_2 \cdot 2\text{H}_2\text{O}$ . The complexation equilibrium time was determined by the kinetic experiment of BPI-COOK film submersion in 1 mol/L metal ion ( $\text{Al}^{3+}$  and  $\text{Cu}^{2+}$ ) solution for 0 – 120 min. The metal ion concentration left in the solution after the complexation was quantified. Equation (3.7) is used to determine the metal removal (%).

$$\text{Metal removal (\%)} = [(C_i - C_e)/C_i] \times 100 \quad (3.7)$$

where the parameters and their definitions are the same as those of Equation (3.1). However, in this case,  $C$  represent the metal ion concentration.  $C_i$  is the initial metal ion concentration (mol/L), and  $C_e$  is the metal ion concentration left in the solution after complexation (mol/L). The equilibrium time was taken from a plot of metal removal over time, where the metal removal is stable.



**Figure 3.3** BPI-COOAl and BPI-COOCu syntheses

An equilibrium time of 30 min (refer to Results & discussion section) was used to observe the metal complexation in different metal ion concentrations. A BPI-COOK film sample was submerged into 10 ml of 0.5, 1, 2, 4, and 6 mol/L metal ion solutions. BPI-COOAl and BPI-COOCu were obtained. Depending on the concentration, the film was dissolved in the metal solution, and/or a precipitate was formed. The separation of the solution and precipitate was done by a filter paper (Whatman™ 11 μm pore). If the film of BPI-COOAl and BPI-COOCu formed without precipitation, they were removed from the solution directly. The complexes were washed with DI water, dried in an oven, and used for further characterization. The metal ions were quantified using inductively coupled plasma atomic emission spectroscopy (ICP-OES, Avio 200, PerkinElmer). The ICP-OES was set up as follows: 1.50 mL/ min peristaltic pump and auto-autosampler flow rate (with autosampler washed between every sample), 20 s flush time, and 30 s normal time.

The thermodynamic properties for the metal complexation were measured under a temperature-controlled environment of 298.15 – 338.15 K (25 – 65 °C), using a closed incubator (NB205-V, N-BIOTEK). The thermodynamics values were determined for the complexation with the metal solution with Al<sup>3+</sup> and Cu<sup>2+</sup>

concentrations of 0.05 – 6 mol/L. The amount of metal bound to a unit of BPI,  $q$  (mol/g), and the metal concentration in the final solution,  $C_e$  (mol/L), were obtained. The thermodynamic parameters were obtained from the linear plot of Equation (2.3) and the calculation of Equation (2.1) In this case the equilibrium constant  $K_{eq}$  was used. The calculation of  $K_{eq}$  for BPI-COOAl and BPI-COOCu are depicted in Equation (3.8) and (3.9), respectively.

$$K_{eq} = \frac{[\text{BPI-COOAl}]^6}{[\text{BPI-COO}^{2-}]^3[\text{Al}^{3+}]^2} \quad (3.8)$$

$$K_{eq} = \frac{\text{BPI-COOCu}}{[\text{BPI-COO}^{2-}][\text{Cu}^{2+}]} \quad (3.9)$$

### 3.9.2 BPI-metal complex characterization

To analyze the changes in the functional groups after metal complexation, reflection infrared spectra were obtained using a FTIR from 400 to 4000  $\text{cm}^{-1}$ . BPI-COOAl and BPI-COOCu from the complexation using 0.5, 1, and 2 mol/L metal ion were analyzed. BPI-COOH and BPI-COOK were also analyzed for comparison.

The study of the metal oxidation state and the local structure in the BPI-metal complex were done using XAS at Beamline 5.2. The electron energy was 1.2 GeV. Due to the unavailability of the energy for Al in the facility, only BPI-COOCu was subjected to this analysis. The resulted complexes of BPI-COOCu from 0.5, 1, and 2 mol/L  $\text{Cu}^{2+}$  were analyzed. XAS spectra were recorded by setting Cu as the probe element (K-edge at 3609 eV). The Silicon (110) double crystals were utilized as a monochromator with the transmission mode applied for the XANES and extended EXAFS. For EXAFS, the structure of  $\text{CuH}_2(\text{CO}_2)_2$  was used as the fitting reference. The probable structure of BPI-COOCu was illustrated using ChemDraw Professional 16.0 (PerkinElmer).

To minimize the metal waste, 1 mol/L metal ion solutions were used to create BPI-metal films for further characterization unless stated otherwise (refer to the RESULTS AND DISCUSSIONS section for more information on the minimum metal ion concentration of film complexation).



BPI-COOAl and BPI-COOCu films and their respective char residues were analyzed by XPS (Shimadzu Kratos AXIS-ULTRA DLD instrument, Kratos) equipped with monochromatic Al-K $\alpha$  radiation. The technique helped in the investigation of metal form found in BPI films and determination if the films were suitable as flame retardant materials after metal removal. The changes in the metal oxidation before and after burning were observed. The char residue was created by burning the films in an open-air oven at 800 °C. The sample weight was  $0.1 \pm 0.01$  g.



## CHAPTER 4

### RESULTS AND DISCUSSION

The screening test for bio-based adsorbents were performed. Only the ones which possessed desirable performance were studied for detailed  $I^-$  adsorption and characterization.  $IO_3^-$  adsorption was also performed with anthocyanin-containing adsorbents while BPI salt complexes were created as the results of  $Al^{3+}$  and  $Cu^{2+}$  removal. In this section, the results of selected cations and anions removal by bio-based adsorbents are presented and discussed.

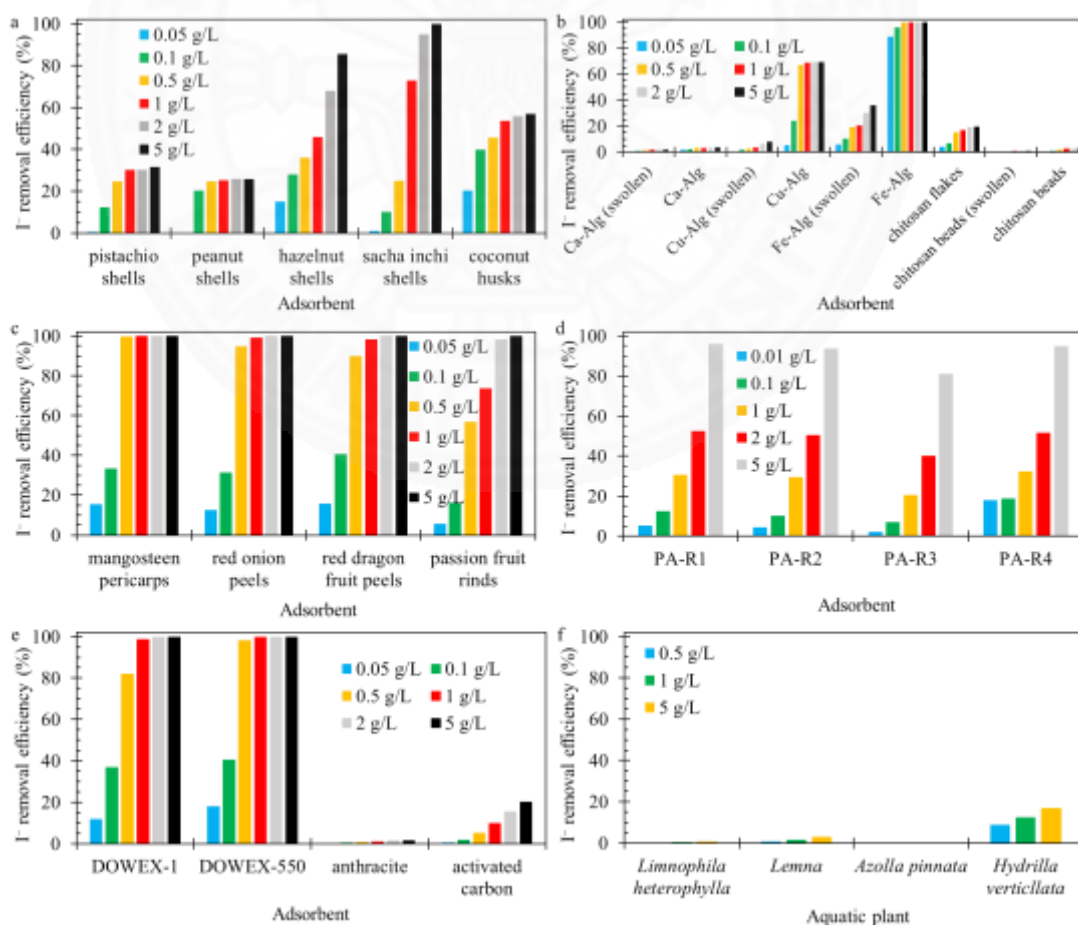
#### 4.1 Screening test and adsorbent doses for iodide adsorption

The screening test for  $I^-$  removal was performed with various adsorbents and doses. The results of the screening test are displayed in **Figure 4.1**. The results of seed shells and husks are shown in **Figure 4.1a**. In 2 h, the hazelnut shells removed about 70% and 85%  $I^-$  at doses of 2 and 5 g/L, respectively. The sacha inchi shells, with a 5 g/L dose, have 100% efficiency. At a longer contact time, hazelnut shells and sacha inchi shells had higher efficiency. **Figure 4.1b** shows that 0.1 g/L Fe-Alg could remove more than 95% of the  $I^-$  in the water, while higher doses yielded 100% efficiency. The Fe-Alg adsorbent was observed to outperform the commercial anion-exchange resins (DOWEX-1 and DOWEX-550), which started to reach a maximum efficiency of 100% at 1 g/L (**Figure 4.1e**). For the anthocyanin-based adsorbents shown in **Figure 4.1c**, 0.5 g/L dose of mangosteen pericarps and red onion peels could remove more than 90% of  $I^-$  surpassing the efficiency of anion-exchange resins. More than 90% of  $I^-$  removal from the solution was observed for 2 and 5 g/L dose of red dragon fruit peels and passion fruit rinds, respectively. At 2 g/L, all cationic biopolyamides can remove up to 50% of the 10 mg/L  $I^-$  in water (**Figure 4.1d**). At 5 g/L, PA-R1, PA-R2, and PA-R4 tend to remove 92 – 95%, while PA-R3 can remove 80% of the same  $I^-$  concentration (**Figure 4.1d**).

From the screening test, some of the adsorbents were selected for detailed adsorption experiment and characterization. For Fe-Alg, mangosteen pericarps, and red onion peels, 0.5 mg/L dose was selected. The optimum dose of 2 g/L was chosen for hazelnut shells, sacha inchi shells and red dragon fruits peels. A 5 g/L dose was assigned to all cationic biopolyamides and passion fruits rinds. Only Dowex-550 was used as a

reference in some of the experiments that were deemed appropriate. The resin optimum dose was decided as 0.5 g/L.

Pistachio shells, peanut shells, coconut husks, Ca-Alg (swollen and non-swollen), Cu-Alg (swollen and non-swollen), Fe-Alg (swollen), chitosan flake, chitosan beads (swollen), chitosan beads, anthracite, and activated carbon could not reach 80% efficiency at all doses including the water plants in **Figure 4.1f**. Thus, they were not used for further experiments. The swollen Fe-Alg, at all doses, was observed to adsorb  $I^-$  at less than 40%. This was due to the presence of water in the complex, which trapped  $Fe^{3+}$  and prevented its interaction with  $I^-$  (Serrano-Aroca et al., 2017). For the other metal-alginate complexes,  $Ca^{2+}$  and  $Cu^{2+}$  may exhibit less  $I^-$  attraction when compared to  $Fe^{3+}$  due to a lower positive charge. The other adsorbents, such as chitosan flakes, pistachio shells, peanut shells, and coconut husks, may not contain cationic functional groups for  $I^-$  removal.



**Figure 4.1** Screening test for various adsorbent doses with 10 mg/L  $I^-$  initial concentration for 2 h at room temperature (a) seed shells and husks, (b) bio-based and metal-based synthetic materials, (c) anthocyanin-containing adsorbents, (d) cationic biopolyamides, (e) commercial adsorbents, (f) living plants

## 4.2 Material characterization for iodide adsorption

### 4.2.1 Surface morphology

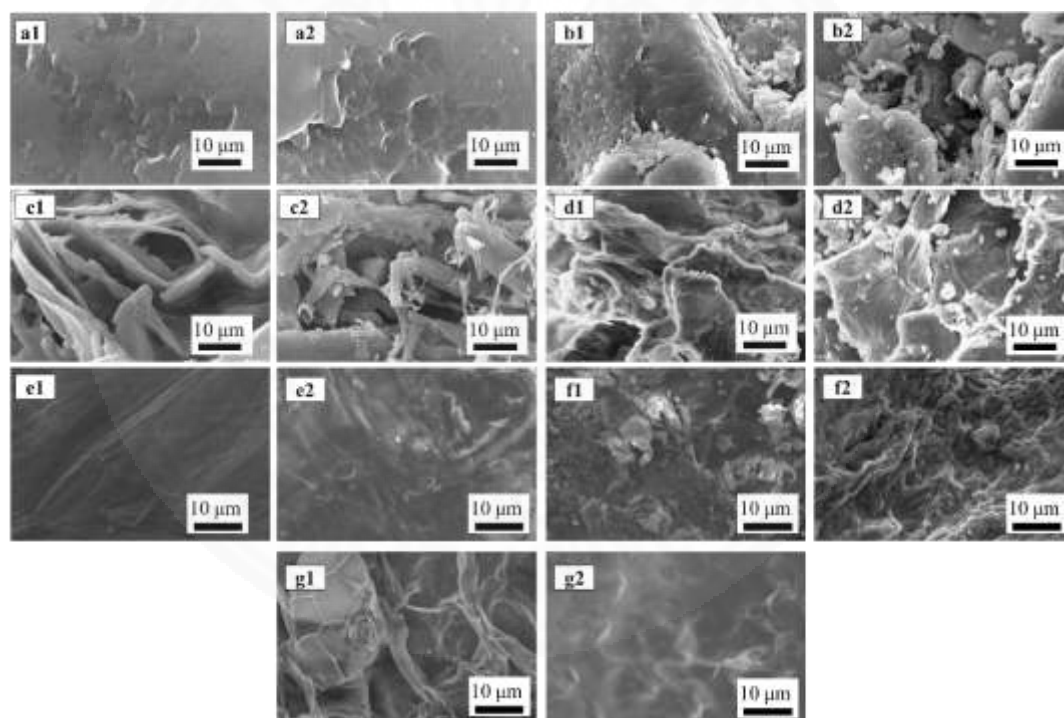
Only the anthocyanin-containing adsorbents were analyzed with  $N_2$  adsorption/desorption technique. The comparison of adsorbents surface and pore characteristics can be found in **Table 4.1**. The BET surface area of all the anthocyanin-containing adsorbents was lower than  $1 \text{ m}^2/\text{g}$ . The total pore volume values were in the range of  $1 \times 10^{-3}$  to  $4 \times 10^{-3} \text{ cm}^3/\text{g}$  with no micropores detected. The characteristics were similar to the raw materials that did not go through carbonization and activation processes (Pathak et al., 2017). From these results, we can infer that the surface area is not the main factor of the  $I^-$  adsorption in these adsorbents. Presence of the specific functional groups plays a more important role in the biosorption of  $I^-$  by the anthocyanin-containing adsorbents. This fact was later proven in the results of adsorption (Chapter 4.3). The mangosteen pericarps possessed the lowest BET surface at  $0.439 \text{ m}^2/\text{g}$  (**Table 4.1**) but yielded the highest  $I^-$  adsorption efficiency.

**Table 4.1** Comparison of surface and pore characteristics for the anthocyanin-containing adsorbents

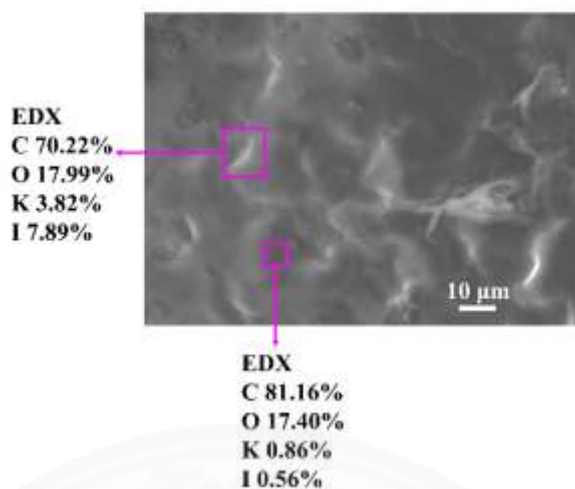
Adsorbent	BET surface area ( $\text{m}^2/\text{g}$ )	Total Pore Volume (DFT method) $\text{cm}^3/\text{g}$	t-plot micropore volume
Mangosteen pericarps	0.439	0.00281	n.d.
Red onion peels	0.622	0.00353	n.d.
Red dragon fruit peels	0.665	0.00142	n.d.
Passionfruit rinds	0.570	0.00186	n.d.

n.d. – not detected

The SEM images before and after  $I^-$  adsorption of all adsorbents show visible surface changes (**Figure 4.2**). The surface of Fe-Alg, hazelnut shells, sacha inchi shells, mangosteen pericarps, red onion peels, and red dragon fruit peels after the adsorption were observed to be more irregular. A similar morphological alteration was reported for a polymer-silver chloride hybrid material, after  $I^-$  adsorption (H. Zhang et al., 2013). Unlike the other adsorbents where  $I^-$  appeared to be adsorbed throughout the surface, the passion fruit rinds only attracted  $I^-$  on some parts of its surface. The white composite indicates the existence of  $I^-$  clusters in the passion fruit peels. This was confirmed by the EDX analysis, and the results are shown in **Figure 4.3**. The same phenomena of  $I^-$  clusters were also observed on the surface of cuprite (Lefèvre et al., 2000).



**Figure 4.2** SEM images of bio-based adsorbents. (a) Fe-Alg, (b) hazelnut shells, (c) sacha inchi shells, (d) mangosteen pericarps, (e) red onion peels, (f) red dragon fruit peels, (g) passion fruit rinds (1 – virgin adsorbent, and 2 – saturated adsorbent)



**Figure 4.3** SEM-EDX analysis showing the elemental composition on different parts of the passion fruit peels

#### 4.2.2 Chemical composition

**Table 4.2** shows the elemental composition before and after  $I^-$  adsorption. All adsorbents had an increased iodine mass percentage after being left in contact with  $I^-$ . Iron (Fe) was calculated to be more than 40%, becoming the dominant species in Fe-Alg. Fe was bound to the alginate through metal-carboxylate interactions, which formed an egg-box model (Li et al., 2007; Nestle and Kimmich, 1996). For hazelnut shells and sacha inchi shells, the EDX analysis detected magnesium (Mg), potassium (K), and calcium (Ca). These compositions were due to the natural cationic mineral constituents that are present in these bio-based adsorbents (Gutiérrez et al., 2011; Lopes et al., 2012). The cationic nature of these adsorbents was potentially responsible for attracting  $I^-$ . A higher reduction of sodium (Na) and K than those of their divalent counterparts were observed. This suggested that the adsorption of  $I^-$  may have a more visible effect on Na and K.

For the anthocyanin-containing adsorbents, the elemental composition reported the replacement of chlorine after the adsorption, and this may suggest an ion-exchange mechanism between  $Cl^-$  and  $I^-$ . EDX was done with accelerated  $I^-$  exposure, and the final iodine composition were 15.9, 13.0, 5.93, and 6.99% for mangosteen pericarps, red onion peels, red dragon fruit peels, and passion fruit rinds, respectively (**Table 4.2**). Among the anthocyanin-containing adsorbents, the mangosteen pericarps contained the highest amount of anthocyanin, and it exhibited the highest iodine composition after

the adsorption. The EDX results emphasized the correlation between the anthocyanin contents and  $I^-$  adsorption.

**Table 4.2** EDX analysis showing the elemental composition of the virgin and  $I^-$  saturated bio-based adsorbents

Adsorbent	Elemental Composition											
	C	O	N	Mg	K	Na	Ca	S	Fe	Cl	I	total
Before $I^-$ adsorption												
Fe-Alg	16.5	27.3	0	0	0	0	0	0	46.2	10.1	0.0	100
hazelnut shells	53.6	39.4	0	3.40	1.50	0.20	2.0	0	0.0	0.0	0.0	100
sacha inchi shells	48.2	33.2	0	9.30	6.40	0.0	2.80	0	0.1	0.0	0.0	100
mangosteen pericarps	38.4	41.8	3.20	0	1.29	0	0	0	0	15.4	0	100
red onion peels	43.2	45.7	0	0.57	0.33	1.26	0	0	0	9.01	0	100
red dragon fruit peels	19.3	55.9	0	0.89	16.2	3.18	0	0	0	4.48	0	100
passion fruit rinds	50.8	37.1	0	0.18	4.41	0.43	0.33	0	0	6.75	0	100
After $I^-$ adsorption												
Fe-Alg	14.4	21.1	0	0	0	0	0	0	40.3	4.10	20.2	100
hazelnut shells	51.8	37.9	0	3.10	1.20	0.20	1.60	0	0	0	4.2	100
sacha inchi shells	43.7	31.1	0	8.2	4.30	0	2.70	0	0	0	10.1	100
mangosteen pericarps	40.1	35.4	3.06	0	5.59	0	0	0	0	0	15.9	100
red onion peels	52.2	29.2	0	0	4.69	0.84	0	0	0	0	13	100

red dragon fruit peels	48.1	40.4	0	0.27	4.78	0.51	0	0	0	0	5.93	100
passion fruit rinds	69.8	20.1	0	0	3.14	0	0	0	0	0	6.99	100

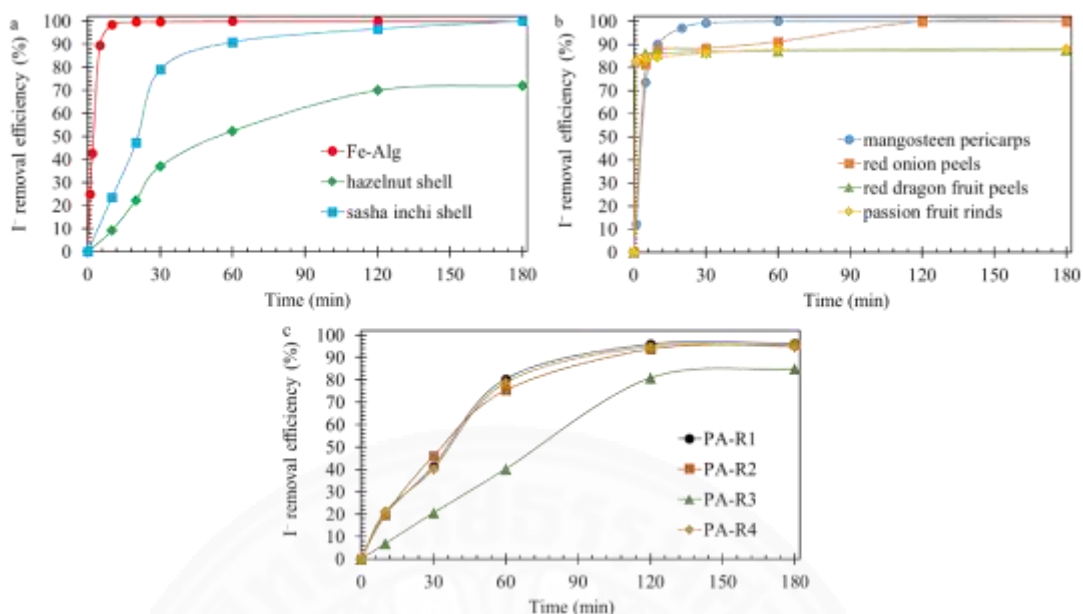
### 4.3 Iodide adsorption study

#### 4.3.1 Adsorption kinetics and pseudo-order reactions

The results of  $I^-$  removal efficiency (for 180 min) are displayed in **Figure 4.4**. Fe-Alg and sachu inchi shells showed 100% removal efficiency. Within 10 min, Fe-Alg could remove more than 99% of the  $I^-$  and became stable at about 30 min while anion-exchange resin took 180 min to adsorb the same amount of  $I^-$ . Sachu inchi shells reached equilibrium at about 120 min. Hazelnut shells showed a maximum of 72%  $I^-$  removal with a 120-min equilibrium time. A 100%-efficiency was achieved for the mangosteen pericarps and red onion peels at about 30 and 120 min, respectively. Red dragon fruit peels and passion fruit rinds possessed nearly 90% efficiency with an equilibrium time of about 60 min. For the cationic biopolyamides, the equilibrium time of contact was determined to be approximately 120 min. PA-R1, PA-R2, and PA-R4 showed a similar  $I^-$  removal pattern, with nearly 100% at equilibrium. PA-R3  $I^-$  adsorption efficiency reached the equilibrium within the same duration but with a lower efficiency (almost 80%). The lower efficiency of PA-R3, compared to that of other BPA, may be due to its lower  $M_w$ . The molecular weight may affect the physical adsorption of  $I^-$ , such that at a low concentration, a higher molecular weight polymer allows for more coiling of polymer chains, leading to entrapment of more  $I^-$  (Janardhan et al., 1990).

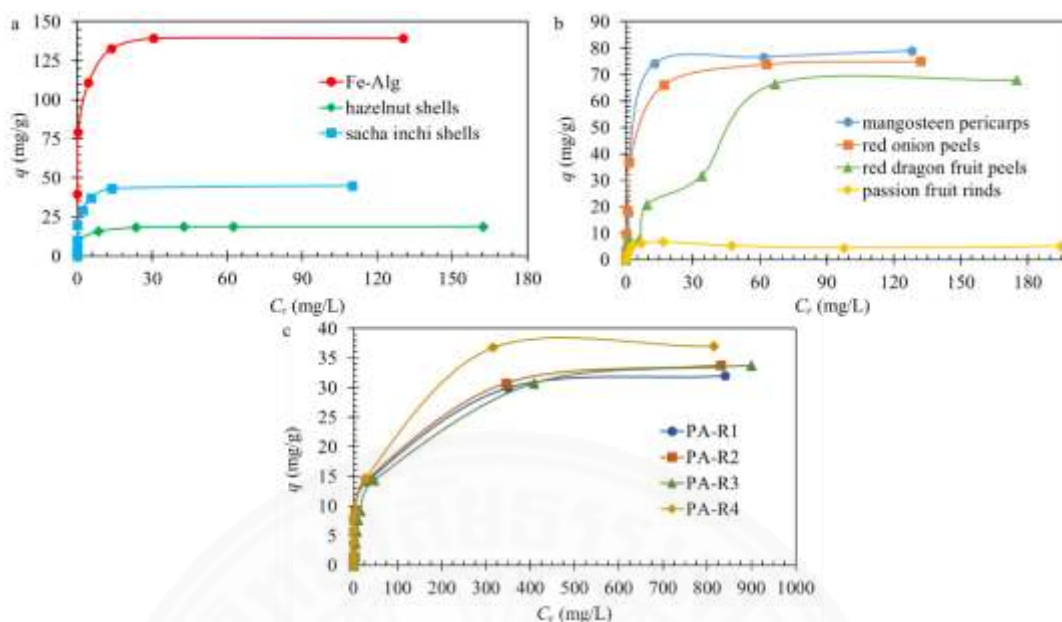
After 8 day contact time, Fe-Alg, hazelnut shells, sachu inchi shells, mangosteen pericarps, passion fruit rinds and all cationic biopolyamides retained the maximum  $I^-$  efficiency for a 10 mg/L initial  $I^-$  concentration. This confirmed that no leaching occurred of the adsorbed  $I^-$ . On the other hand, about 8% and 20% of  $I^-$  were desorbed from red onion peels and red dragon fruit peels, respectively.





**Figure 4.4** Kinetic study showing I<sup>-</sup> removal efficiency (%) for 180 min with optimum adsorbent dose and 10 mg/L I<sup>-</sup> initial concentration at room temperature. (a) Fe-Alg, hazelnut shells, and sacha inchi shells, (b) anthocyanin-containing adsorbents, (c) cation biopolyamides

The concentration-dependent adsorption is represented by the plots of  $q$  vs.  $C_e$ , as presented in **Figure 4.5**. Fe-Alg and sacha inchi shells had maximum experimental  $q$  values of about 139 and 48.4 mg/g, respectively. The hazelnut shells possessed a lower  $q$  value of 18.9 mg/g. For the anthocyanin-containing adsorbents, 79.0, 75.0, 68.0, and 10.0 mg/g were yielded as adsorption capacities of mangosteen pericarps, red onion peels, red dragon fruit peels, and passion fruit rinds, respectively. The low  $q$  value of passion fruit rinds might be due to its low anthocyanin content. PA-R4 possessed 37.0 mg/g adsorption capacity and became the cationic biopolyamides with the highest  $q$  value. PA-R1, PA-R2, and PA-R4 had 32.0, 33.8, and 20.0 mg/g as their maximum  $q$ , respectively. Some of the important results such as optimum dosage, equilibrium time, I<sup>-</sup> removal efficiency at the equilibrium time and after an 8-day contact, and maximum experimental  $q$  values are tabulated in **Table 4.3**.



**Figure 4.5** Batch experiment showing adsorption capacity,  $q$  (mg/g) over final  $I^-$  concentration,  $C_e$  (mg/L) with optimum adsorbent dose and equilibrium time. (a) Fe-Alg, hazelnut shells, and sacha inchi shells (2 – 200 mg/L initial  $I^-$  concentration), (b) anthocyanin-containing adsorbents (2 – 200 mg/L initial  $I^-$  concentration), (c) cation biopolyamides (5 – 1000 mg/L initial  $I^-$  concentration)

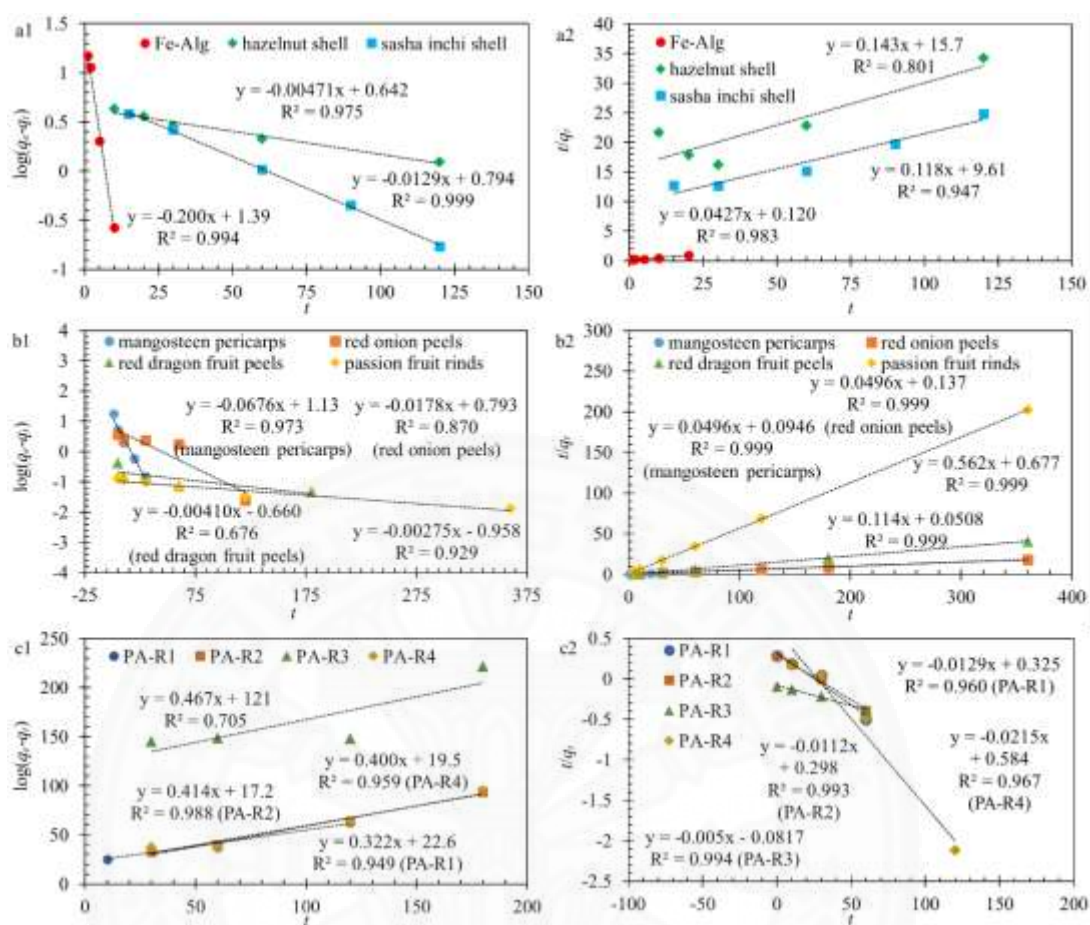
**Table 4.3** Summary of  $I^-$  adsorption experiment values, 8-day efficiency, and experimental adsorption capacity

Adsorbent	Optimum Dosage (g/L)	Equilibrium Time (min)	$I^-$ removal efficiency (%) <sup>a</sup>	$I^-$ removal efficiency after 8 days (%) <sup>a</sup>	Maximum experimental $q$ (mg/g)
Fe-Alg	0.5	30	>99.0	>99	139
hazelnut shells	2	120	72.0	72.0	18.9
sacha inchi shells	2	120	>99	>99	48.4
mangosteen pericarps	0.5	30	>99	>99	79.0

red onion peels	0.5	120	>99	>99	75.0
red dragon fruit peels	2	60	90	82	68.0
passion fruit rinds	5	60	90	70	10.0
PA-R1	5	120	>99	>99	32.0
PA-R2	5	120	>99	>99	33.8
PA-R3	5	120	80	80	20.0
PA-R4	5	120	>99	>99	37.0

<sup>a</sup>Experiment was conducted with 10 mg/L initial  $I^-$  concentration

The linear fittings of pseudo-first-order [Equation (2.14)] and pseudo-second-order [Equation (2.16)] reactions are shown in **Figure 4.6** with important calculated parameters tabulated in **Table 4.4**. Some of the data points close to equilibrium were omitted to avoid biasness, as suggested by a study (Simonin, 2016). According to the values of  $R^2$ , the rate-limiting step in adsorption processes for Fe-Alg, hazelnut shells, sacha inchi shells, and all cationic biopolyamides were better explained by the pseudo-first-order reaction. The pseudo-first-order reaction in Equation (2.14) was integrated by a reaction of an order higher than 1, which is supposedly dependent on more than one reactant. However, only one of the reactants was considered and another was neglected as an excess reactant (Schwarzenbach et al., 2002). By default, the term “physisorption” was given as the underlying rate-limiting step process, in which only one reactant was considered. As a result, the adsorption of  $I^-$  by these adsorbents was more likely to be governed by physisorption processes. On the other hand, the rate-limiting step of  $I^-$  adsorption by anthocyanin-containing adsorbents was better explained by chemisorption. This is due to their results fitted better with the pseudo-second-order model.



**Figure 4.6** Linear fits of pseudo-order-reaction. (a) Fe-Alg, hazelnut shells, and sacha inchi shells, (b) anthocyanin-containing adsorbents, (c) cation biopolyamides (a1, b1, c1 – first-order; a2, b2, c2 – second-order)

**Table 4.4** Derived parameters of the linear fitting pseudo-order reactions

Adsorbents	pseudo-first-order reaction <sup>a</sup>			pseudo-second-order reaction <sup>b</sup>		
	$k_t$ (L/min)	$Q_e$ (mg/g)	$R^2$	$k_2$ (g/mg/m in)	$Q_e$ (mg/g)	$R^2$
Fe-Alg	0.461	24.5	0.994	$7.33 \times 10^{-3}$	29.7	0.957
hazelnut shells	0.0108	4.39	0.975	$1.30 \times 10^{-3}$	7.0	0.801

sacha inchi shells	0.0297	6.22	0.999	$1.45 \times 10^{-3}$	8.47	0.947
mangosteen pericarps	0.152	7.28	0.973	0.104	5.04	0.999
red onion peels	2.0	6.21	0.870	0.0716	5.10	0.999
red dragon fruit peels	$9.44 \times 10^{-3}$	0.219	0.676	0.0560	5.04	0.999
passion fruit rinds	$6.22 \times 10^{-3}$	0.110	0.929	0.0187	44.4	0.999
PA-R1	0.0297	2.11	0.960	$4.59 \times 10^{-3}$	3.11	0.949
PA-R2	0.0258	1.99	0.993	$9.96 \times 10^{-3}$	2.42	0.988
PA-R3	0.0115	0.829	0.994	$1.80 \times 10^{-3}$	2.14	0.705
PA-R4	0.0495	3.84	0.967	$8.21 \times 10^{-3}$	2.50	0.959

<sup>a</sup>Equation (2.14), <sup>b</sup>Equation (2.16)

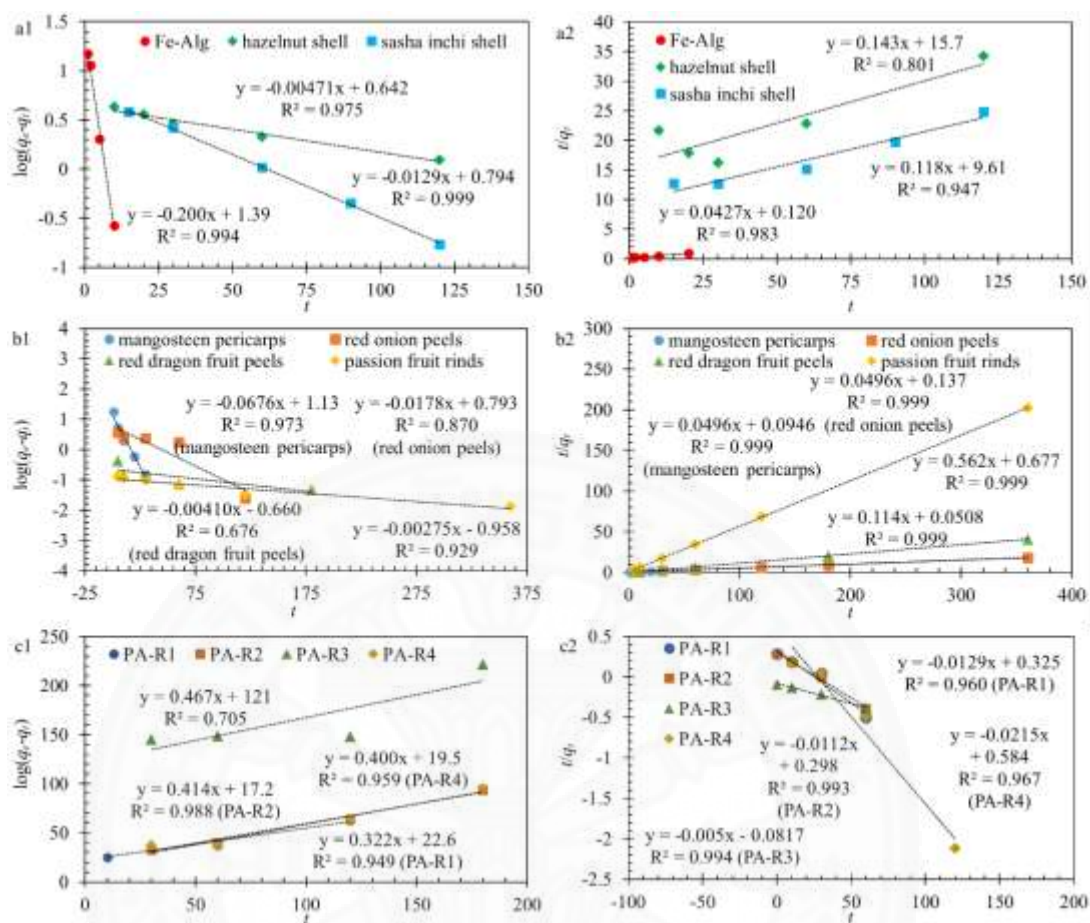
#### 4.3.2 Isotherms

The linear fits of the Langmuir and Freundlich models [calculated by Equation (2.8) and (2.10)] are displayed in **Figure 4.7**. Derived parameters for isotherm models can be found in **Table 4.5**. The Langmuir model produced better fits ( $R^2 = 0.997 - 0.998$ ) for all the adsorbents except for the red dragon fruit peel. The isothermal process describes the equal energy of all adsorption sites where the interactions between neighboring adsorbed molecules were neglected (Delle Site, 2001; Hamdaoui and Naffrechoux, 2007). This may be true for Fe-Alg, in which the attraction by  $Fe^{3+}$  was regarded as the main mechanism, while the anthocyanin is the main functional group responsible for the anthocyanin-containing adsorbents. The calculation with Langmuir model ( $q_{max}$ ) yielded the maximum adsorption capacities of 140, 18.8, and 45.0 mg/g for Fe-Alg, hazelnut shells, and sacha inchi shells, respectively. Except the passion fruit

rinds, the anthocyanin-containing adsorbents had more than 70 mg/g  $q_{max}$  value with the highest predicted  $q_{max}$  of 79.4 mg/g in the mangosteen pericarps. The Langmuir model revealed that PA-R4 possessed the highest  $q_{max}$  value (37.6 mg/g) among the cationic biopolyamides. The values of  $q_{max}$  calculated from the Langmuir model are similar to those of the experimental  $q$  (**Figure 4.5**).

The log-transformed results of sachu inchi shells also fit the Freundlich model, with  $R^2$  values of more than 0.950 (**Figure 4.7c**). The model considered the difference in energy for different adsorption sites. This could be from the effects of  $I^-$  attraction by different cation species on the surface of the adsorbents (Delle Site, 2001; Hamdaoui and Naffrechoux, 2007).  $n$  values of higher than 1 (**Table 4.5**) suggested that the increase in  $I^-$  concentration enhanced the adsorption free energy of sachu inchi shells at all sites for further sorption.

With the kinetic experiment, batch concentration studies, and isothermal models fittings, Fe-Alg became the most efficient bio-based synthetic adsorbent for removing  $I^-$ . On the other hand, mangosteen pericarps removed the highest amount of  $I^-$  when compared with the other minimal-processing adsorbents. Fe-Alg still offered the highest  $I^-$  removal efficiency as compared with all other adsorbents. This is maybe due to strong  $I^-$  attraction by  $Fe^{3+}$ . However, the overall performance of all the adsorbents was needed to be assessed in different water condition.



**Figure 4.7** Linear fits of isothermal models. (a) Fe-Alg, hazelnut shells, and sacha inchi shells, (b) anthocyanin-containing adsorbents, (c) cation biopolyamides (a1, b, c1 – Langmuir; a2, b2, c2 – Freundlich)

**Table 4.5** Derived parameters of the linear fitting isotherm models

Adsorbents	Langmuir isotherm <sup>a</sup>			Freundlich isotherm <sup>b</sup>		
	$K_L$ (L/g)	$q_{max}$ (mg/g)	$R^2$	$K_F$ (mg/g· mg/L) <sup>1/n</sup>	$n$	$R^2$
Fe-Alg	2.72	140	0.999	61.6	3.89	0.875
hazelnut shells	1.81	18.8	0.999	8.59	4.95	0.817
sacha inchi shells	2.39	45.0	0.999	25.5	5.92	0.974
mangosteen pericarps	0.486	79.4	0.997	17.8	2.60	0.8927

red onion peels	0.514	75.8	0.999	16.9	2.61	0.8619
red dragon fruit peels	0.0378	78.7	0.587	6.61	2.17	0.916
passion fruit rinds	0.586	7.38	0.998	3.65	11.1	0.2469
PA-R1	0.0785	32.3	0.998	6.05	3.88	0.949
PA-R2	0.0566	34.1	0.999	4.95	3.31	0.923
PA-R3	0.0279	20.6	0.998	0.756	1.75	0.709
PA-R4	0.0864	37.6	0.998	5.26	3.14	0.891

<sup>a</sup>Equation (2.8), <sup>b</sup>Equation (2.10)

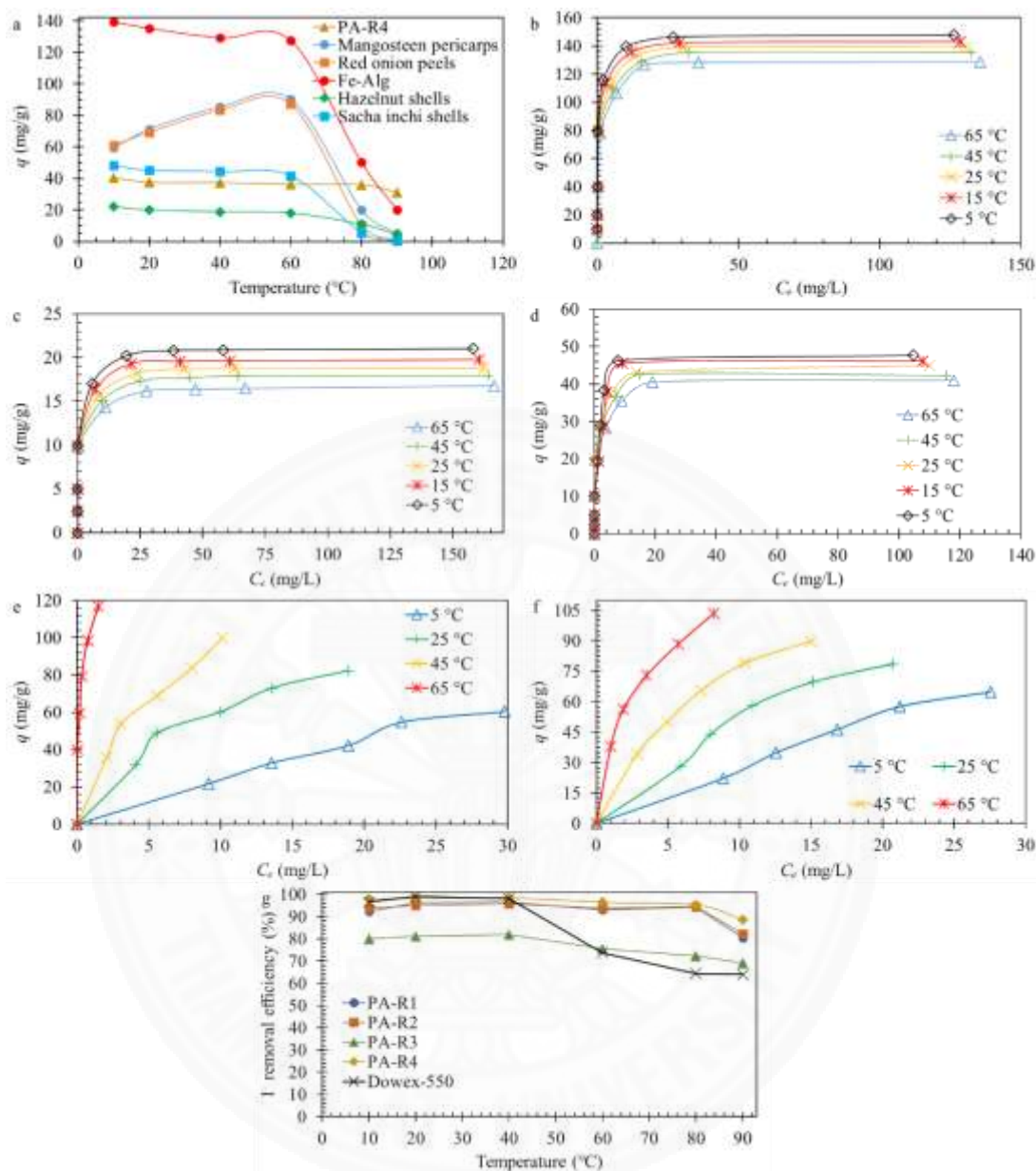
### 4.3.3 Effects of temperature and thermodynamics

**Figure 4.8** exhibits the  $I^-$  adsorption by bio-based adsorbents at different temperature. **Figure 4.8a** reveals that at the temperature 80 – 90 °C, adsorption capacity of all the adsorbents, except for that of PA-R4 dropped significantly (more than 50% of the capacity at room temperature). Even when compared to DOWEX-550, all cationic biopolyamides adsorbed higher amount of  $I^-$  at the temperature more than 60 °C (**Figure 4.8g**). At 20 °C, DOWEX-550 was found to be superior for  $I^-$  adsorption, as it has 100%  $I^-$  removal capacity, while PA-R4  $I^-$  adsorption was up to 98%. An increase in the temperature led to a significant loss in the  $I^-$  adsorption efficiency for the conventional resin. In contrast, the BPA maintained their anion-exchange efficiency throughout the measured temperature range, and the performance began to fall after 80 °C. From 40 °C, except for PA-R3, the  $I^-$  removal efficiency of BPA started to surpass that of DOWEX-550. The lower efficiency of the commercial-grade resin may be attributed to the low thermal stability of the polystyrene resin. According to the literature, the commercial polystyrene resin for water treatment had a  $T_{d10}$  of approximately 100 °C (Ezzeldin et al., 2010). Moreover, the water absorption characteristics of the BPA may increase the  $OH^- (H_2O)_x$  clusters in the complex, subsequently preventing the degradation of quaternary ammonium to further facilitate the uniform adsorption of the dissolved impurities at a higher temperature (Dekel et al., 2017; Monson et al., 2008). This phenomenon was less observed in a polystyrene-based material like Dowex-550, as reported during water immersion tests (Cai et al., 2017).



The adsorption capacities for Fe-Alg, hazelnut shells, and sacha inchi shells were observed to decrease as the temperature increased from 5 to 65 °C (**Figure 4.8b-d**). The phenomenon illustrated an exothermic nature, with heat dissipation during the adsorption process. This was confirmed with the thermodynamic calculation (**Table 4.6**), as  $\Delta H$  values for Fe-Alg, hazelnut shells, and sacha inchi shells were -13.3, -0.0124, and -9.23, respectively. The results of  $\Delta G$  indicated a spontaneous reaction, and  $\Delta S$  for all systems was calculated to be negative, implying a more ordered adsorbed state (Erkey, 2011). From the fitting of Arrhenius equation [Equation (3.3)], the bio-based adsorbents have negative  $E_a$ . The values are displayed in the inset of **Figure 4.9**.  $E_a$  values of less than 40 kJ/mol suggest physisorption processes (Inglezakis and Zorpas, 2012). In addition, negative  $E_a$  was also possible because an adsorbent with physisorption properties may not require activation energy to adsorb on a target solute rapidly (Erkey, 2011). Consequently, the adsorption of  $I^-$  by Fe-Alg, hazelnut shells, and sacha inchi shells was determined to be governed by physical processes. This coincided with the fittings of the pseudo-first-order reaction (**Figure 4.7a1**).

On the contrary, the adsorption capacities for the anthocyanin-containing adsorbents increases as the temperature increase (**Figure 4.8e,f**). The behavior indicated the endothermic and chemisorption nature of the adsorption of  $I^-$  by anthocyanin. This was reconfirmed by the fitting of Arrhenius equation (**Figure 4.9**) which yielded 88.1 and 55.8 kJ/mol of  $E_a$  for mangosteen pericarps and red onion peels, respectively. The results coincided with the fittings of the pseudo-first-order reaction (**Figure 4.7a2**). Therefore, it can be assumed that the  $I^-$  adsorption in the anthocyanin-based adsorbents mainly occurred through chemisorption. It was also noted that a higher intensity of red solution was observed in the experiment with red dragon fruit peels at a higher temperature, which might indicate a loss of more anthocyanin from the adsorbent, leading to lower  $I^-$  adsorption.

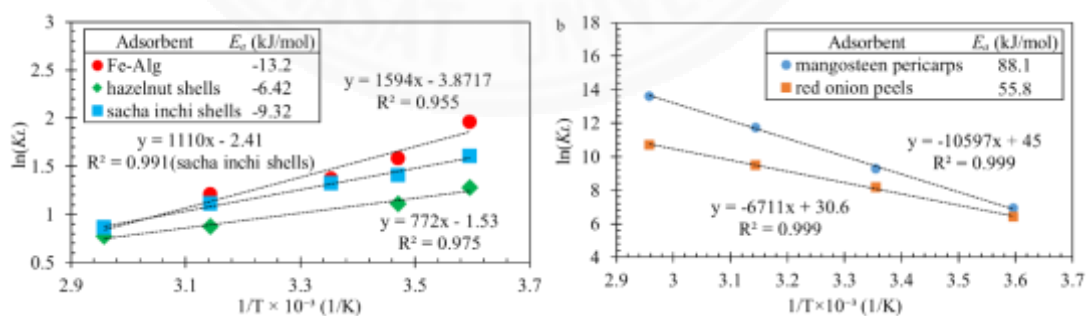


**Figure 4.8** Effects of temperature on  $I^-$  adsorption. (a) overall effects on adsorption capacity, (b) concentration-dependent adsorption of Fe-Alg, (c) concentration-dependent adsorption of hazelnut shells, (d) concentration-dependent adsorption of Sacha inchi shells, (e) concentration-dependent adsorption of mangosteen pericarps, (f) concentration-dependent adsorption of red onion peels, (g)  $I^-$  removal efficiency of cationic biopolyamides with 10 mg/L  $I^-$  initial concentration

**Table 4.6** Thermodynamic parameters of the  $I^-$  adsorption by bio-based adsorbents at 5 – 65 °C

Adsorbent	$T$ ( $^{\circ}\text{C}$ ) <sup>a</sup>	$K_L$ (L/g) <sup>b</sup>	$\Delta H$ (kJ/mol) <sup>c</sup>	$\Delta S$ (kJ/K/mol) <sup>c</sup>	$\Delta G$ (K/mol) <sup>d</sup>
Fe-Alg	5	7.10	-13.3	-0.0322	-4.29
	15	4.87			-3.97
	25	3.95			-3.65
	45	3.35			-3.06
	65	3.32			-2.36
hazelnut shells	5	3.61	-15.2	-0.0124	-2.83
	15	3.03			-2.70
	25	2.64			-2.58
	45	2.40			-2.33
	65	2.17			-2.08
sacha inchi shells	5	4.98	-9.23	-0.0200	-3.67
	15	4.09			-3.47
	25	3.76			-3.27
	45	3.04			-2.87
	65	2.37			-2.47

<sup>a</sup>temperature of  $\text{I}^-$  solution, <sup>b</sup>Langmuir constant calculated by Equation (2.8), <sup>c</sup>change in enthalpy and entropy calculated by Equation (2.3), <sup>d</sup>change in Gibbs free energy calculated by Equation (2.1)



**Figure 4.9** Linear fits of the Arrhenius model. (a) Fe-Alg, hazelnut shells, and sacha inchi shells, (b) mangosteen pericarps and red onion peels (insets - Arrhenius activation energy,  $E_a$ )

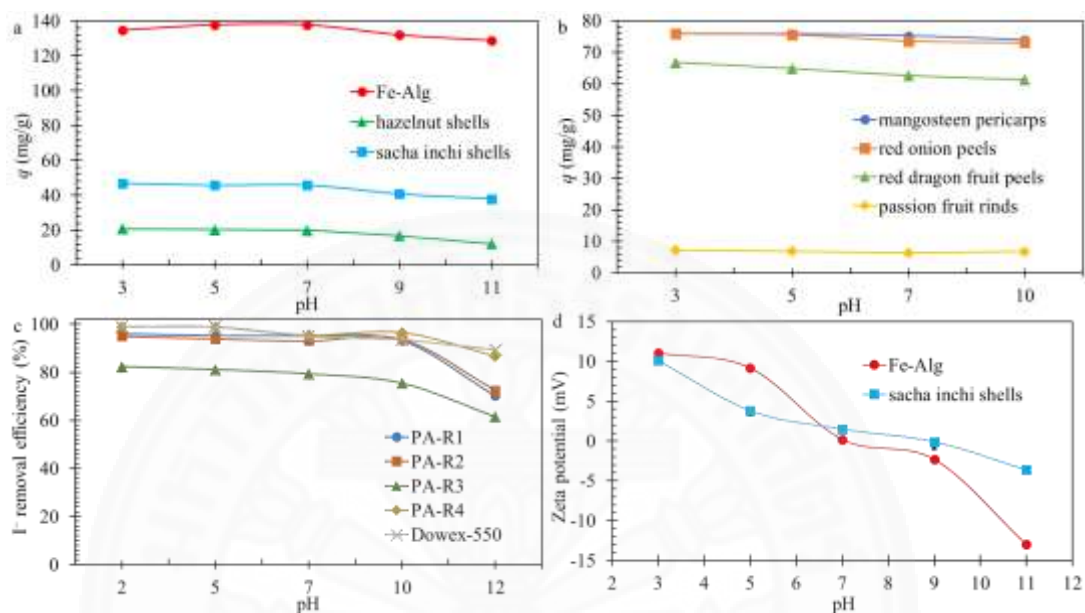
#### 4.3.4 Effects of pH and zeta potential, competitive anions, and regeneration

The effects of pH are depicted in **Figure 4.10**. As the pH increases, the  $I^-$  adsorption capacity is observed to decrease for all the adsorbents. The adsorbents sustained their adsorption capacities until pH 7. At pH 11, the  $q$  values dropped. This may be due to the competition by  $OH^-$  in basic conditions. Decreasing pH maximized the  $I^-$  adsorption. This is due to the variation of the surface charge and functional group activity of the adsorbents (Long et al., 2013). In some cases, it is assumed that at a lower pH, protons could generate a repulsive force that hinders the approach of  $I^-$  anions. Some functional groups are protonated, leaving ionized groups behind that can compete with  $I^-$  (Madrakian et al., 2012). However, in the case of anthocyanin-containing adsorbents, the stability of flavylum cation containing  $O^+$  in acidic conditions promoted the attraction of  $I^-$ , while the form of the functional group in basic conditions did not favor such a mechanism (Oancea and Drăghici, 2013). The stability of the  $q$  value for the passion fruit rinds might be due to the low amount of anthocyanin in the adsorbent, which was not affected by changes in pH.

The results of zeta potential (**Figure 4.10b**) can be used to explain the pH effect in the adsorption of  $I^-$  by Fe-Alg and sacha inchi shells. pH at the point of zero charge ( $pH_{PZC}$ ) for Fe-Alg and sacha inchi shells were 7 and 9, respectively. At  $pH_{PZC}$ , the net charge on the adsorbent surface was equal to zero. This may be due to the addition of  $OH^-$ , which was attracted by the positive charges on the adsorbent surface. At higher pH ( $>pH_{PZC}$ ), the net charge on the adsorbent surface was negative due to the  $OH^-$  layer. This may create repulsion force between the  $OH^-$  layer and  $I^-$ , leading to a decrease in  $q$ . The same adsorption behavior across different pH condition was observed in the adsorption of  $F^-$  by fumarate-based metal-organic frameworks and the removal of microalgae by cationic cassava starch composite (Jangyubol et al., 2018; Ke et al., 2018).

There was a significant difference in an isoelectric charge (IEC), the pH condition in which particles remain stationary. For the sacha inchi shells, IEC was observed to be similar to  $pH_{PZC}$ . On the other hand, IEC of Fe-Alg was observed at about pH 8. This indicates the adsorption of ions other than  $H^+$  and  $OH^-$  during the zeta potential test (Sposito, 1998). At higher pH, there is a possibility for a highly insoluble  $Fe(OH)_4^-$  to form at the surface of the Fe-Alg (Ren et al., 2018). This anion can be

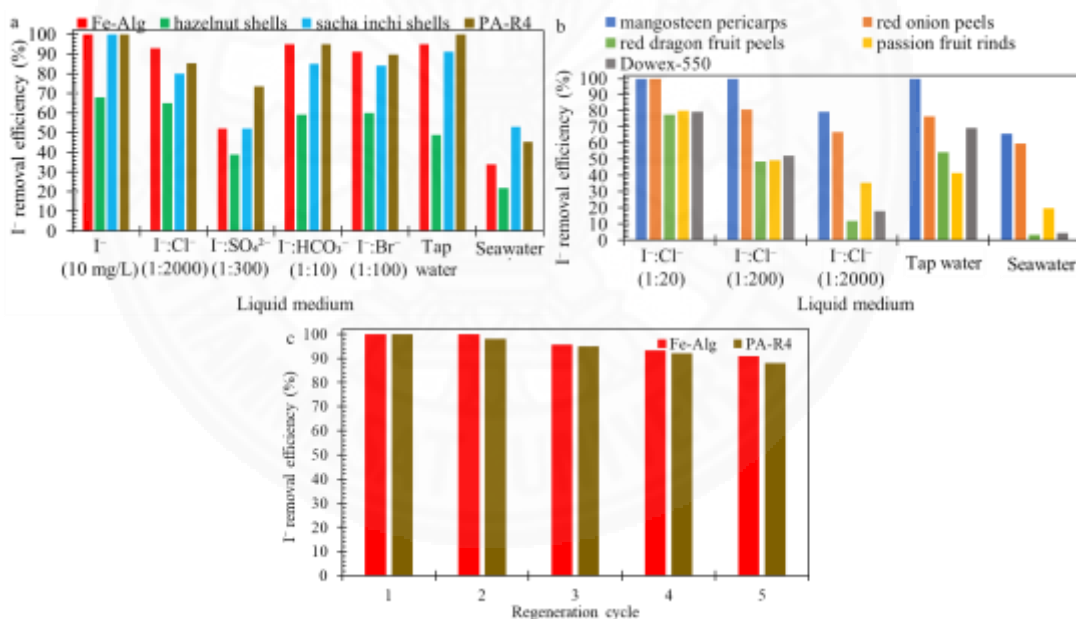
attracted by the remaining  $\text{Fe}^{3+}$  in Fe-Alg. This phenomenon can help to explain a highly unstable zeta potential at pH 9 – 10 (**Figure 4.10d**), and a noticeable decrease in  $q$  value of Fe-Alg at pH 8 onwards (**Figure 4.10a**).



**Figure 4.10**  $\text{I}^-$  adsorption efficiency at various pH (a) Fe-Alg, hazelnut shells, and sachal inchi shells, (b) anthocyanin-containing adsorbents, (c) cation biopolyamides at 10 mg/L initial  $\text{I}^-$  concentration, (d) zeta potential of Fe-Alg and sachal inchi shells

The results of  $\text{I}^-$  removal efficiency in the presence of other anions is exhibited in **Figure 4.11**. The removal efficiency of Fe-Alg, hazelnut shells, sachal inchi shells, and PA-R4 was highly affected by  $\text{SO}_4^{2-}$  (**Figure 4.11a**). This was perhaps due to the higher negative charge of the ion that created a higher attraction toward the adsorbents. In seawater, the  $\text{I}^-$  removal efficiency of Fe-Alg was observed to decrease from 100% to 34%, while sachal inchi shells adsorbed 53% of  $\text{I}^-$  and became the most efficient adsorbent. The other anions in seawater compete for the adsorption sites in sachal inchi shells and hazelnut shells. However, the significant drop in the  $\text{I}^-$  removal efficiency of Fe-Alg was due to the leaching of iron, as the change of solute color was apparent. In seawater conditions, the leaching of inorganic iron could occur by hydrolysis reactions and subsequent precipitation (Rose and Waite, 2003).

**Figure 4.11b** depicts the effects of  $\text{Cl}^-$  on the  $\text{I}^-$  adsorption efficiency of the anthocyanin-containing adsorbents. For  $\text{I}^-:\text{Cl}^-$  (1:20), the mangosteen pericarps and red onion peels were not affected by the addition of  $\text{Cl}^-$ . The other adsorbents could remove about 80% of  $\text{I}^-$  in the solution. When the chloride increases 10-fold, about a 20% reduction in adsorption efficiency was seen in the red onion peels, while the mangosteen pericarps remained unaffected. The other adsorbents have about 50% removal efficiency. For  $\text{I}^-:\text{Cl}^-$  (1:2000), all the anthocyanin-containing adsorbents were affected, but the mangosteen pericarps still maintained the highest adsorption efficiency. The adsorbent was also unaffected by the ions that were present in the tap water. In seawater, low efficiency was expected due to more anion competitors such as bicarbonate and sulfate. Nevertheless, mangosteen pericarps and red onion peels removed more than 50% of  $\text{I}^-$  in seawater.



**Figure 4.11**  $\text{I}^-$  adsorption efficiency in the presence of competitive anions and regeneration cycle at 10 mg/L initial  $\text{I}^-$  concentration. (a) Fe-Alg, hazelnut shells, sacha inchi shells, and PA-R4 in the presence of competitive anions (b) anthocyanin-containing adsorbents in the presence of competitive anions, (c) Fe-Alg and PA-R4 efficiency of 5-cycle regeneration

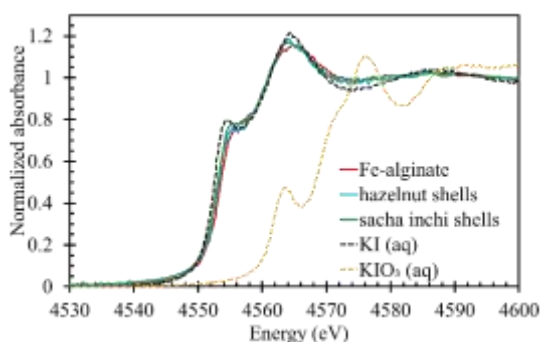
The adsorption-regeneration was assessed for 5 cycles (**Figure 4.11c**). In cycle 2, Fe-Alg still maintained 100%  $\text{I}^-$  removal efficiency, while in cycle 5, the efficiency

decreased to 90.9%. The  $I^-$  adsorption efficiency of PA-R4 was maintained above 90% in the second cycle. After the fifth cycle of regeneration, the  $I^-$  adsorption yielded an efficiency of less than 90%. Each regeneration cycle reduced the adsorption performance, possibly due to a loss of active surface functional groups to the solute (Lata et al., 2015). Moreover, this study only investigated one set of conditions for adsorbent regeneration. By increasing the time or changing the temperature, the  $I^-$  removal performance per regeneration cycle can be improved (Yao et al., 2009).

#### 4.4 Mechanism of iodide adsorption by bio-based adsorbents

##### 4.4.1 Cationic metal species as iodide adsorption functional group

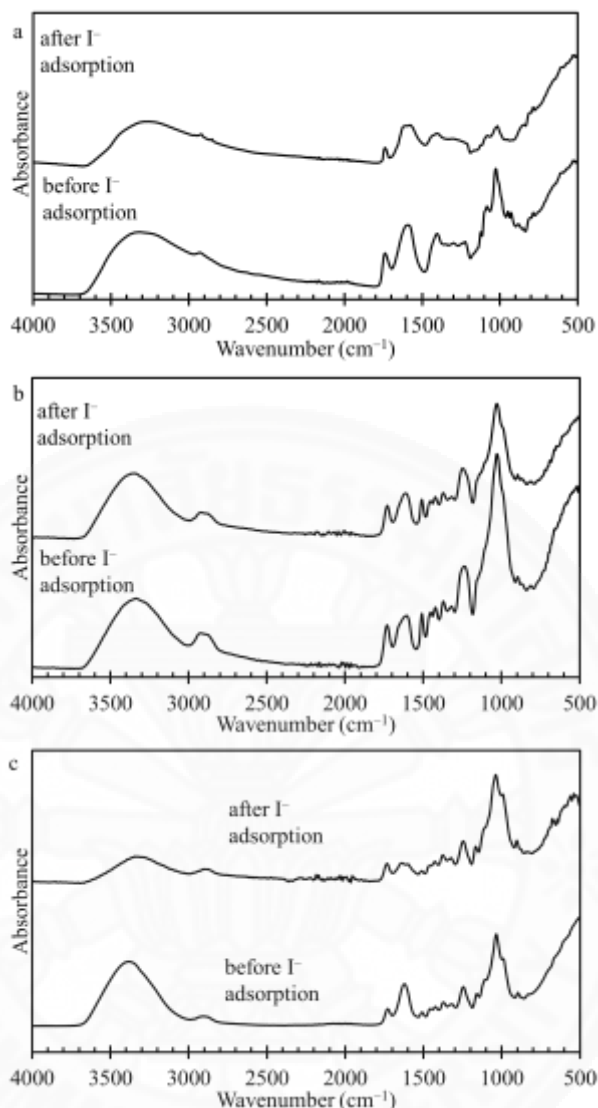
The results of XANES analyses for Fe-Alg, hazelnut shells and sachu inchi shells are presented with a graph of normalized absorbance vs. energy in **Figure 4.12**. The characteristic absorption edges of the iodine species in the bio-adsorbents were 4552.83 – 4553.40 eV. The absorption edges were closer to that of the KI reference at 4552.83 eV than  $KIO_3$  at 4560.77 eV (**Figure 4.12**). This verified that the oxidation state of iodine in the adsorbent was -1 (Yoon et al., 2009). The mechanism in the adsorption could be confirmed as physisorption.  $I^-$  was attracted to the adsorbent without a chemical reaction or change in the iodine oxidation number. This agreed with the adsorption experiment and thermodynamic calculations. Physisorption is explained as the attraction between adsorbents and adsorbates via processes such as hydrogen bonding, electrostatic forces, hydrophobic interactions, or combinations (Zhang et al., 2016). Due to the cationic nature of the adsorbents, the attraction of  $I^-$  by electrostatic forces was the most probable mechanism.



**Figure 4.12** Normalized iodine  $L_{III}$ -edge XANES spectra of the saturated Fe-Alg, hazelnut shells, and sachu inchi shells with KI (aq) and  $KIO_3$  (aq) as references

The FTIR analysis was then employed to determine the functional groups or chemical species involved in the attraction of  $I^-$  by electrostatic forces. The spectra in **Figure 4.13a** reveal peak modifications of the Fe-Alg. The asymmetric stretching of  $COO^-$  at  $1585\text{ cm}^{-1}$  and symmetric stretching of  $COO^-$  at  $1402\text{ cm}^{-1}$  were observed with weaker intensity after  $I^-$  adsorption. These corresponded to the carboxylate functional groups, which cross-linked with  $Fe^{3+}$  in Fe-Alg (Papageorgiou et al., 2010). A decrease in the C-O stretching peak at  $1021\text{ cm}^{-1}$  was also observed. The FTIR analysis could not detect the electrostatic interaction between  $Fe^{3+}$  and  $I^-$ . However, this phenomenon may indirectly influence the structure of the neighboring deprotonated carboxyl molecules, causing the peak intensity to decrease (Coates, 2004). The FTIR results of sachu inchi shells (**Figure 4.13b**) and hazelnut shells (**Figure 4.13c**) exhibited, to some extent, a deprotonated carboxyl peak intensity modification at  $1540 - 1650\text{ cm}^{-1}$ . Additionally, for sachu inchi shells, the O-H stretching at  $3372\text{ cm}^{-1}$  (before  $I^-$  adsorption) shifted to  $3320\text{ cm}^{-1}$  (after  $I^-$  adsorption), while the C-O stretching at  $1024\text{ cm}^{-1}$  experienced a minor intensity decrease after the adsorption (**Figure 4.13c**). According to the EDX analysis, sachu inchi shells and hazelnut shells contain several cationic minerals, such as K, Mg, and Ca (**Table 4.2**). These minerals were presumed to form complexes with the proteins or lipids in plants (Chen et al., 2018). Moreover, tannin was found to be abundant in hazelnut shells and sachu inchi shells. Tannin can bind cationic metals, mostly through the chelation by the aromatic C-O (Chirinos et al., 2016; Lopes et al., 2012; Oladoja et al., 2011). The electrostatic attraction of  $I^-$  may cause alteration in the neighboring functional groups of the cationic mineral.





**Figure 4.13** FTIR spectra of the virgin and saturated bio-based adsorbents. (a) Fe-Alg, (b) hazelnut shells, (c) sachu inchi shells

#### 4.4.2 Investigation of anthocyanin involvement in iodide adsorption

The results of the *TAC* calculated by Equation (3.4) are shown in **Table 4.7**. The mangosteen pericarps contained the highest anthocyanin content with 25.1 mg/100 g. This value is similar to that of the results in the literature, which reported 20.83 to 23.54 mg/100 g *TAC* (Hiranrangsee et al., 2016). The passion fruit rinds yielded the lowest value of 10.9 mg/100 g, while the red dragon fruit peels adsorb low intensity at wavelength 700 nm, leading to a low value of 12.4 mg/100 g. The anthocyanin leached from red dragon fruit peels and red onion peels, was found to be 0.668 and 0.334

mg/100 g, respectively, while there was no leaching detected in the other adsorbents. The higher *TAC* values corresponded to higher  $I^-$  adsorption in the kinetic study previously reported. The observed orange and red solvent were due to the variation of hydroxyl and methoxy groups in the anthocyanin (He and Giusti, 2010).

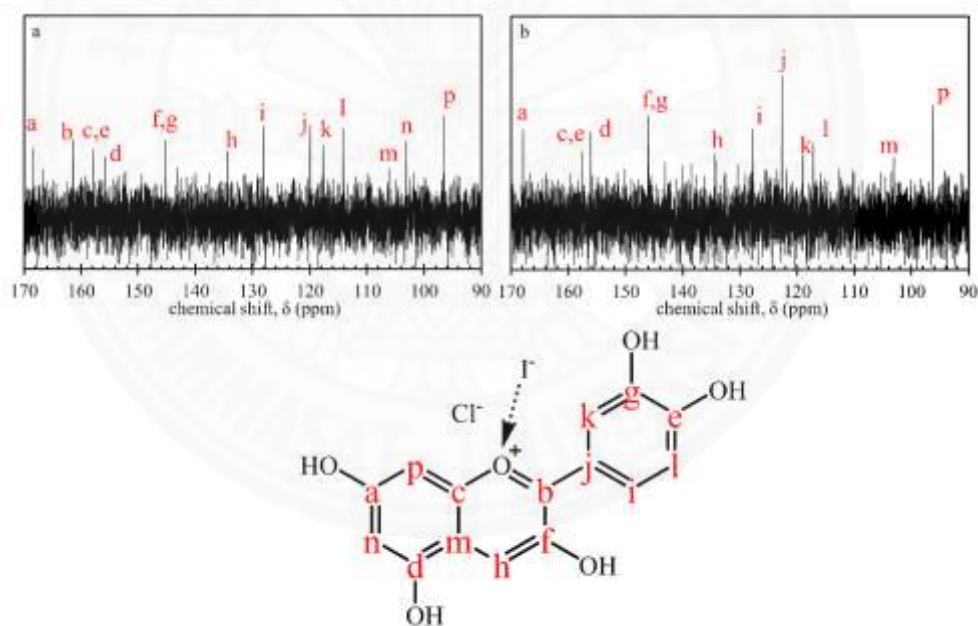
**Table 4.7** Total anthocyanin content (*TAC*) from the anthocyanin quantification, using the ultrasound-assisted extraction method, and the leaching experiment, using 10 mg/L  $I^-$  solution with 2 h contact time.

Experiment	Adsorbent	pH 1.0 <sup>a</sup>		pH 4.5 <sup>a</sup>		<i>TAC</i> <sup>b</sup> (mg/100g)	observable color in solvent
		A510 (nm)	A700 (nm)	A510 (nm)	A700 (nm)		
Anthocyanin quantification	mangosteen pericarps	1.31	0.809	0.900	0.547	25.1	orange
	red onion peels	0.584	0.204	0.375	0.134	23.2	red
	red dragon fruit peels	0.346	0.026	0.318	0.072	12.4	red
	passion fruit rinds	0.109	0.014	0.051	0.021	10.9	orange
Leaching of anthocyanin	mangosteen pericarps	0.002	0	0.002	0	0	-
	red onion peels	0.005	0.001	0.003	0.001	0.334	pale red
	red dragon fruit peels	0.004	0	0.004	0.004	0.668	red
	passion fruit rinds	0.001	0	0.003	0.002	0	-

<sup>a</sup>parameter calculated by Equation (3.4), <sup>b</sup>calculated by Equation (3.5)

The  $^{13}C$  chemical shifts of the cyanidin chloride from  $^{13}C$  NMR (400 MHz,  $D_2O$ ,  $\delta$ , ppm) were: 96.5, 103.1, 106.1, 114.1, 117.6, 119.9, 128.0, 134.35, 145.2, 155.7,

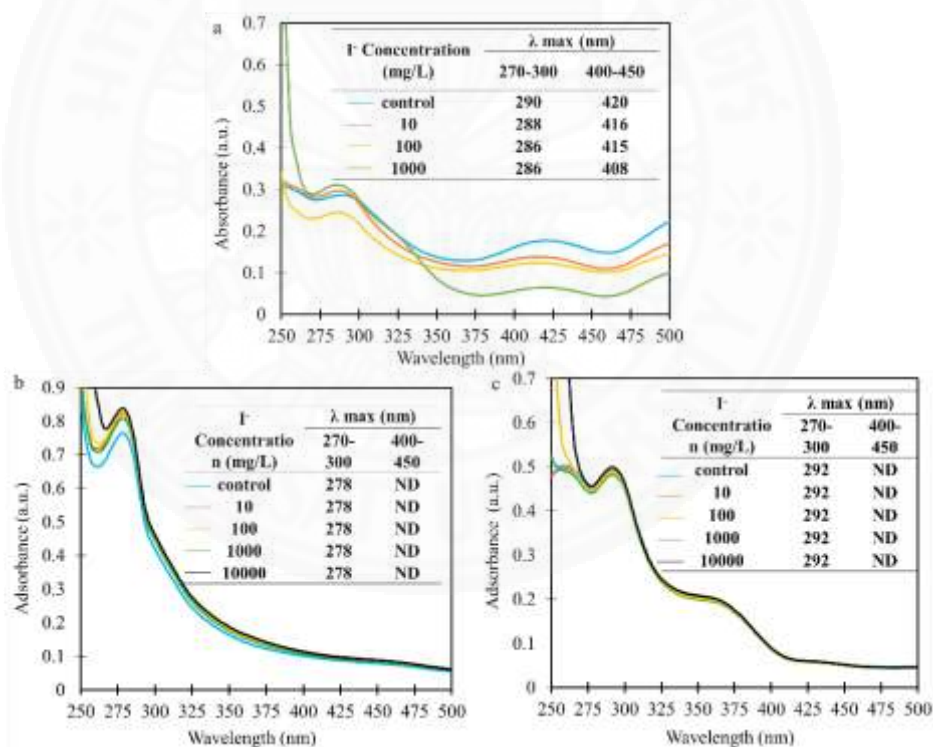
157.9, 161.4, 168.5. The actual spectrum is depicted in **Figure 4.14a**. Although the signal is noisy due to the minute amount of the samples, the assigned chemical shifts correspond to those previously reported (Wolniak and Wawer, 2008). **Figure 4.14b** is a spectrum of the cyanidin chloride-KI mixture. The carbon atom assigned at 161.4 ppm is no longer observable, while the chemical shift at 157.9 ppm decreased. These chemical shifts correspond to the two carbon atoms nearest to  $O^+$ . This suggests the occurrence of ion-exchange, bonding or the electrostatic forces that pull  $I^-$  nearer to the cyanidin molecules. There are additional decreases in the chemical shifts at 103.1, 106.1, 114.1, 117.6, 128.0, and 134.35 ppm. The binding of different anions could create conformational alterations in the structure of the molecules, affecting the chemical shifts in the NMR spectrum (Makuc et al., 2011). In this case, the decrease or disappearance occurred, and the low sample concentration does not allow for actual peak broadening (Hartman and Kelusky, 1979).



**Figure 4.14** Study of cyanidin ion-exchange properties. (a) cyanidin chloride solution, (b) cyanidin chloride in KI solution (equimolar ratio of cyanidin to  $I^-$ )

The  $\lambda_{max}$  between 400 and 450 nm indicates a solution color of crimson and magenta, which was prominent in the cyanidin chloride solution (**Figure 4.15a**). Slight hypochromic shifts (blue shifts) for the cyanidin chloride was observed as  $I^-$  increased. The values of  $\lambda_{max}$  appear between 270 and 300 nm, corresponding to the benzoyl

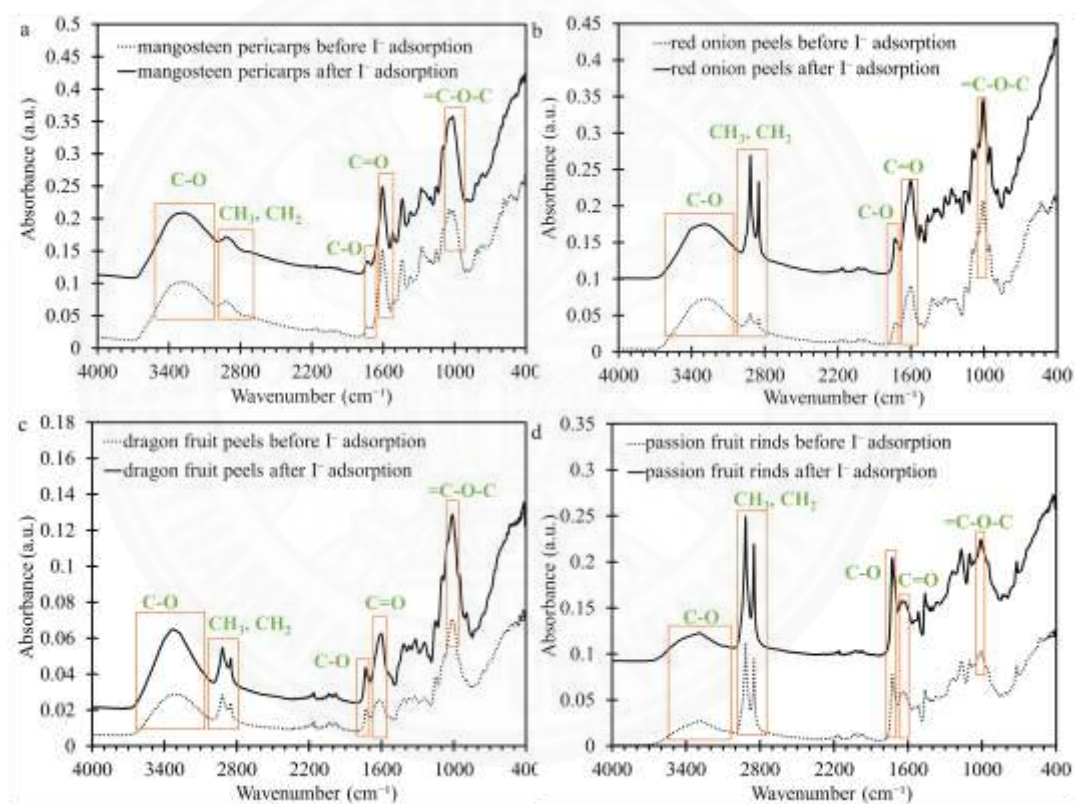
functional group of flavylium cation (Syukri et al., 2013). The pH effects and solvent polarity could be neglected because KI is considered to be neutral, and only water was used as the solvent. Therefore, the blue-shift phenomena can be explained by electrostatic interactions or chemical bonding. As  $I^-$  was increasing, more anions were pulled towards the flavylium cation, available in the cyanidin solution. This affected the electronic transition ( $n \rightarrow \pi^*$ ) and caused the blue shifts (Haldar and Bagchi, 2016). The spectra of mangosteen pericarps and red onion peels anthocyanin extract are shown in **Figure 4.15b** and **Figure 4.15c**, respectively. The non-shifting absorbance in the raw materials is due to the presence of other molecules in the extract. The hydration of flavylium cations and the formation of neutral hemiketal anthocyanin could also prevent the shifts from occurring (Basílio and Pina, 2016).



**Figure 4.15** UV-visible spectrum of anthocyanin in different  $I^-$  concentrations. (a) cyanidin chloride, (b) anthocyanin extract of mangosteen pericarps, (c) anthocyanin extract of red onion peels

FTIR was used to observe the vibrational bands in the peaks corresponding to the anthocyanin content. The results are shown in **Figure 4.16**. The numerical

wavelength values are shown in **Table 4.8**. Upon comparing the spectra before and after the adsorption process of each adsorbent, a shift was observed for mainly C=O (stretching) at 1820 – 1670  $\text{cm}^{-1}$ . The shifts in the other regions of FTIR spectra were observed to be minimal. The interaction between the adsorbent and  $\text{I}^-$  might affect the stretching and bending of the adsorbent functional groups to a small extent. However, the change in the peak shape of =C-O-C (aromatic) for the mangosteen pericarps, red dragon fruit peels and passion fruit rinds could still be observed. All the corresponding peaks shown on the spectra are associated with the oxygen-containing functional groups in the anthocyanin.



**Figure 4.16** FTIR spectra of virgin and saturated anthocyanin-containing adsorbents. (a) mangosteen pericarps, (b) red onion peels, (c) red dragon fruit peels, (d) passion fruit rinds

**Table 4.8** Comparison of FTIR peaks corresponding to the dominant functional groups in anthocyanin of virgin and saturated anthocyanin-containing adsorbents

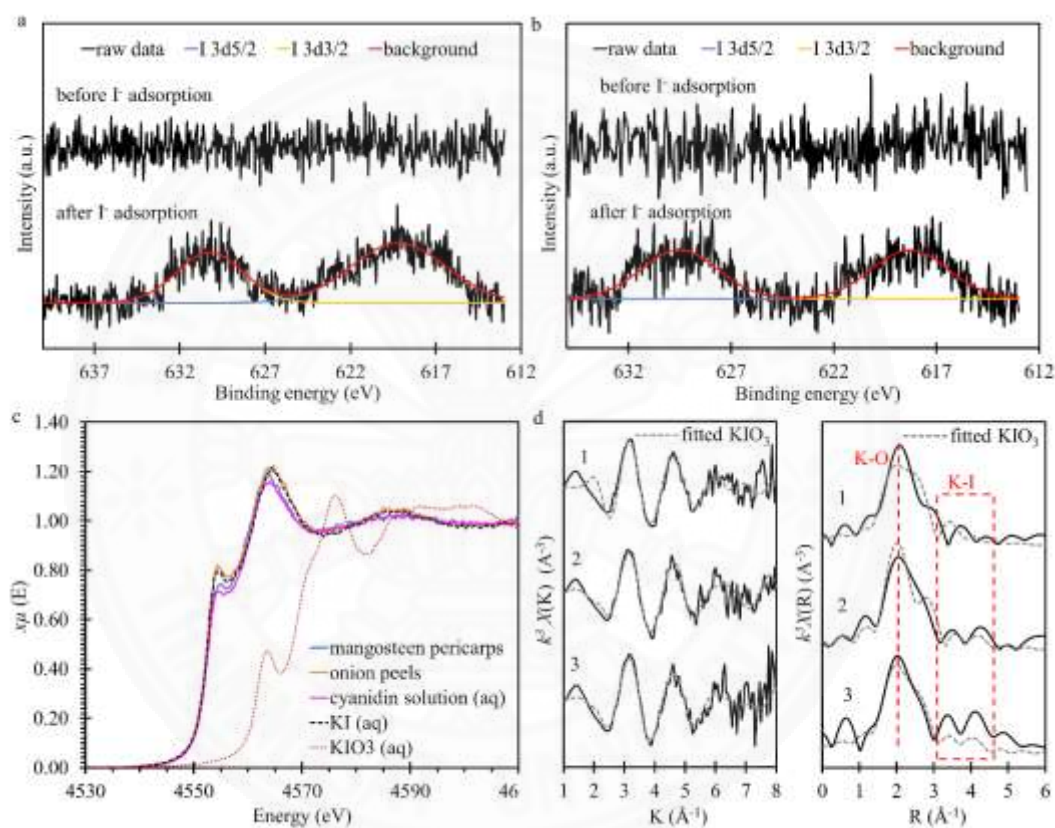
Functional group	FTIR peaks corresponding to the functional group (cm <sup>-1</sup> )							
	Mangosteen pericarps		Red onion peels		Red dragon fruit peels		Passion fruit rinds	
	virgin	saturated	virgin	saturated	virgin	saturated	virgin	saturated
O-H	3274.42	3277.22	3270.60	3293.26	3318.15	3331.91	3286.95	3294.17
CH <sub>2</sub> , CH <sub>3</sub>	2913.48,	2915.19,	2850.11,	2849.44,	2850.25,	2850.15,	2849.27,	2849.35,
	2964.01	ND	2918.25	2917.83	2918.59	2917.64	2917.06	2917.07
C-O	1730.05	1734.27	1730.30	1732.58	1731.71	1731.92	1727.88	1728.06
C=O	1605.37	1604.90	1601.71	1601.48	1617.52	1603.28	1631.98	1648.99
C-O-C	1042.93	N.D.	1008.82	1008.93	1016.28	1011.98	1011.11	1010.16

The appearance of iodine bands is evidence of the I<sup>-</sup> presence in the adsorbent. Before adsorption, no iodine bands were detected in any adsorbent. I<sub>3d5/2</sub> and I<sub>3d3/2</sub> peaks can be seen at 619 and 631 eV for all adsorbents after the I<sup>-</sup> adsorption (**Figure 4.17a – b**). The appearance of these peaks can confirm the presence of iodine at the -1 oxidation state, I<sup>-</sup> (Ahlberg et al., 2015). Similar I<sub>3d</sub> spin-orbital doublets were also observed with the adsorption of I<sup>-</sup> on the metal adsorbent, indicating interactions such as CuI and AgI (K. Li et al., 2016; Yang et al., 2011). The XPS results for all adsorbents can be found in the appendices.

XANES data in **Figure 4.17c** show that the adsorbents and cyanidin solution have characteristic absorption edges (4552.83 – 4552.90 eV) closer to that of KI (4552.83 eV) than KIO<sub>3</sub> (4560.77 eV). This confirmed that the iodine species in the adsorbents had the same oxidation state of -1. Therefore, the mechanism involved in the adsorption can be confirmed as an ion-exchange process. The iodine L<sub>III</sub>-edge shifts in this study were similar to the literature for the I<sup>-</sup> adsorption by organo-bentonites (Yoon et al., 2009).

As explained in the methodology section, the obtained EXAFS iodine L<sub>III</sub>-edge spectra could not be fitted. I-probing EXAFS spectra can be found in the appendices. To gain insights into I-O interactions, the EXAFS results of potassium K-edge were fitted with the model of the KIO<sub>3</sub> crystal structure. **Figure 4.17d** shows comparable EXAFS spectra in K-space. The results of the EXAFS fits are shown in **Table 4.9** with

values of R-factor (fractional misfit) below 0.02. They are deemed acceptable for all paths. In R-space, K ions were surrounded by several O atoms, and this produced the fitted peak centered at  $2.576 - 3.574 \text{ \AA}$  (**Figure 4.17d**). The K-I peak appeared at  $4.255$  and  $4.173 \text{ \AA}$  for red onion peels and cyanidin solution, respectively, while the results of mangosteen pericarps had the peak shifted to  $3.593 \text{ \AA}$ . With the results, we can assume that I is located nearer to O in the local structure of all adsorbents, with respect to the K atom.



**Figure 4.17** Iodine oxidation state and local structure in the presence of anthocyanin. (a) I<sub>3d5</sub> XPS spectra of mangosteen pericarps, (b) I<sub>3d5</sub> XPS spectra of red onion peels (c) normalized iodine L<sub>III</sub>-edge XANES spectra of the anthocyanin-based adsorbents, (d) graph of transformed K-space and R-space for potassium K-edge [1. mangosteen pericarps, 2. red onions peels, 3. cyanidin solution]

**Table 4.9** EXAFS quick-first shell fit

Sample	Path	N <sup>a</sup>	S <sub>0</sub> <sup>2b</sup>	e <sup>0c</sup>	R (Å) <sup>d</sup>	σ <sup>2</sup> (Å <sup>2</sup> ) <sup>e</sup>	R-factor <sup>f</sup>
mangosteen pericarps	K-O1	1	1	-6.695	2.576	0.01423	0.011
	K-O2	1	1	-6.695	2.578	0.01203	0.011
	K-O3	2	1	-6.695	3.137	0.00454	0.011
	K-O4	2	1	-6.695	3.198	0.00857	0.011
	K-I1	4	1	-6.695	3.593	0.03993	0.011
red onion peels	K-O1	1	1	-2.495	2.582	0.00565	0.013
	K-O2	2	1	-2.495	2.693	0.01203	0.013
	K-O3	2	1	-2.495	3.352	0.00355	0.013
	K-O4	1	1	-2.495	3.574	0.00656	0.013
	K-I1	4	1	-2.495	4.255	0.03993	0.013
cyanidin solution	K-O1	2	1	-4.686	2.611	0.01232	0.011
	K-O2	1	1	-4.686	2.629	0.02772	0.011
	K-O3	1	1	-4.686	3.210	0.00688	0.011
	K-O4	2	1	-4.686	3.292	0.00157	0.011
	K-O5	1	1	-4.686	3.498	0.01244	0.011
	K-O6	2	1	-4.686	3.513	0.00716	0.011
	K-I1	4	1	-4.686	4.173	0.04034	0.011

<sup>a</sup>coordination number, <sup>b</sup>amplitude reduction term, <sup>c</sup>energy shift (where k = 0), <sup>d</sup>near-neighbor distance, <sup>e</sup>mean-square disorder in R, <sup>f</sup>fractional misfit

The optimized structure of cyanidin and the counterpart atom partial charges are shown in **Figure 4.18** and **Table 4.10**, respectively. Out of 100 possibilities calculated by the program, there were two most stable Cyanidin-I conformations with ~3.28 Å radial distance between O<sup>+</sup> and I<sup>-</sup> (**Figure 4.19**). The total estimated binding energy was calculated to be -2.21 kcal/mol for both conformations, and the dominant bonding mechanism is electrostatic interactions with an estimated energy of -1.40 kcal/mol. The binding energy (-0.80 kcal/mol) was attributed to the other attractive forces between opposite charges.



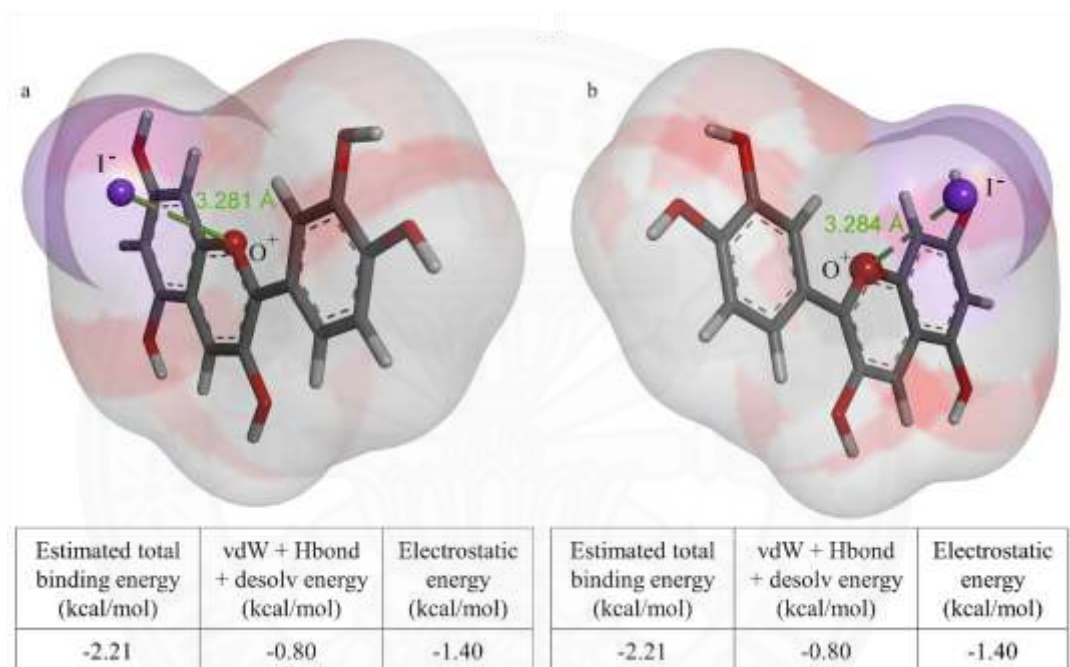


**Figure 4.18** Optimized structure of cyanidin by Gaussian 09 with DFT method

**Table 4.10** Partial charge of the atoms in the optimized cyanidin

Atom	Label ( <b>Figure 4.18</b> )	$\delta$
carbon	1	+0.124
	2	+0.022
	3	+0.131
	4	+0.062
	5	+0.143
	6	+0.023
	7	-0.002
	8	+0.160
	9	+0.177
	11	+0.025
	13	-0.047
	14	-0.016
	15	+0.158
	16	+0.159
17	-0.006	
Oxygen	10	+1.000
	12, 20, 21	-0.503

	18	-0.507
	19	-0.506
Hydrogen	24, 25 ,26	+0.292
	27, 28	+0.069
	29, 30, 32	+0.066
	31	+0.063



**Figure 4.19** Cyanidin- $I^-$  conformations with the lowest total estimated binding energy obtained from the program, AutoDock 4. (a) conformation 1 (b) conformation 2 (vdW – Van der Waals, Hbond – hydrogen bond, desolv – desolvation)

Previous research with a computational methodology using Gaussian software can predict the interactions between a C atom of fullerene and  $I^-$  (Kobayashi and Yokoyama, 2016). The distance was predicted to be 3 Å (0.3 nm), similar to the distance of I-O in this study due to the same binding mechanism and similar atomic radius of the host atoms (C and O). Another study predicted a shorter distance between an atom of Ti and  $I^-$  in the range of 2.64 – 2.72 Å (Asaduzzaman and Schreckenbach, 2011). A closer atomic distance and stronger binding energy were expected for such a metal-halide bond.

The computational results also confirmed that, in addition to the ion-exchange shown previously,  $O^+$  in the anthocyanin-based adsorbents attracted  $I^-$  by electrostatic force. A similar adsorption mechanism (for cationic and anionic contaminants removal in the water) which involves ion-exchange and electrostatic force was also reported by other researchers (M. Li et al., 2016; Wang et al., 2018).

#### 4.5 Comparative study of adsorbents for iodide removal

Recent studies on  $I^-$  adsorption were compared with the bio-based adsorbents in this research. The experimental  $I^-$  adsorption capacity, equilibrium time, and mechanism are tabulated in **Table 4.11**. Fe-Alg was observed to be comparable to the silica-based poly(4-vinyl pyridine), in terms of adsorption capacity and equilibrium time. It outperformed Fe-based MOF, which incorporated bismuth (Bi) to assist Fe in the  $I^-$  attraction. Among all the adsorbents presented in **Table 4.11**, the cryogel incorporated with silver was observed to possess the highest adsorption (326 mg/g). However, it required a long equilibrium time (32 h). Sacha inchi shells, mangosteen pericarps and red onion peels were unmodified adsorbents. The experimental  $I^-$  adsorption capacities were higher than those of palygorskite-based polymer microspheres, silver-based chitosan microspheres, and commercial resin. The palygorskite-based polymer microspheres had the fastest equilibrium time. With a higher initial  $I^-$  concentration, the palygorskite-based polymer microspheres could yield higher performance.

The usage of waste in water treatment process could help to reduce operation cost and boost the circular economy (Hossain et al., 2020). The fruit waste containing anthocyanin is free. The incurred costs might come from the preparation of adsorbents (rinsing and drying). On the other hand, the costs of conventional polystyrene resin and metal-based adsorbent came from limited resources, syntheses, and chemical waste handling. With the same adsorbent dose, the waste containing  $I^-$  adsorption functional group is viewed as more sustainable as well as economical.

**Table 4.11** Comparison with other adsorbents in term of experimental I<sup>-</sup> adsorption capacity and proposed mechanism

Adsorbent	Experimental I <sup>-</sup> adsorption capacity (mg/g)	Equilibrium time	Initial I <sup>-</sup> concentration (mg/L)	Proposed mechanism of I <sup>-</sup> adsorption	Ref.
Fe-Alg	139	30 min	2 – 200	electrostatic attraction by Fe <sup>3+</sup>	This work
Sacha inchi shells	48.4	120 min	2 – 200	electrostatic interactions, ion-exchange and chemisorption on the flavylum cation of the anthocyanin	This work
Mangosteen pericarps	79.0	30 min	2 – 200	electrostatic interactions on the flavylum cation of the anthocyanin	This work
Onion peels	75.0	120 min	2 – 200		This work
PA-R4	37.0	120 min	2 – 200	ion-exchange with OH <sup>-</sup> at quaternary ammonium groups	This work
DOWEX-550	39.4	180 min	2 – 200	ion-exchange with Cl <sup>-</sup> at quaternary ammonium groups	This work

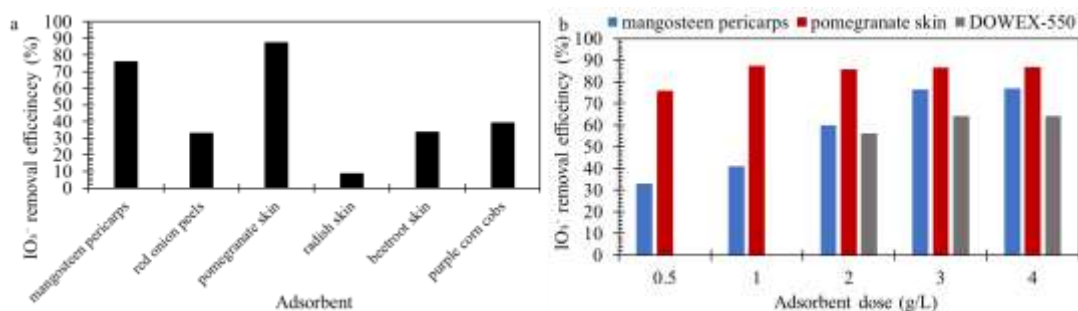
Silica-based ion-exchange resin made from poly(4-vinyl pyridine)	149	30 min	12.69 – 63.45	ion-exchange at quaternary ammonium groups	(Ye et al., 2019)
Cryogel incorporated with silver	326	~ 32 h	n/a	formation of AgI colloid on the cryogel surface	(Baimenov et al., 2020)
LDH incorporated with Fe <sub>3</sub> O <sub>4</sub>	70	5 h	50	electrostatic attraction	(Jung et al., 2020)
MOF with Fe and Bi(NO <sub>3</sub> ) <sub>3</sub>	~ 190	20 min	200	Electrostatic attraction created by Fe and Bi	(Xu et al., 2019)
Palygorskite-based polymer microspheres	~ 0.152 (1.20 mmol/g)	5 min	~ 0.0253 – 0.381 (0.2 – 3 mM)	electrostatic attraction by quaternary ammonium of polymer poly(2-(diethylamine) ethyl methacrylate)	(Mao et al., 2020)
Chitosan microspheres incorporated with silver	~ 0.194 (1.53 mmol/g)	20 min	0.0127 – 2.54 (0.1 – 20 mM)	chemisorption forming AgI	(Li et al., 2020)

From the results of this study, it can be concluded that the anthocyanin-containing adsorbents, sacha inchi shells and hazelnut shells are readily available wastes. They are minimally modified and are economical, incurring no costs associated with syntheses. As plant-based adsorbents, they do not produce secondary pollution and are suitable for open environment remediation. Fe-Alg needed synthesis but the inclusion of  $\text{Fe}^{3+}$  required a simple complexation reaction in water. This saved time and the usage of other solvents. Fe-Alg exhibited comparable equilibrium time and adsorption capacity to the other adsorbents with more complicated synthesis routes. Alginate is readily available due to its source being brown algae. However, with a metal in the adsorbent, the adsorbent is only suitable for closed-environment remediation. PA-R4 may need a more elaborate synthesis route but the adsorbent was tested to be stable even at elevated temperature and became suitable for a closed-environment remediation process that involve near-boiling temperature condition.

#### 4.6 Iodate adsorption by anthocyanin-containing adsorbents

Due to the successful  $\text{I}^-$  adsorption by anthocyanin-containing adsorbents, the adsorbents were briefly assessed for their ability to remove  $\text{IO}_3^-$  in the water. More kinds of anthocyanin-based waste materials were added to the screening test. The results of the test are shown in **Figure 4.20a**. Pomegranate skin and mangosteen pericarps exhibited satisfactory removal efficiency with 87.5% and 76.3%, respectively. They were selected for detailed adsorption experiment. Red onion peels, radish skin, beetroot skin, and purple corn cobs could not remove more than 50% of 10 mg/L  $\text{IO}_3^-$ . They are deemed unsuitable for the application of  $\text{IO}_3^-$  removal and were not taken for further studies.

In **Figure 4.20b**, the results of dosage variation for mangosteen pericarps and pomegranate skin are shown. The  $\text{IO}_3^-$  removal efficiency of mangosteen pericarps increased with adsorbent dose until it reached 77% removal efficiency at 3 g/L. At 4 g/L, the mangosteen pericarps yielded a similar efficiency, so 3 g/L was considered as its optimum dose. For the pomegranate skin, it had an optimum dose at 1 g/L which 86% of  $\text{IO}_3^-$  was removed from the solution. DOWEX-550 was used to compared. It possessed the same optimum dose as mangosteen pericarps (3 g/L) but the removal was found to be about 64%.

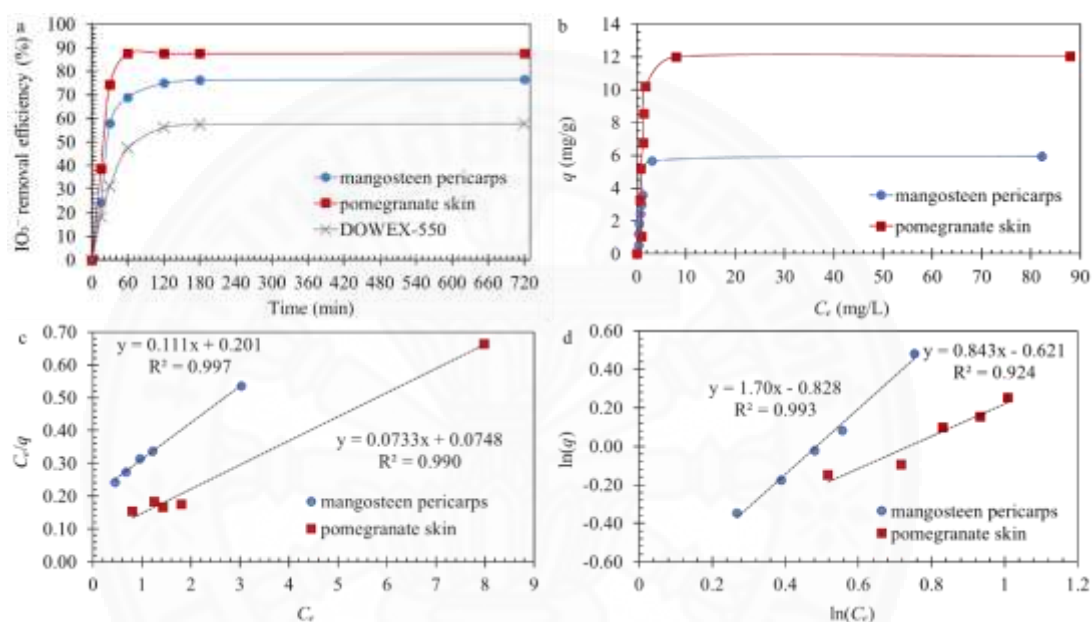


**Figure 4.20** Removal of  $\text{IO}_3^-$  by anthocyanin-containing adsorbents. (a) screening test with 1 g/L dose in 10 mg/L  $\text{IO}_3^-$  solution for 2 h, (b) adsorbent dose of the selected adsorbents in 10 mg/L  $\text{IO}_3^-$  solution for 2 h

The results of  $\text{IO}_3^-$  removal by anthocyanin-containing adsorbents for 720 min is shown in **Figure 4.21a**. For pomegranate skin, the results revealed that the adsorption time at 60 min provided the highest  $\text{IO}_3^-$  removal which was 87.6%. However, for mangosteen pericarps, the  $\text{IO}_3^-$  removal reached the saturation at 120 min with 75% efficiency. The equilibrium time was determined to be 60 min and 120 for the pomegranate skin and mangosteen pericarps, respectively. DOWEX-550 was used as the reference in the kinetic study. The synthetic resin has the equilibrium time of 120 min but its efficiency was 56.2%. Compared with the previous studies on duckweed and corn stalk as adsorbents (Zhang and Chen, 2018a, 2018b). The natural adsorbents required approximately 4 – 5 days to reach an adsorption equilibrium. In addition, the results confirmed that there was no desorption after 12 h in both pomegranate skin and mangosteen pericarps.

With the equilibrium time and optimum dose, pomegranate skin and mangosteen pericarps were taken for batch studies. The concentration dependent  $\text{IO}_3^-$  adsorption graphs ( $q$  over  $C_e$ ) are plotted in **Figure 4.21b**. The maximum  $q$  value for pomegranate skin was 12.0 mg/g. For the mangosteen pericarps, the  $\text{IO}_3^-$  adsorption capacity was lower at 5.94 mg/g. The results were taken to fit the isotherm models. Linear fits of Langmuir model and Freundlich models were displayed in **Figure 4.21c** and **Figure 4.21d**, respectively. The calculated parameters for both models were tabulated in **Table 4.12**. The adsorbents fitted better with the Langmuir model ( $R^2 > 0.990$ ). The model predicted  $q_{max}$  values of 13.6 and 9.09 mg/g for pomegranate skin

and mangosteen pericarps, respectively. The overestimation of adsorption capacities was due to the neglect of effects created by neighboring adsorbed molecules, which could prevent further adsorption to a certain extent (Delle Site, 2001; Hamdaoui and Naffrechoux, 2007). In addition, the fittings of Freundlich models yielded  $R^2$  values of 0.924 and 0.993 for pomegranate skin and mangosteen pericarps, respectively. Both isothermal models can be used to explain the behavior of  $\text{IO}_3^-$  removal by anthocyanin-containing adsorbents.



**Figure 4.21** Kinetic and batch experiment of  $\text{IO}_3^-$  removal by anthocyanin-containing adsorbents. (a) Kinetic experiment for 720 min using 10 mg/L  $\text{IO}_3^-$  initial concentration and optimum adsorbent doses at room temperature, (b) graph of concentration-dependent adsorption ( $q$  over  $C_e$ ) for 0 – 100  $\text{IO}_3^-$  initial concentration, optimum adsorbent doses and equilibrium time of contact at room temperature, (c) linear fits of Langmuir model, (d) linear fits of Freundlich model

**Table 4.12** Derived parameters of the linear fitting isotherm models

Adsorbents	Langmuir isotherm <sup>a</sup>			Freundlich isotherm <sup>b</sup>		
	$K_L$ (L/g)	$q_{max}$ (mg/g)	$R^2$	$K_F$ (L/g)	$n$	$R^2$
pomegranate skin	0.935	13.6	0.997	0.437	0.588	0.993
mangosteen pericarps	0.547	9.09	0.990	0.537	1.19	0.924

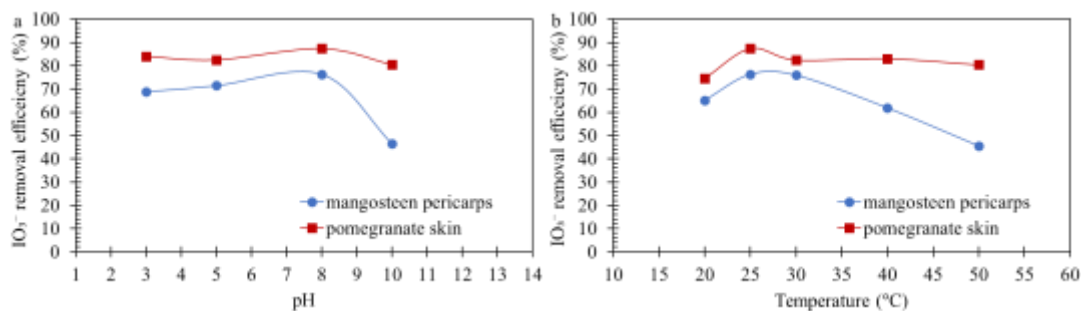


<sup>a</sup>Equation (2.8), <sup>b</sup>Equation (2.10)

The effect of pH in aqueous solution was investigated from pH 3 to 10. As shown in **Figure 4.22a**, it can be demonstrated that the  $\text{IO}_3^-$  removal was almost stable in the acid environment and slightly increased until pH 8. Then it was observed to significantly decreased for pomegranate skin at pH 10. The mangosteen pericarps seemed to be more affected at pH 10 as the efficiency dropped to about 40%. The colors of anthocyanin in pomegranate skin and mangosteen pericarps were observed to be red and orange, respectively. According to a previous study, methoxy groups is prominent in the red anthocyanin, while hydroxyl groups were observed more frequently in the orange one (He and Giusti, 2010). This might bring about a higher stability in pomegranate skin to absorb the  $\text{IO}_3^-$  at high pH. Nevertheless, pomegranate skin may just contain higher amount of anthocyanin and retain higher  $\text{IO}_3^-$  in any condition. A similar pattern was observed previously in the adsorption of  $\text{I}^-$  by anthocyanin-containing adsorbents. At high pH, the presence of  $\text{OH}^-$  could compete for the adsorption sites and hinder the adsorption ability of  $\text{IO}_3^-$ . Under an acidic environment, the presence of  $\text{H}^+$  might also repulse  $\text{IO}_3^-$ . Moreover, the cationic form of anthocyanin was present more in an acidic condition.

In a changing temperature environment,  $\text{IO}_3^-$  adsorption by anthocyanin-containing adsorbents yielded a similar pattern to that of  $\text{I}^-$  adsorption. **Figure 4.22b** depicts the effect of temperature. For pomegranate skin, the results show that changing temperature slightly affected the  $\text{IO}_3^-$  removal. However, the  $\text{IO}_3^-$  removal was increasing from 20 °C to 30 °C. According to Le Chatelier's principle, the  $\text{IO}_3^-$  adsorption by the adsorbents was assumed to be an endothermic process if the process is governed by the chemisorption process (Dorman and Steinberg, 2010). However, at higher temperature condition, the anthocyanin was assumed to be disintegrated, leading to low  $\text{IO}_3^-$  adsorption.

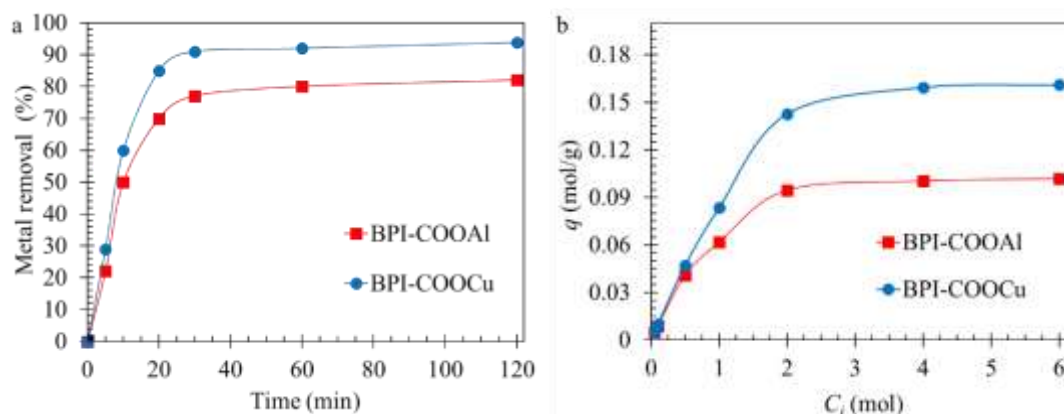
The overall results show that mangosteen pericarps could remove  $\text{I}^-$  better than  $\text{IO}_3^-$  in all adsorption conditions. This suggests that the steric hindrance created by  $\text{IO}_3^-$  structure played an important role in the anion adsorption (refer to Chapter 2.2).



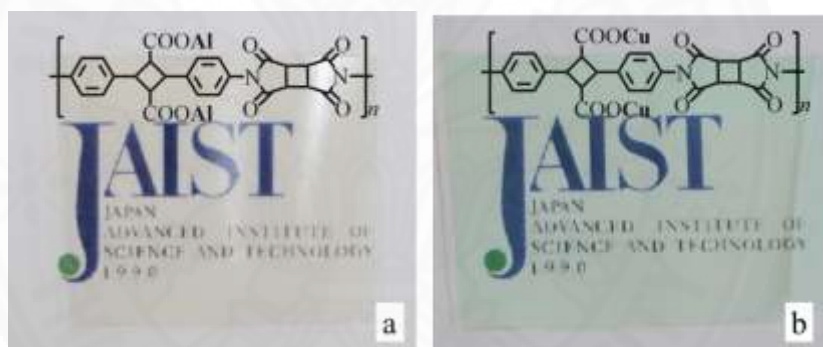
**Figure 4.22** Effect of changing condition to  $\text{IO}_3^-$  removal by anthocyanin-containing adsorbents using optimum dose and equilibrium contact time in 10 mg/L  $\text{IO}_3^-$  initial concentration. (a) variation of pH, (b) variation of temperature

#### 4.7 Complexation of polyimide with copper and aluminium

The metal removal over time (min) is exhibited in **Figure 4.23a**. Both complexation systems had an equilibrium at about 30 min, where the metal removal became stable. With 1 mol/L initial metal ion concentration, BPI can bind more with  $\text{Cu}^{2+}$  (more than 90%  $\text{Cu}^{2+}$  removal) than  $\text{Al}^{3+}$  (more than 80%  $\text{Al}^{3+}$  removal). The maximum values of  $q$ , the amount of metal (bound to a unit of BPI), were 0.101 and 0.161 mol/g for the binding of  $\text{Al}^{3+}$  and  $\text{Cu}^{2+}$ , respectively. The  $q$  results were used to plot against  $C_i$ , initial metal ion concentration (mol/L), and the graph is depicted in **Figure 4.23b**. For both complexation systems, while  $q$  started to stabilize at 2 mol/L  $C_i$ , BPI-COOAl and BPI-COOCu films could be obtained at a  $C_i$  of 1 mol/L. With a  $C_i$  of less than 1 mol/L, the metal ions were not concentrated enough, and the submerged BPI-COOK film was observed to scatter in the metal solution, forming precipitates. As a result, 1 mol/L was used as the minimum metal ion concentration for BPI-metal complexation. The actual images of BPI-COOAl and BPI-COOCu made from 1 mol/L  $C_i$  are shown in **Figure 4.24**. The thickness of the films was  $0.143 \pm 0.015$  mm.

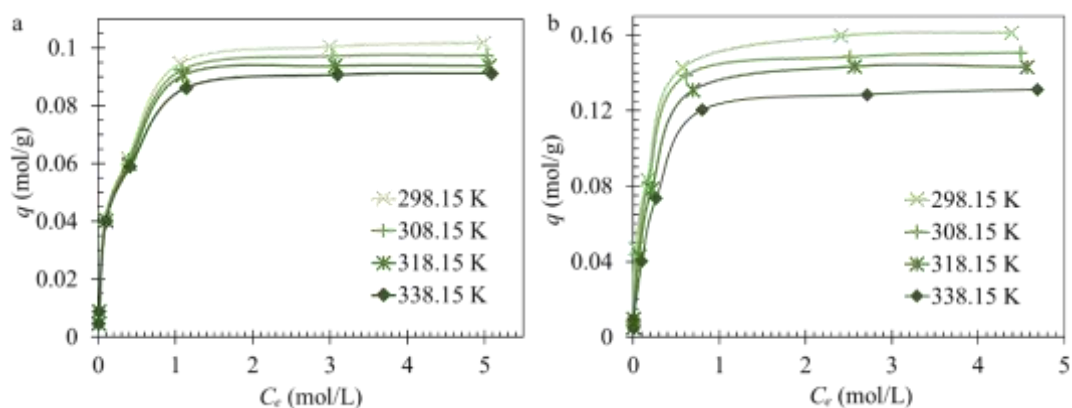


**Figure 4.23** Kinetic study of metal complexation. (a) metal removal (%) calculated by Equation (3.7) over time for 0 – 120 min of BPI-COOK submerged in 1 mol/L  $\text{Al}^{3+}$  and  $\text{Cu}^{2+}$  solution, (b) batch experiment of BPI-COOK submerged in 0.5 – 6 mol/L  $\text{Al}^{3+}$  and  $\text{Cu}^{2+}$  solution for 30 min.  $q$  is the amount of metal bound to a unit of BPI (mol/g), and  $C_i$  is the initial metal ion concentration (mol/L).



**Figure 4.24** BPI films made from 1 mol/L metal ion. (a) BPI-COOAl, (b) BPI-COOCu

The graphs of  $q$  (mol/g) vs.  $C_e$  (mol/L) for 25 – 65 °C (298.15 – 338.15 K) and the linear fitting of the Langmuir isotherm are found in **Figure 4.25**. The capacity of metal complexation decreased as the temperature increased (**Figure 4.25a – b**). This reflected the exothermic reaction, which corresponded to the negative values of  $\Delta H$  and  $\Delta S$  (**Table 4.13**). The parameters of thermodynamics are displayed in **Table 4.13**.



**Figure 4.25** Graphs for thermodynamic parameters. (a)  $q$  (mol/g) over  $C_e$  for BPI-COOAl, (b)  $q$  over  $C_e$  for BPI-COOCu

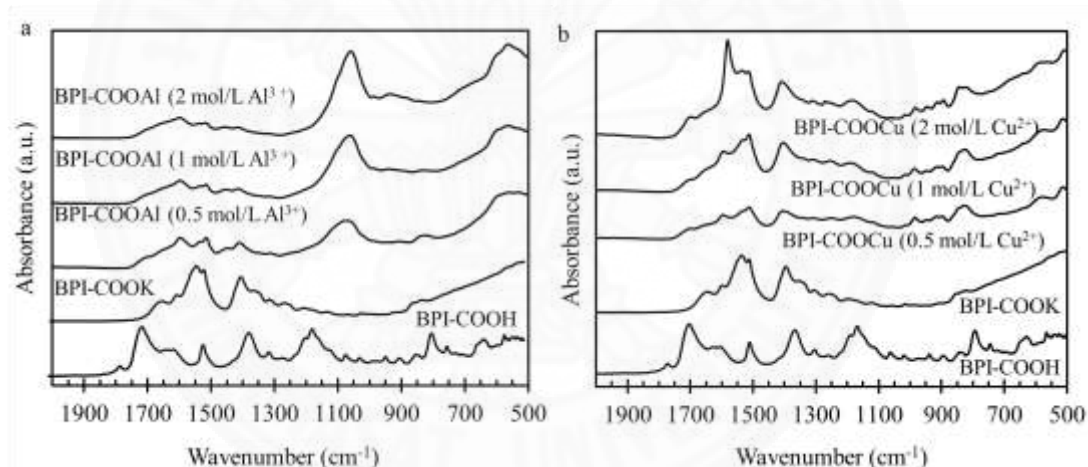
**Table 4.13** Thermodynamic parameters for the complexation of BPI-COOAl and BPI-COOCu

sample	$T$ (K) <sup>a</sup>	$K_{eq}$ <sup>b</sup>	$\Delta H$ (kJ/mol) <sup>c</sup>	$\Delta S$ (kJ/K/mol) <sup>c</sup>	$\Delta G$ (K/mol) <sup>d</sup>
BPI-COOAl	298.15	46.8	-0.00249	-0.0191	-4.97
	308.15	24.2			-4.83
	318.15	16.6			-4.70
	338.15	12.6			-4.43
BPI-COOCu	298.15	8.40	-0.00083	-0.0258	-6.66
	308.15	2.37			-6.37
	318.15	1.12			-6.08
	338.15	0.646			-5.51

<sup>a</sup>metal ion solution temperature controlled by closed incubator, <sup>b</sup>equilibrium constant calculated by Equation (3.8) and (3.9), <sup>c</sup>change in enthalpy and entropy calculated by Equation (2.3), <sup>d</sup>change in Gibbs free energy calculated by Equation (2.1)

The ATR-FTIR spectra, focusing on the fingerprint region of BPI-COOAl and BPI-COOCu, are shown in **Figure 4.26**. The full spectra can be found in the appendix.

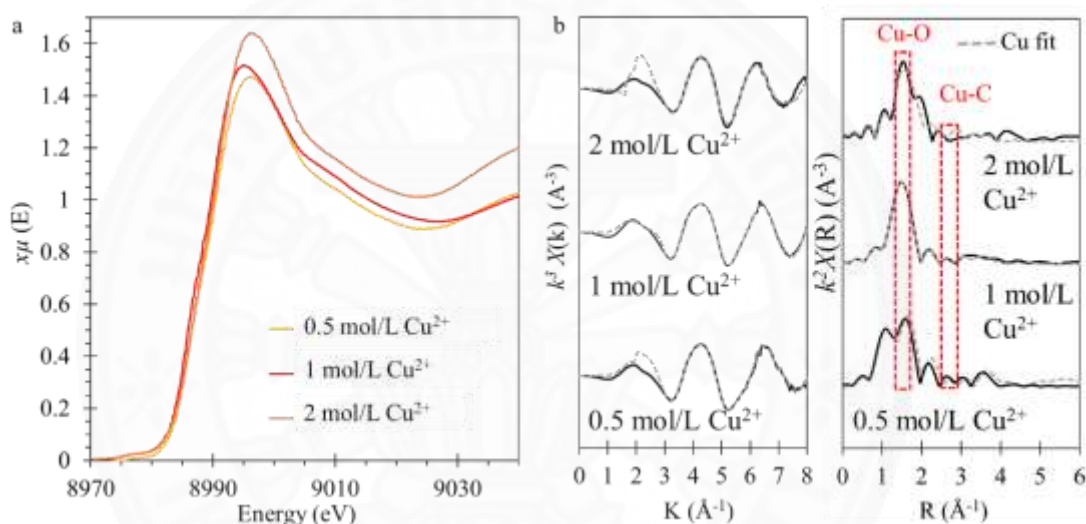
BPI-COOH and BPI-COOK were used for comparison. A high-intensity band of carboxylic acid stretch ( $1690 - 1750 \text{ cm}^{-1}$ ) could be observed in BPI-COOH. In contrast, the deprotonated carboxylic acid stretches ( $1540 - 1650 \text{ cm}^{-1}$  and  $1300 - 1420 \text{ cm}^{-1}$ ) appeared in the spectra of BPI-COOK, BPI-COOAl, and BPI-COOCu. Such alteration could be explained by metal-carboxylate coordination. The same phenomenon was reported when the alginic acid formed metal-alginate in a metal solution (Papageorgiou et al., 2010). The increase in  $\text{Cu}^{2+}$  led to a higher intensity of the deprotonated carboxylic acid stretches of BPI-COOCu, while the opposite occurred in the system of  $\text{Al}^{3+}$  and BPI-COOAl. A band corresponding to C-N aromatic amine at about  $1300 \text{ cm}^{-1}$  appeared in all kinds of polyimides, but a weaker intensity could be observed in BPI-COOAl and BPI-COOCu. The bands at  $1050$  and  $550 \text{ cm}^{-1}$  correspond to sulfur from the added  $\text{Al}_2(\text{SO}_4)_3$  (**Figure 4.6a**).



**Figure 4.26** FTIR spectra in the fingerprint region of BPI-metal complex made from various metal ion concentrations with the spectra of BPI-COOH and BPI-COOK as references. (a) BPI-COOAl, (b) BPI-COOCu

XANES data of the Cu K-edge can be found in **Figure 4.27a**. The characteristic absorption edge was observed at about  $8995.52 - 8996.63 \text{ eV}$ , with no pre-edge peaks. This coincides with the previously reported XANES results of  $\text{Cu}^{2+}$  in  $\text{Cu}(\text{OH})_2$  (Okamoto et al., 1998). The graph of transformed K-space/R-space **Figure 4.27b**, while the EXAFS fits data for Cu K-edge is displayed in **Table 4.14**. The fitting of all samples yielded values of R-factor (fractional misfit) below 0.02. The local structure focused on

Cu atom with radial distances taken from the fit of BPI-COOCu (**Table 4.14**) is illustrated in **Figure 4.28**. The distance between the single-bonded O atoms of carboxyl groups and the Cu atom is 1.94 Å. With respect to the Cu atom, the carboxyl C atom and double-bonded O atom are located at 2.85 and 4.26 Å, respectively. The local structure displayed monodentate metal-carboxylate formation. This was also the case for Cu<sup>2+</sup> and α-L-gulonate anions of alginates (Plazinski and Drachb, 2015). For both complexes, Al<sup>3+</sup> and Cu<sup>2+</sup> attract the surrounding water molecules to achieve a stable geometry since the BPI has no other available hydroxyl groups (except on the carboxylate) (Motekait and Martell, 1984; Zaafarany, 2010).



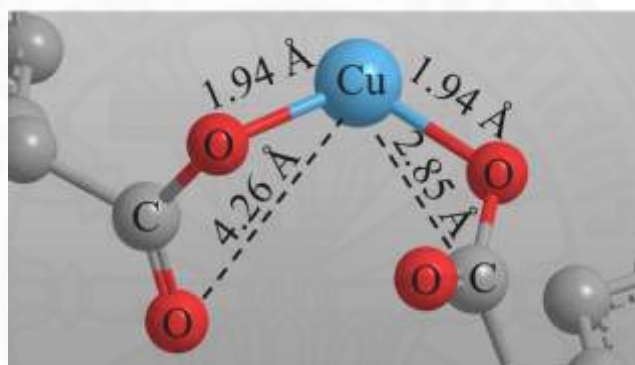
**Figure 4.27** XAS of BPI-COOCu at Cu k-edge. (a) XANES, (b) EXAFS K-space and R-space

**Table 4.14** BPI-COOCu EXAFS fit with the model structure of CuH<sub>2</sub>(CO<sub>2</sub>)<sub>2</sub>

Sample	Path	N <sup>a</sup>	S <sub>0</sub> <sup>2b</sup>	e <sup>0c</sup>	R (Å) <sup>d</sup>	σ <sup>2</sup> (Å <sup>2</sup> ) <sup>e</sup>	R-factor <sup>f</sup>
BPI-COOCu (0.5 mol/ L Cu <sup>2+</sup> )	Cu-O(1)	6	0.901	2.932	1.930	0.01188	0.006
	Cu-C(1)	4	0.901	2.932	2.826	0.01873	
	Cu-O(1)-C(1)	8	0.901	2.932	3.008	0.01919	
	Cu-O(2)	4	0.901	2.932	4.259	0.00478	
BPI-COOCu (1 mol/ L Cu <sup>2+</sup> )	Cu-O(1)	4	0.968	3.338	1.943	0.00644	0.002
	Cu-C(1)	4	0.968	3.338	2.854	0.04017	

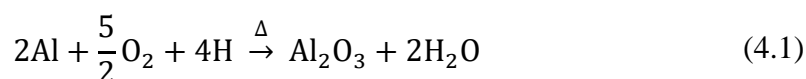
	Cu-O(1)-C(1)	8	0.968	3.338	3.055	0.01912	
	Cu-O(2)	4	0.968	3.338	4.045	0.01203	
BPI-COOCu (2 mol/ L Cu <sup>2+</sup> )	Cu-O(1)	6	0.944	9.767	2.014	0.01275	0.010
	Cu-C(1)	4	0.944	9.767	3.167	0.00656	
	Cu-O(1)-C(1)	8	0.944	9.767	3.291	0.01101	
	Cu-O(2)	4	0.944	9.767	4.314	0.01704	

<sup>a</sup>coordination number, <sup>b</sup>amplitude reduction term, <sup>c</sup>energy shift (where  $k = 0$ ), <sup>d</sup>near-neighbor distance, <sup>e</sup>mean-square disorder in R, <sup>f</sup>fractional misfit



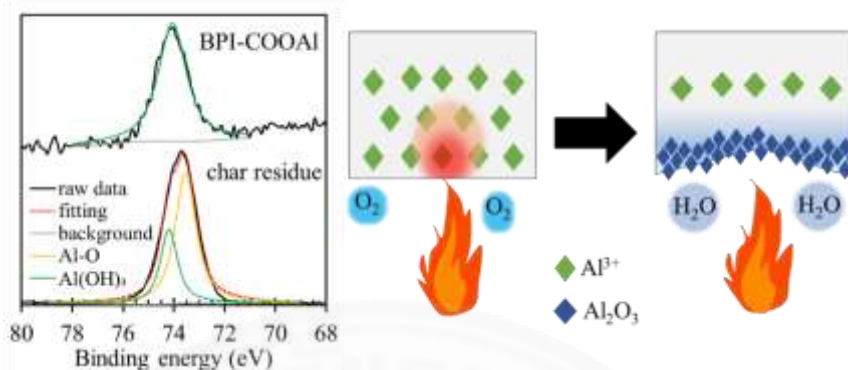
**Figure 4.28** Local structure at Cu atom of BPI-COOCu made from 1 mol/L Cu<sup>2+</sup> initial concentration

The fitting of Al2p XPS spectra for BPI-COOAl in **Figure 4.29** was adopted from the literature (Corsi et al., 2019). The results showed Al(OH)<sub>3</sub> from Al<sup>3+</sup> of aluminum carboxylate (~74 eV) as the main species in BPI-COOAl. The BPI-COOAl char residue contained Al(OH)<sub>3</sub> and Al-O from Al<sub>2</sub>O<sub>3</sub> (~73.7 eV). The latter was formed according to Equation (4.1) with the O<sub>2</sub> from the atmosphere. H may also come from the atmosphere or the degradation of cyclobutene and benzene rings in the BPI structure.



The mechanism in **Figure 4.29** shows that an Al<sub>2</sub>O<sub>3</sub> char layer formed and prevented the spreading of heat. Moreover, the water molecules released during the

reaction suppressed smoke, prevented access to O<sub>2</sub>, and provided further support for flame retardancy.

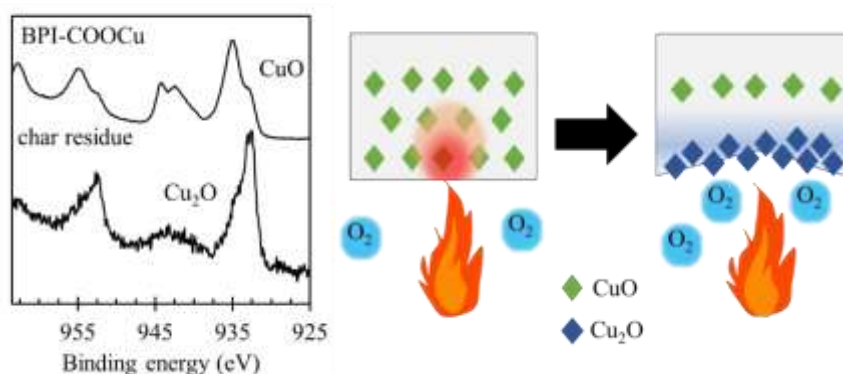


**Figure 4.29** Proposed flame retardant mechanism of BPI-COOAl with Al2p XPS spectra and flame retardant mechanism diagram

XPS spectra of BPI-COOCu, focusing on the Cu2p3 region, is displayed in **Figure 4.30**. The results show that CuO from the carboxylation of Cu<sup>2+</sup> is the main species of BPI-COOCu. Cu<sub>2</sub>O was observed in the film char residue. This suggests that the Cu<sub>2</sub>O char layer is an intumescent material during burning (**Figure 4.30**). The accumulation of the char layer can also be explained by Equation (4.2).



In the formation of Cu<sub>2</sub>O at high temperatures, a previous study revealed that about 10% oxygen (O<sub>2</sub>) was created in the process (Hu et al., 2016). Cu<sub>2</sub>O could act as an intumescent material that prevented the transfer of heat, but the addition of O<sub>2</sub> promoted fire.





**Figure 4.30** Proposed flame retardant mechanism of BPI-COOCu with Cu<sub>2</sub>p<sub>3</sub> with XPS spectra



## CHAPTER 5

### CONCLUSIONS AND RECOMMENDATIONS

The selected adsorbents after the screening test were Fe-Alg, hazelnut shells, sacha inchi shells, anthocyanin-containing adsorbents, and cationic biopolyamides. They exhibited more than 70% efficiency (2 h contact time and 10 mg/L  $I^-$  initial concentration) at all doses.

As a bio-based adsorbent with metal incorporation, Fe-Alg yielded 139 mg/g adsorption capacity and 30 min equilibrium time. The adsorbent outperformed the commercial polystyrene-based resin and was comparable to some recently synthesized materials in removing  $I^-$  from water. However, it was not stable in the presence of other anions, and the iron leakage was observed in the seawater medium. This made Fe-Alg suitable for the application of  $I^-$  remediation in closed and controlled environment. The cationic biopolyamides were previously derived from glucose and bacterial fermentation. The quaternary ammonium bearing adsorbents possessed a maximum of 37 mg/g capacity (PA-R4), however, the polymers were stable even at 90 °C. This made the biopolymer suitable for specific applications that required  $I^-$  adsorption in a near-boiling environment. Both types of adsorbents were explained by the pseudo-first-order reaction as well as Langmuir isotherm. This infer the physical nature of adsorbent by an equal localized adsorption energy created by the incorporated  $Fe^{3+}$  (in Fe-Alg) and quaternary ammonium (in cationic biopolyamides).

Unlike Fe-Alg and cationic biopolyamides, the other selected adsorbents were unmodified plant parts. Sacha inchi shells possessed 48.4 mg/g of  $I^-$  adsorption capacity. This value was higher than the commercial resin and some of the adsorbents in the literature. Hazelnut shells showed a low adsorption capacity of 18.9 mg/g. The mechanism of  $I^-$  adsorption by sacha inchi shells and hazelnut shells was governed by an electrostatic attraction by cationic minerals (Mg, K, and Ca). The changes in FTIR peaks were observed mostly at those corresponding to the neighboring functional groups of the mentioned cationic minerals. The anthocyanin-containing adsorbents exhibited promising results as 79.0 and 75.0 mg/g adsorption capacity were reported for mangosteen pericarps and red onion peels, respectively. Leakage in anthocyanin was observed for red dragon fruit peels, and low adsorption capacity of 10 mg/g was

observed for passion fruit rinds. The characterizations confirmed the role of anthocyanin as the primary functional group involved in chemically attracting  $I^-$ . The change in functional group related to anthocyanin was observed where  $I^-$  was located near  $O^+$  with  $\sim 3.28 \text{ \AA}$  radial distance. According to the isothermal model fits, sacha inchi shells and hazelnut shells exhibited a physical adsorption (better fitting for the pseudo-first-order reaction model). The negative activation energy ( $E_a$ ) by the fittings of Arrhenius model confirmed the physical adsorption. Contrastingly, the results of the anthocyanin-containing adsorbents fitted better with the pseudo-second-order reaction model. Moreover, 88.1 and 55.8 kJ/mol of  $E_a$  were required in the  $I^-$  adsorption by mangosteen pericarps and red onion peels. These results infer, to a large extent, that the attraction by anthocyanin was a chemical-driven mechanism.

The same mechanism involving anthocyanin as an active functional group was assumed in the experiment of  $IO_3^-$  adsorption. In this case, the pomegranate skin was added as one of the adsorbents, and it outperformed the mangosteen pericarps with a  $q$  value of 12.0 mg/g. Although the  $IO_3^-$  adsorption performance was met with lower efficiency than that of  $I^-$  adsorption, the study has demonstrated a potential bio-based adsorbent for the  $IO_3^-$  pollution. The results also infer that more unmodified materials containing cations should be explored for the adsorption of anions pollutants. This will add to more sustainable options for such an application.

Lastly, the complexation of BPI to  $Al^{3+}$  and  $Cu^{2+}$  yielded 0.101 and 0.161 mol/g metal removal capacity, respectively. The equilibrium time to create stable BPI-metal films was about 30 min. Such complexation was governed by the exothermic reaction as the negative values of  $\Delta H$  and  $\Delta S$  were yielded in the thermodynamic study. The XPS results revealed  $Al(OH)_3$  and  $CuO$  as the metal form of BPI-COOAl and BPI-COOCu films, respectively. After burning, both films were observed with crystallized char layers ( $Al_2O_3$  and  $Cu_2O$ ) that may act as a protective layer preventing the spread of fire. As a result, the films can be used further for the fire safety application, especially for PI-COOAl as the water was created during the burning to suppress the fire.

All in all, this research has shown successful removal of inorganic pollutant ( $I^-$ ,  $IO_3^-$ ,  $Al^{3+}$ , and  $Cu^{2+}$ ) by bio-based adsorbents in the aqueous environment. The bio-based adsorbents such as mangosteen pericarps, pomegranate skins, hazelnut shells, and sacha inchi shells could be employed for the remediation of ionic pollutants in the

natural water environment as they pose minimal negative affects to human and organisms. They are free and can be used with minimal processing (rinsing and drying). On the other hand, the costs of conventional polystyrene resin and metal-based adsorbent came from limited resources, syntheses, and chemical waste handling. With the same adsorbent dose, the fruit waste containing anthocyanin is viewed as more sustainable as well as economical. Fe-Alg, cationic biopolyamides, and BPI are more suitable as industrial-based materials for pollutants removal because they are more stable in controlled and extreme condition. These adsorbents represent more sustainable options for the applications of environmental engineering and waste management.

### **Recommendations**

Modifications in environmental conditions should be performed to improve the  $I^-$  adsorption capacities for some of the adsorbents. For instance, EDX suggested that Na and K in hazelnut shells and sacha inchi shells involve more significantly in the  $I^-$  adsorption process. A method of adding more of these cations in the adsorbents should be explored.

Due to the successful regeneration tests in some of the adsorbents, further studies should be carried out to access the adsorbents reusability after I-131 is decayed to Xenon-131 (Xe-131). This will contribute to the spent adsorbent handling technique and help minimize waste in the future.

For the adsorption study, future screening tests should consider the competing alternatives through the fine-tuning of additional criteria. This includes other variation of adsorbent doses, time of contact as well as initial  $I^-$  concentration.

Overall, future work should be an exploration of more adsorbents with minimal processing and high removal efficiency. Also, syntheses of new bio-based materials (with green chemical and methods) should be geared toward better stability and reusability in a closed environment condition. This study indicates the importance of the continue examination of bio-based adsorbents in the removal of ionic and radioactive substances from the water.

## REFERENCES

- Ablouh, E.H., Hanani, Z., Eladlani, N., Rhazi, M., & Taourirte, M., (2019). Chitosan microspheres/sodium alginate hybrid beads: An efficient green adsorbent for heavy metals removal from aqueous solutions. *Sustainable Environment Research*, 1(1). doi:10.1186/s42834-019-0004-9
- Adams, R.E., & Browning Jr, W.E., (1960). Removal of radioiodine from air streams by activated charcoal. Oak Ridge. doi:10.2172/4200026
- Afkhami, A., Madrakian, T., & Zarei, A.R., (2001). Spectrophotometric determination of periodate, iodate and bromate mixtures based on their reaction with iodide. *Analytical Sciences*, 17(10), 1199–1202. doi:10.2116/analsci.17.1199
- Agency for Toxic Substances and Disease Registry, (2004). Toxicological profile for iodine (pp 33–80). Atlanta: U.S. Department of Health and Human Services.
- Ahlberg, P., Hinnemo, M., Song, M., Gao, X., Olsson, J., Zhang, S.L., & Zhang, Z.B., (2015). A two-in-one process for reliable graphene transistors processed with photo-lithography. *Applied Physics Letters*, 107(20), 203104. doi:10.1063/1.4935985
- Al-Saydeh, S.A., El-Naas, M.H., & Zaidi, S.J., (2017). Copper removal from industrial wastewater: A comprehensive review. *Journal of Industrial and Engineering Chemistry*, 56, 35–44. doi:10.1016/j.jiec.2017.07.026
- Aldahan, A., Kekli, A., & Possnert, G., (2006). Distribution and sources of <sup>129</sup>I in rivers of the Baltic region. *Journal of Environmental Radioactivity*, 88, 49–73.
- Anderson, H.L., Balsley, S.D., & Brady, P. V, (1995). *Iodide retention by cinnabar (HgS) and chalcocite (Cu<sub>2</sub>S)*. Albuquerque: Sandia National Laboratories.
- Ar Gall, E., Küpper, F.C., & Kloareg, B., (2004). A survey of iodine content in *Laminaria digitata*. *Botanica Marina*, 47(1), 30–37. doi:10.1515/BOT.2004.004
- Araya, M., McGoldrick, M.C., Klevay, L.M., Strain, J.J., Robson, P., Nielsen, F., Olivares, M., Pizarro, F., Johnson, L.A., & Poirier, K.A., (2001). Determination of an acute no-observed-adverse-effect level (NOAEL) for copper in water. *Regulatory Toxicology and Pharmacology*, 34(2), 137–145. doi:10.1006/rtph.2001.1492

- Arnal, J.M., Esteban, J.M.C., Garcla, J.L., Fernandez, M.S., Clar, I.I., & Miranda, I.A., (2000). Declassification of radioactive waste solutions of iodine (I125) from radioimmune analysis (RIA) using membrane techniques. *Desalination*, 129, 101–105. doi:10.1016/S0011-9164(00)00053-9
- Asaduzzaman, A.M., & Schreckenbach, G., (2011). Computational studies of the interactions of I<sup>-</sup> and I<sub>3</sub><sup>-</sup> with TiO<sub>2</sub> clusters: implications for dye-sensitized solar cells. *Theoretical Chemistry Accounts*, 129(2), 199–208. doi:10.1007/s00214-011-0920-1
- Asrarian, R., Jadidian, R., Parham, H., & Haghtalab, S., (2014). Removal of Aluminum from water and wastewater using magnetic iron oxide nanoparticles. *Advanced Materials Research*, 829, 752–756. doi:10.4028/www.scientific.net/AMR.829.752
- Atkinson, A., & Nickerson, A.K., (1988). Diffusion and sorption of cesium, strontium, and iodine in water-saturated cement. *Nuclear Technology*, 81(1), 100–113. doi:10.13182/NT88-A34082
- Ayoub, G.M., Sermerjian, L., Acra, A., El Fadel, M., & Koopman, B., (2001). Heavy metal removal by coagulation with seawater liquid bittern. *Journal of Environmental Engineering*, 127(3), 196–207. doi:10.1061/(ASCE)0733-9372(2001)127:3(196)
- Badawi, M.A., Negm, N.A., Abou Kana, M.T.H., Hefni, H.H., & Abdel Moneem, M.M., (2017). Adsorption of aluminum and lead from wastewater by chitosan-tannic acid modified biopolymers: Isotherms, kinetics, thermodynamics and process mechanism. *International Journal of Biological Macromolecules*, 99, 465–476. doi:10.1016/j.ijbiomac.2017.03.003
- Baily, N.A., & Kelly, S., (1955). Iodine exchange in *Ascophyllum*. *Biological Bullentin*, 109(1), 13–21. doi:10.2307/1538655
- Baily, N.A., & Kelly, S., (1951). The uptake of radioactive iodine by *Ascophyllum*. *Biological Bullentin*, 100(3), 188–190. doi:10.2307/1538529
- Baimenov, A.Z., Berillo, D.A., & Inglezakis, V.J., (2020). Cryogel-based Ag<sup>0</sup>/Ag<sub>2</sub>O nanocomposites for iodide removal from water. *Journal of Molecular Liquids*, 299, 112134. doi:10.1016/j.molliq.2019.112134
- Barkauskas, J., & Dervinyte, M., (2004). An investigation of the functional groups on

- the surface of activated carbons. *Journal of the Serbian Chemical Society*, 69(5), 363–375. doi:10.2298/JSC0405363B
- Basílio, N., & Pina, F., (2016). Chemistry and photochemistry of anthocyanins and related compounds: a thermodynamic and kinetic approach. *Molecules*, 21(11), 1502. doi:10.3390/molecules21111502
- Bauman, W., & Mckeller, R., (1952). *Anion exchange resins*. Midland: The Dow Chemical Company.
- Bo, A., Sarina, S., Liu, H., Zheng, Z., Xiao, Q., Gu, Y., Ayoko, G.A., & Zhu, H., (2016). Efficient Removal of Cationic and Anionic Radioactive Pollutants from Water Using Hydrotalcite-Based Getters. *Applied Materials and Interfaces*, 8(25), 16503–16510. doi:10.1021/acsami.6b04632
- Boaventura, A. R., Duarte, A. S. A. & Almeida, M.F., (2000). Aluminium recovery from water treatment sludges. *IV International Conference Water Supply and water quality*, (pp 1–4). Kraków, Poland: The International Water Association Poland.
- Bonhoure, I., Scheidegger, A.M., Wieland, E., & Dähn, R., (2002). Iodine species uptake by cement and CSH studied by I K-edge X-ray absorption spectroscopy. *Radiochimica Acta*, 90(9–11), 647–651. doi:10.1524/ract.2002.90.9-11\_2002.647
- Boonamnuayvitaya, V., Chaiya, C., Tanthapanichakoon, W., & Jarudilokkul, S., (2004). Removal of heavy metals by adsorbent prepared from pyrolyzed coffee residues and clay. *Separation and Purification Technology*, 35(1), 11–22. doi:10.1016/S1383-5866(03)00110-2
- Boonamnuayvitaya, V., Sae-Ung, S., & Tanthapanichakoon, W., (2005). Preparation of activated carbons from coffee residue for the adsorption of formaldehyde. *Separation and Purification Technology*, 42(2), 159–168. doi:10.1016/j.seppur.2004.07.007
- Braverman MD, L.E., & Cooper, D., (2005). *The Thyroid. A Fundamental and Clinical Text*. Philadelphia: Lippincott Williams & Wilking.
- Brunauer, S., Emmett, P.H., & Teller, E., (1938). Adsorption of gases in multimolecular layers. *Journal of the American Chemical Society*, 60(2), 309–319. doi:10.1021/ja01269a023
- Bürgi, H., Schaffner, T., & Seiler, J.P., (2001). The toxicology of iodate: A review of

- the literature. *Thyroid*, 11(5), 449–456. doi:10.1089/105072501300176408
- Cai, S., Zhang, B., & Cremaschi, L., (2017). Review of moisture behavior and thermal performance of polystyrene insulation in building applications. *Building and Environment*, 123, 50–65. doi:10.1016/j.buildenv.2017.06.034
- Cao, Z., Ge, H., & Lai, S., (2001). Studies on synthesis and adsorption properties of chitosan cross-linked by glutaraldehyde and Cu(II) as template under microwave irradiation. *European Polymer Journal*, 37(10), 2141–2143. doi:10.1016/S0014-3057(01)00070-2
- Carpenter, L.J., Malin, G., Liss, P.S., & Küpper, F.C., (2000). Novel biogenic iodine-containing trihalomethanes and other short-lived halocarbons in the coastal East Atlantic. *Global Biogeochemical Cycles*, 14(4), 1191–1204. doi:10.1029/2000GB001257
- Carpenter, L.J., Sturges, W.T., Penkett, S.A., Liss, P.S., Aliche, B., Hebestreit, K., & Platt, U., (1999). Short-lived alkyl iodides and bromides at Mace Head, Ireland: Links to biogenic sources and halogen oxide production. *Journal of Geophysical Research*, 104(D1), 1679–1689. doi:10.1029/98jd02746
- Chae, S., & Kin, C., (2014). Removal of cesium (<sup>137</sup> Cs) and iodide (<sup>127</sup> I) by microfiltration nanofiltration reverse osmosis membranes. *Journal of Korean Society of Water and Wastewater*, 28(5), 549–554. doi:10.11001/jksww.2014.28.5.549
- Chen, C., Habert, G., Bouzidi, Y., & Jullien, A., (2010). Environmental impact of cement production: detail of the different processes and cement plant variability evaluation. *Journal of Cleaner Production*, 18(5), 478–485. doi:10.1016/j.jclepro.2009.12.014
- Chen, S., & Wang, Y., (2001). Study on  $\beta$ -cyclodextrin grafting with chitosan and slow release of its inclusion complex with radioactive iodine. *Journal of Applied Polymer Science*, 82(10), 2414–2421. doi:10.1002/app.2092
- Chen, Y., Zhang, F., & Xue, Z., (2016). Iodine capture by ionic liquids and recovery by compressed CO<sub>2</sub>. *Journal of Molecular Liquids*, 223, 202–208. doi:10.1016/j.molliq.2016.08.036
- Chen, Z.C., Peng, W.T., Li, J., & Liao, H., (2018). Functional dissection and transport mechanism of magnesium in plants. *Seminars in Cell and Developmental Biology*,



- 74, 142–152. doi:10.1016/j.semcd.2017.08.005
- Chirinos, R., Necochea, O., Pedreschi, R., & Campos, D., (2016). Sacha inchi (*Plukenetia volubilis L.*) shell: An alternative source of phenolic compounds and antioxidants. *International Journal of Food Science and Technology*, 51(4), 986–993. doi:10.1111/ijfs.13049
- Choi, B.S., Park, G. Il, Kim, J.H., Lee, J.W., & Ryu, S.K., (2001). Adsorption equilibrium and dynamics of methyl iodide in a silver ion-exchanged zeolite column at high temperatures. *Adsorption*, 7, 91–103. doi:10.1023/A:1011660121182
- Choung, S., Kim, M., Yang, J.S., Kim, M.G., & Um, W., (2014). Effects of radiation and temperature on iodide sorption by surfactant-modified bentonite. *Environmental Science and Technology*, 48(16), 9684–9691. doi:10.1021/es501661z
- Christiansen, J.V., & Lars, C., (1989). *Iodine in the environment revisited. An evaluation of the chemical- and physico chemical processes possibly controlling the migration behaviour of iodine in the terrestrial environment*. Roskilde: Risø National Laboratory.
- Clesceri, L.S., (1999). *Standard Methods for the Examination of Water and Wastewater*, 20th ed. Washington, D.C.: American Public Health Association.
- Coates, J., (2004). Interpretation of Infrared Spectra, A Practical Approach. *Encyclopedia of Analytical Chemistry*, (pp 1–23). Newtown: John Wiley & Sons, Ltd.
- Corsi, J.S., Fu, J., Wang, Z., Lee, T., Ng, A.K., & Detsi, E., (2019). Hierarchical Bulk Nanoporous Aluminum for On-Site Generation of Hydrogen by Hydrolysis in Pure Water and Combustion of Solid Fuels. *ACS Sustainable Chemistry and Engineering*, 7(13), 11194–11204. doi:10.1021/acssuschemeng.9b00481
- Dąbrowski, A., (2001). Adsorption - From theory to practice. *Advances in Colloid and Interface Science*, 93(1–3), 135–224. doi:10.1016/S0001-8686(00)00082-8
- Dai, J.L., Zhang, M., Hu, Q.H., Huang, Y.Z., Wang, R.Q., & Zhu, Y.G., (2009). Adsorption and desorption of iodine by various Chinese soils: II Iodide and iodate. *Geoderma*, 153(1–2), 130–135. doi:10.1016/j.geoderma.2009.07.020
- Dekel, D.R., Amar, M., Willdorf, S., Kosa, M., Dhara, S., & Diesendruck, C.E., (2017).

- Effect of Water on the Stability of Quaternary Ammonium Groups for Anion Exchange Membrane Fuel Cell Applications. *Chemistry of Materials*, 29(10), 4425–4431. doi:10.1021/acs.chemmater.7b00958
- Delle Site, A., (2001). Factors affecting sorption of organic compounds in natural sorbent/water systems and sorption coefficients for selected pollutants. A review. *Journal of Physical and Chemical Reference Data*, 30(1), 187–439. doi:10.1063/1.1347984
- Devivier, K., Devol-Brown, I., & Savoye, S., (2004). Study of iodide sorption to the argillite of Tournemire in alkaline media. *Applied Clay Science*, 26(1-4 SPEC. ISS.), 171–179. doi:10.1016/j.clay.2003.07.010
- Dorman, J.W., & Steinberg, S.M., (2010). Analysis of iodide and iodate in Lake Mead, Nevada using a headspace derivatization gas chromatography-mass spectrometry. *Environmental Monitoring and Assessment*, 161(1–4), 229–236. doi:10.1007/s10661-008-0740-5
- Druehl, L.D., Cacklette, M., & D’Auria, J.M., (1988). Geographical and Temporal Distribution of iodine-131 in the Brown Seaweed *Fucus* Subsequent to the Chernobyl Incident. *Marine Biology*, 98, 125–129.
- Eden, G.E., Downing, A.L., & Wheatland, A.B., (1952). Observations on the Removal of Radio-Isotopes During Purification of Domestic Water Supplies: Radio-Iodine. *Journal of Instrumentation Water Engineering*, 6, 511–532.
- Erkey, C., (2011). Chapter 4 - Thermodynamics and dynamics of adsorption of metal complexes on surfaces from supercritical solutions. *Supercritical Fluid Science and Technology*, 1, 41–77. doi:10.1016/B978-0-08-045329-3.00004-4
- Evans, G.J., & Hammad, K.A., (1995). Radioanalytical studies of iodine behavior in the environment. *Journal of Radioanalytical and Nuclear Chemistry*, 192(239–247).
- Ewing, D., & Jones, S.R., (1987). Superoxide removal and radiation protection in bacteria. *Archives of Biochemistry and Biophysics*, 254(1), 53–62. doi:10.1016/0003-9861(87)90080-4
- Ezzeldin, H.A., Apblett, A., & Foutch, G.L., (2010). Synthesis and properties of anion exchangers derived from chloromethyl styrene codivinylbenzene and their use in water treatment. *International Journal of Polymer Science*, 1–9.

doi:10.1155/2010/684051

- Fabryka-Martin, J.T., (1984). *Natural iodine-129 as a ground-water tracer*. Tucson: The University of Arizona.
- Faur-Brasquet, C., Kadirvelu, K., & Le Cloirec, P., (2002). Removal of metal ions from aqueous solution by adsorption onto activated carbon cloths: Adsorption competition with organic matter. *Carbon*, 40(13), 2387–2392. doi:10.1016/S0008-6223(02)00117-3
- Fielman, K.T., Woodin, S.A., Walla, M.D., & Lincoln, D.E., (1999). Widespread occurrence of natural halogenated organics among temperate marine infauna. *Marine Ecology Progress Series*, 181, 1–12. doi:10.3354/meps181001
- Fukui, M., Fujikawa, Y., & Satta, N., (1996). Factors affecting interaction of radioiodide and iodate species with soil. *Journal of Environmental Radioactivity*, 31(2), 199–216. doi:10.1016/0265-931X(95)00039-D
- Galarneau, A., Villemot, F., Rodriguez, J., Fajula, F., & Coasne, B., (2014). Validity of the t-plot method to assess microporosity in hierarchical micro/mesoporous materials. *Langmuir*, 30(44), 13266–13274. doi:10.1021/la5026679
- Ganchev, T., Dyankov, E., Zacharieva, R., Pachalieva, I., Velikova, M., & B, K., (1998). Influence of aluminium on erythropoiesis, iron metabolism and some functional characteristics of erythrocytes in rats. *Acta Physiologica et Pharmacologica Bulgarica*, 23(1), 27–31.
- Gao, R., Lu, Y., Xiao, S., & Li, J., (2017). Facile Fabrication of Nanofibrillated Chitin/Ag<sub>2</sub>O Heterostructured Aerogels with High Iodine Capture Efficiency. *Scientific Reports*, 7(1), 1–9. doi:10.1038/s41598-017-04436-8
- Goher, M.E., Hassan, A.M., Abdel-Moniem, I.A., Fahmy, A.H., Abdo, M.H., & El-sayed, S.M., (2015). Removal of aluminum, iron and manganese ions from industrial wastes using granular activated carbon and Amberlite IR-120H. *Egyptian Journal of Aquatic Research*, 41(2), 155–164. doi:10.1016/j.ejar.2015.04.002
- Goodman, W.G., Gilligan, J., & Horst, R., (1984). Short-term aluminum administration in the rat: effects on bone formation and relationship to renal steomalacia. *The Journal of Clinical Investigation, Inc.*, 73, 171–181.
- Gunatilake, S.K., (2015). Methods of removing heavy metals from industrial

- wastewater. *Journal of Multidisciplinary Engineering Science Studies Industrial Wastewater*, 1(1), 13–18.
- Gutiérrez, L.-F., Rosada, L.-M., & Jiménez, Á., (2011). Chemical composition of Sacha Inchi (*Plukenetia volubilis* L.) seeds and characteristics of their lipid fraction. *Grasas y Aceites*, 62(1), 76–83. doi:10.3989/gya044510
- Haldar, T., & Bagchi, S., (2016). Electrostatic interactions are key to C=O n- $\pi^*$  shifts: An experimental proof. *Journal of Physical Chemistry Letters*, 7(12), 2270–2275. doi:10.1021/acs.jpcclett.6b01052
- Hall, P., Berg, G., Bjelkengren, G., Boice, J.D., Ericsson, U.-B., Hallquist, A., Lidberg, M., Lundell, Gör., Tennvall, J., Wiklund, K., & Holm, L.-E., (1992). Cancer mortality after iodine-131 therapy for hyperthyroidism. *International Journal of Cancer*, 50(6), 886–890. doi:10.1002/ijc.2910500611
- Hamasaki, T., Nakamichi, N., Teruya, K., & Shirahata, S., (2014). Removal efficiency of radioactive cesium and iodine ions by a flow-type apparatus designed for electrochemically reduced water production. *PLoS ONE*, 9(7). doi:10.1371/journal.pone.0102218
- Hamdaoui, O., & Naffrechoux, E., (2007). Modeling of adsorption isotherms of phenol and chlorophenols onto granular activated carbon. Part I. Two-parameter models and equations allowing determination of thermodynamic parameters. *Journal of Hazardous Materials*, 147(1–2), 381–394. doi:10.1016/j.jhazmat.2007.01.021
- Harfouche, M., Wieland, E., Dähn, R., Fujita, T., Tits, J., Kunz, D., & Tsukamoto, M., (2006). EXAFS study of U(VI) uptake by calcium silicate hydrates. *Journal of Colloid and Interface Science*, 303(1), 195–204. doi:10.1016/j.jcis.2006.07.019
- Hartman, J.S., & Kelusky, E.C., (1979). A  $^{13}\text{C}$  nmr study of metal ion binding to pyridoxine. *Canadian Journal of Chemistry*, 57, 2118–2323. doi:10.1139/v79-340
- Harvey, P.J., Handley, H.K., & Taylor, M.P., (2016). Widespread copper and lead contamination of household drinking water, New South Wales, Australia. *Environmental Research*, 151, 275–285. doi:10.1016/j.envres.2016.07.041
- Havens, K.E., (1993). Acid and aluminum effects on the survival of littoral macro-invertebrates during acute bioassays. *Environmental Pollution*, 80(1), 95–100. doi:10.1016/0269-7491(93)90016-H
- He, J., & Giusti, M.M., (2010). Anthocyanins: Natural colorants with health-promoting

- properties. *Annual Review of Food Science and Technology*, 1, 163–167. doi:10.1146/annurev.food.080708.100754
- Hieu, T.T., Russell, A.W., Cuneo, R., Clark, J., Kron, T., Hall, P., & Doi, S.A.R., (2012). Cancer risk after medical exposure to radioactive iodine in benign thyroid diseases: a meta-analysis. *Endocrine-Related Cancer*, 19(5), 645–655. doi:10.1530/ERC-12-0176
- Hiranrangsee, L., Kumaree, K.K., Sadiq, M.B., & Anal, A.K., (2016). Extraction of anthocyanins from pericarp and lipids from seeds of mangosteen (*Garcinia mangostana* L.) by Ultrasound-assisted extraction (UAE) and evaluation of pericarp extract enriched functional ice-cream. *Journal of Food Science and Technology*, 53(10), 3806–3813. doi:10.1007/s13197-016-2368-8
- Hoskins, J.S., & Karafil, T., (2002). Removal and sequestration of iodide using silver-impregnated activated carbon. *Environmental Science and Technology*, 36(4), 784–789. doi:10.1021/es010972m
- Hossain, N., Bhuiyan, M.A., Pramanik, B.K., Nizamuddin, S., & Griffin, G., (2020). Waste materials for wastewater treatment and waste adsorbents for biofuel and cement supplement applications: A critical review. *Journal of Cleaner Production*, 255. doi:10.1016/j.jclepro.2020.120261
- Hosseini, Syed Abbas, Hosseini, Syed Ali, & Mehr, J.P.J., (2013). The role of temperature on radio iodine adsorption behavior in the sandy-loam soil. *Asian Journal of Scientific Research*, 6(1), 129–134.
- Hou, X., Povinec, P.P., Zhang, L., Shi, K., Biddulph, D., Chang, C., Fan, Y., Golser, R., Hou, Y., Jeřkovsky, M., Jull, A.J.Ti., Liu, Q., Luo, M., Steier, P., & Zhou, W., (2013). Iodine-129 in seawater offshore fukushima: distribution, inorganic speciation, sources, and budget. *Environmental Science and Technology*, 47, 3091–3098. doi:dx.doi.org/10.1021/es304460k
- Hou, X., Yan, X., & Chai, C., (1999). Chemical species of iodine in some seaweeds – II. Iodine-bound biological macromolecules. *Radioanalytical and Nuclear Chemistry*, 245(3), 461–467.
- Hu, W., Donat, F., Scott, S.A., & Dennis, J.S., (2016). The interaction between CuO and Al<sub>2</sub>O<sub>3</sub> and the reactivity of copper aluminates below 1000 °C and their implication on the use of the Cu-Al-O system for oxygen storage and production.

- RSC Advances*, 6(114), 113016–113024. doi:10.1039/c6ra22712k
- Huang, E., (2007). Use of fish scales as biosorbent for the removal of copper in water. *Water Research*, 30, 1985–1990.
- Huang, T.T., Tsai, C.L., Tateyama, S., Kaneko, T., & Liou, G.S., (2016). Highly transparent and flexible bio-based polyimide/TiO<sub>2</sub> and ZrO<sub>2</sub> hybrid films with tunable refractive index, Abbe number, and memory properties. *Nanoscale*, 8(25), 12793–12802. doi:10.1039/c6nr03963d
- Hughes, J.T., Sava, D.F., Nenoff, T.M., & Navrotsky, A., (2013). Thermochemical evidence for strong iodine chemisorption by ZIF-8. *Journal of the American Chemical Society*, 135(44), 16256–16259. doi:10.1021/ja406081r
- Inglezakis, V.J., & Zorpas, A.A., (2012). Heat of adsorption, adsorption energy and activation energy in adsorption and ion exchange systems. *Desalination and Water Treatment*, 39(1–3), 149–157. doi:10.1080/19443994.2012.669169
- Inoue, H., (2004). Effects of co-ions on transport of iodide ions through a non-conventional anion exchange paper membrane. *Journal of Membrane Science*, 228(2), 209–215. doi:10.1016/j.memsci.2003.10.009
- Inoue, H., & Kagoshima, M., (2000). Removal of <sup>125</sup>I from radioactive experimental waste with an anion exchange paper membrane. *Applied Radiation and Isotopes*, 52, 1407–1412.
- International Atomic Energy Agency, (2006). *Chernobyl's legacy: Health, environmental and socio-economic impacts and recommendations to the governments of Belarus, the Russian federation and Ukraine*. Vienna: International Atomic Energy Agency.
- Janardhan, R., Gedam, P.H., & Sampathkumaran, P.S., (1990). The effect of polymer molecular weight in the adsorption process. *Journal of Colloid And Interface Science*, 140(2), 391–400. doi:10.1016/0021-9797(90)90359-V
- Jangyubol, K., Kasemwong, K., Charoenrat, T., & Chittapun, S., (2018). Magnetic-cationic cassava starch composite for harvesting *Chlorella* sp. TISTR8236. *Algal Research*, 35(April), 561–568. doi:10.1016/j.algal.2018.09.027
- Jhiang, S.M., Smanik, P.A., & Mazzaferri, E.L., (1994). Development of a single-step duplex RT-PCR detecting different forms of ret activation, and identification of the third form of in vivo ret activation in human papillary thyroid carcinoma.

- Cancer Letters*, 78(1–3), 69–76. doi:10.1016/0304-3835(94)90033-7
- Johnson, K.E., (2007). What's an Ionic Liquid? *Electrochemical Society Interface*, 16(1), 38–41. doi:10.1038/nmat2448
- Jubin, R.T., (1979). *A literature survey of methods to remove iodine from off-gas streams using solid sorbents*. Oak Ridge: Oak Ridge National Laboratory.
- Jung, I.K., Jo, Y., Han, S.C., & Yun, J. Il, (2020). Efficient removal of iodide anion from aqueous solution with recyclable core-shell magnetic Fe<sub>3</sub>O<sub>4</sub>@Mg/Al layered double hydroxide (LDH). *Science of the Total Environment*, 705, 135814. doi:10.1016/j.scitotenv.2019.135814
- Kamei, D., Kuno, T., Sato, S., Nitta, K., & Akiba, T., (2012). Impact of the Fukushima Daiichi Nuclear Power Plant accident on hemodialysis facilities: An evaluation of radioactive contaminants in water used for hemodialysis. *Therapeutic Apheresis and Dialysis*, 16(1), 87–90. doi:10.1111/j.1744-9987.2011.01029.x
- Kantati, Y., Kodjo, M., Gnandi, K., Ketoh, G., & Gbeassor, M., (2013). Effects of pollution on oxidative stress in aquatic species: case of the fish *Sarotherodon melanotheron* in Bè Lagoon (Lomé). *International Journal of Biological and Chemical Sciences*, 7(2). doi:10.4314/ijbcs.v7i2.26
- Kaplan, D I, Denham, M.E., Zhang, S., Yeager, C., Xu, C., Schwehr, K.A., Li, H.P., Ho, Y.F., Wellman, D., & Santschi, P.H., (2014). Radioiodine biogeochemistry and prevalence in groundwater. *Critical reviews in environmental science and technology*, 44(20), 2287–2335. doi:10.1080/10643389.2013.828273
- Kaplan, D.I., Knox, A.S., Crapse, K.P., Li, D., & Diprete, P., (2015). Organo-modified clays for removal of aqueous radioactive anions. US20150129504A1.
- Kaplan, Daniel I., Zhang, S., Roberts, K.A., Schwehr, K., Xu, C., Creeley, D., Ho, Y.F., Li, H.P., Yeager, C.M., & Santschi, P.H., (2014). Radioiodine concentrated in a wetland. *Journal of Environmental Radioactivity*, 131. doi:10.1016/j.jenvrad.2013.09.001
- Karkhanei, N., Sepehrian, H., & Cheraghali, R., (2015). Preparation, characterization, and iodide sorption performance of silver-loaded mesoporous MCM-41. *Desalination and Water Treatment*, 56, 3096–3105. doi:10.1080/19443994.2014.963684
- Kaufhold, S., Pohlmann-Lortz, M., Dohrmann, R., & Nüesch, R., (2007). About the

- possible upgrade of bentonite with respect to iodide retention capacity. *Applied Clay Science*, 35(1–2), 39–46. doi:10.1016/j.clay.2006.08.001
- Kawamura, H., Kobayashi, T., Furuno, A., In, T., Ishikawa, Y., Nakayama, T., Shima, S., & Awaji, T., (2011). Preliminary numerical experiments on oceanic dispersion of <sup>131</sup>I and <sup>137</sup>Cs discharged into the ocean because of the Fukushima Daiichi nuclear power plant. *Journal of Nuclear Science and Technology*, 48(11), 1349–1356. doi:10.3327/jnst.48.1349
- Ke, F., Peng, C., Zhang, T., Zhang, M., Zhou, C., Cai, H., Zhu, J., & Wan, X., (2018). Fumarate-based metal-organic frameworks as a new platform for highly selective removal of fluoride from brick tea. *Scientific Reports*, 8(1), 1–12. doi:10.1038/s41598-018-19277-2
- Keogh, S.M., Aldahan, A., Possnert, G., Finegan, P., Leon Vintro, L., & Mitchell, P.I., (2007). Trends in the spatial and temporal distribution of <sup>129</sup>I and <sup>99</sup>Tc in coastal waters surrounding Ireland using *Fucus vesiculosus* as a bio-indicator. *Journal of Environmental Radioactivity*, 95, 23–38.
- Kester, D.R., Deudall, I.W., Connors, D.N., & Pytkowicz, R.M., (1967). Preparation of artificial seawater. *Limnology and Oceanography*, 12(1), 176–179. doi:10.4319/lo.1967.12.1.0176
- Kitada, S., Oikawa, T., Watanabe, S., Nagai, K., Kobayashi, Y., Matsuki, M., Tsuchiya, K., Nakamura, K., Sasaki, M., Shinoda, Y., & Iwamoto, T., (2015). Removal of radioactive iodine and cesium in water purification. *Desalination and Water Treatment*, 54(13), 3494–3501. doi:10.1080/19443994.2014.923205
- Kobayashi, T., & Yokoyama, K., (2016). Theoretical study of the adsorption of Cs, Cs<sup>+</sup>, I, I<sup>-</sup>, and CsI on C<sub>60</sub> fullerene. *Journal of Nuclear Science and Technology*, 53(10), 1489–1493. doi:10.1080/00223131.2015.1126206
- Kocasoy, G., & Şahin, V., (2007). Heavy metal removal from industrial wastewater by clinoptilolite. *Journal of Environmental Science and Health - Part A Toxic/Hazardous Substances and Environmental Engineering*, 42(14), 2139–2146. doi:10.1080/10934520701629617
- Kong, Q., & Lin, C.L.G., (2010). Oxidative damage to RNA: Mechanisms, consequences, and diseases. *Cellular and Molecular Life Sciences*,. doi:10.1007/s00018-010-0277-y



- Konings, R.J.M., Wiss, T., & Beneš, O., (2015). Predicting material release during a nuclear reactor accident. *Nature Materials*, 14(March), 247–252. doi:10.1038/nmat4224
- Kosaka, K., Asami, M., Kobashigawa, N., Ohkubo, K., Terada, H., Kishida, N., & Akiba, M., (2012). Removal of radioactive iodine and cesium in water purification processes after an explosion at a nuclear power plant due to the Great East Japan Earthquake. *Water Research*, 46(14), 4397–4404. doi:10.1016/j.watres.2012.05.055
- Koter, S., (1999). Comparative investigations of ion-exchange membranes. *Journal of Membrane Science*, 153(1), 83–90. doi:10.1016/S0376-7388(98)00242-7
- Langmuir, I., (1918). The adsorption of gases on plane surfaces of glass, mica and platinum. *Journal of the American Chemical Society*, 40(9), 1361–1403. doi:10.1021/ja02242a004
- Lata, S., Singh, P.K., & Samadder, S.R., (2015). Regeneration of adsorbents and recovery of heavy metals: A review. *International Journal of Environmental Science and Technology*, 12(4), 1461–1478. doi:10.1007/s13762-014-0714-9
- Leblanc, C., Colin, C., Cosse, A., Delage, L., La Barre, S., Morin, P., Fiévet, B., Voiseux, C., Ambroise, Y., Verhaeghe, E., Amouroux, D., Donard, O., Tessier, E., & Potin, P., (2006). Iodine transfers in the coastal marine environment: the key role of brown algae and of their vanadium-dependent haloperoxidases. *Biochimie*, 88(11), 1773–1785. doi:10.1016/j.biochi.2006.09.001
- Lefèvre, G., Bessière, J., Ehrhardt, J.J., & Walcarius, A., (2003). Immobilization of iodide on copper(I) sulfide minerals. *Journal of Environmental Radioactivity*, 70(1–2), 73–83. doi:10.1016/S0265-931X(03)00119-X
- Lefèvre, G., Walcarius, A., Ehrhardt, J.-J., & Bessière, J., (2000). Sorption of iodide on cuprite (Cu<sub>2</sub>O). *Langmuir*, 16(10), 4519–4527. doi:10.1021/la9903999
- Lemma, F.G. Di, Colle, J.Y., Bene, O., & Konings, R.J.M., (2015). A separate effect study of the influence of metallic fission products on CsI radioactive release from nuclear fuel. *Journal of Nuclear Materials*, 465, 499–508. doi:10.1016/j.jnucmat.2015.05.037
- Li, D., Kaplan, D.I., Knox, A.S., Crapse, K.P., & Diprete, D.P., (2014). Aqueous <sup>99</sup>Tc, <sup>129</sup>I and <sup>137</sup>Cs removal from contaminated groundwater and sediments using highly

- effective low-cost sorbents. *Journal of Environmental Radioactivity*, 136, 56–63. doi:10.1016/j.jenvrad.2014.05.010
- Li, K., Zhao, Y., Zhang, P., He, C., Deng, J., Ding, S., & Shi, W., (2016). Combined DFT and XPS investigation of iodine anions adsorption on the sulfur terminated (001) chalcopyrite surface. *Applied Surface Science*, 390, 412–421. doi:10.1016/j.apsusc.2016.08.095
- Li, L., Fang, Y., Vreeker, R., Appelqvist, I., & Mendes, E., (2007). Reexamining the egg-box model in calcium - Alginate gels with X-ray diffraction. *Biomacromolecules*, 8(2), 464–468. doi:10.1021/bm060550a
- Li, M., Liu, J., Xu, Y., & Qian, G., (2016). Phosphate adsorption on metal oxides and metal hydroxides: A comparative review. *Environmental Reviews*, 24(3), 319–332. doi:10.1139/er-2015-0080
- Li, Q., Mao, Q., Li, M., Zhang, S., He, G., & Zhang, W., (2020). Cross-linked chitosan microspheres entrapping silver chloride via the improved emulsion technology for iodide ion adsorption. *Carbohydrate Polymers*, 234(January), 115926. doi:10.1016/j.carbpol.2020.115926
- Liu, R., Gong, W., Lan, H., Yang, T., Liu, H., & Qu, J., (2012). Simultaneous removal of arsenate and fluoride by iron and aluminum binary oxide: Competitive adsorption effects. *Separation and Purification Technology*, 92, 100–105. doi:10.1016/j.seppur.2012.03.020
- Liu, S., Kang, S., Wang, H., Wang, G., Zhao, H., & Cai, W., (2016). Nanosheets-built flowerlike micro/nanostructured Bi<sub>2</sub>O<sub>2.33</sub> and its highly efficient iodine removal performances. *Chemical Engineering Journal*, 289, 219–230. doi:10.1016/j.cej.2015.12.101
- Liu, Y., (2009). Is the free energy change of adsorption correctly calculated? *Journal of Chemical and Engineering Data*, 54(7), 1981–1985. doi:10.1021/jc800661q
- Liu, Y., Gu, P., Yang, Y., Jia, L., Zhang, M., & Zhang, G., (2016). Removal of radioactive iodide from simulated liquid waste in an integrated precipitation reactor and membrane separator (PR-MS) system. *Separation and Purification Technology*, 171, 221–228. doi:10.1016/j.seppur.2016.07.034
- Loderio, P., Cordero, B., Barriada, J.L., Herrero, R., & Sastre de Vicente, M.E., (2005). Biosorption of Cadmium by Biomass of Brown Marine Macroalgae. *Bioresource*

- Technology*, 96(16), 1796–1803.
- Long, H., Wu, P., & Zhu, N., (2013). Evaluation of Cs<sup>+</sup> removal from aqueous solution by adsorption on ethylamine-modified montmorillonite. *Chemical Engineering Journal*, 225, 237–244. doi:10.1016/j.cej.2013.03.088
- Lonin, A.Y., Levenets, V. V., Neklyudov, I.M., & Shchur, A.O., (2015). The usage of zeolites for dynamic sorption of cesium from waste waters of nuclear power plants. *Journal of Radioanalytical and Nuclear Chemistry*, 303(1), 831–836. doi:10.1007/s10967-014-3597-9
- Lopes, L.P.C., Martins, J., Esteves, B., & Lemos, L.T.D.E., (2012). New products From hazelnut shell. *ECOWOOD' 12 - Towards Forest Products and Processes with Lower Environmental Impact*, (pp 83–90).
- Madrakian, T., Afkhami, A., Zolfigol, M.A., Ahmadi, M., & Koukabi, N., (2012). Application of modified silica coated magnetite nanoparticles for removal of iodine from water samples. *Nano-Micro Letters*, 4(1), 57–63. doi:10.1007/BF03353693
- Majidnia, Z., & Idris, A., (2015). Photocatalytic reduction of iodine in radioactive waste water using maghemite and titania nanoparticles in PVA-alginate beads. *Journal of the Taiwan Institute of Chemical Engineers*, 54, 137–144. doi:10.1016/j.jtice.2015.03.005
- Makuc, D., Hiscock, J.R., Light, M.E., Gale, P.A., & Plavec, J., (2011). NMR studies of anion-induced conformational changes in diindolylureas and diindolylthioureas. *Beilstein Journal of Organic Chemistry*, 7, 1205–1214. doi:10.3762/bjoc.7.140
- Malhotra, N., Ger, T.R., Uapipatanakul, B., Huang, J.C., Chen, K.H.C., & Hsiao, C. Der, (2020). Review of copper and copper nanoparticle toxicity in fish. *Nanomaterials*, 10(6), 1–28. doi:10.3390/nano10061126
- Mao, P., Yu, X., Liu, K., Sun, A., Shen, J., Yang, Y., Ni, L., Yue, F., & Wang, Z., (2020). Rapid and reversible adsorption of radioactive iodide from wastewaters by green and low-cost palygorskite-based microspheres. *Journal of Radioanalytical and Nuclear Chemistry*, 325(1), 303–313. doi:10.1007/s10967-020-07231-4
- Martinelango, P.K., Tian, K., & Dasgupta, P.K., (2006). Perchlorate in seawater: Bioconcentration of iodide and perchlorate by various seaweed species. *Analytica*

- Chimica Acta*, 567(1 SPEC. ISS.), 100–107. doi:10.1016/j.aca.2006.02.015
- Matsui, Y., Ishikawa, T.B., Kimura, M., Machida, K., Shirasaki, N., & Matsushita, T., (2013). Aluminum concentrations of sand filter and polymeric membrane filtrates: A comparative study. *Separation and Purification Technology*, 119, 58–65. doi:10.1016/j.seppur.2013.09.006
- Matthiessen, P., Reed, J., & Johnson, M., (1999). Sources and potential effects of copper and zinc concentrations in the estuarine waters of Essex and Suffolk, United Kingdom. *Marine Pollution Bulletin*, 38(10), 908–920. doi:10.1016/S0025-326X(99)00090-9
- Medrano-Macías, J., Leija-Martínez, P., González-Morales, S., Juárez-Maldonado, A., & Benavides-Mendoza, A., (2016). Use of iodine to biofortify and promote growth and stress tolerance in crops. *Frontiers in Plant Science*, 7(AUG2016). doi:10.3389/fpls.2016.01146
- Min, J.H., & Hering, J.G., (1998). Arsenate sorption by Fe(III)-doped alginate gels. *Water Research*, 32(5), 1544–1552. doi:10.1016/S0043-1354(97)00349-7
- Mishra, T., & Tiwari, S.K., (2006). Studies on sorption properties of zeolite derived from Indian fly ash. *Journal of Hazardous Materials*, 137(1), 299–303. doi:10.1016/j.jhazmat.2006.02.004
- Miyake, Y., Matsuzaki, H., Fujiwara, T., Saito, T., Yamagata, T., Honda, M., & Muramatsu, Y., (2012). Isotopic ratio of radioactive iodine ( $^{129}\text{I}/^{131}\text{I}$ ) released from Fukushima Daiichi NPP accident. *Geochemical Journal*, 46(4), 327–333. doi:10.2343/geochemj.2.0210
- Monson, L., Braunwarth, M., & Extrand, C.W., (2008). Moisture absorption by various polyamides and their associated dimensional changes. *Journal of Applied Polymer Science*, 107, 355–363. doi:10.1002/app.27057
- Moreno, C., Baeza-Romero, M.-T., Sanz, M., Gálvez, Ó., Arza, V.L., Ianni, J.C., & Espíldora, E., (2020). Iodide conversion to iodate in aqueous and solid aerosols exposed to ozone. *Physical Chemistry Chemical Physics*, 22(10), 5625–5637. doi:10.1039/C9CP05601G
- Morita, T., Niwa, K., Fujimoto, K., Kasai, H., Yamada, H., Nishiuchi, K., Sakamoto, T., Godo, W., Taino, S., Hayashi, Y., Takeno, K., Nishigaki, T., Fujiwara, K., Aratake, H., Kamonoshita, S., Hashimoto, H., Kobayashi, T., Otsuka, S., &

- Imanaka, T., (2010). Detection and activity of iodine-131 in brown algae collected in the Japanese coastal areas. *Science of The Total Environment*, 408(16), 3443–3447. doi:10.1016/j.scitotenv.2010.04.001
- Motekait, R.J., & Martell, A.E., (1984). Complexes of aluminum(III) with hydroxy carboxylic acids. *Inorganic Chemistry*, 23(1), 18–23. doi:10.1021/ic00169a006
- Nanakoudis, A., (2019). What is SEM? Scanning electron microscopy explained. Retrieved from <https://www.thermofisher.com/blog/microscopy/what-is-sem-scanning-electron-microscopy-explained/>
- Nath, T., Raha, P., & Rakshit, A., (2010). Sorption and desorption behaviour of iodine in alluvial soils of Varanasi, India. *Agricultura*, 14, 9–14.
- National Academy of Science, (1999). Exposure of the American People to Iodine-131 from Nevada Nuclear-Bomb Tests: Review of the National Cancer Institute Report and Public Health Implication, National Academy Press.
- Nestle, N., & Kimmich, R., (1996). Heavy metal uptake of alginate gels studied by NMR microscopy. *Colloids and Surfaces A: Physicochemical and Engineering Aspects*, 115, 141–147. doi:10.1016/0927-7757(96)03608-4
- Nwosu, F.O., Olu-Owolabi, B.I., Adebowale, K.O., Henle, T., & Schwarzenbolz, U., (2009). Pore Structure and Surface Functional Groups on Six Tropical Fruit Nutshell Active Carbons. *Bioremediation, Biodiversity and Bioavailability*,.
- O'Donohue, J.W., REID, M.A., Portmann, B., & Williams, R., (1993). Micronodular cirrhosis and acute liver failure due to chronic copper self-intoxication. *European Journal of gastroenterology & hepatology*, 5(7), 561–562.
- O'Dowd, C.D., Jimenez, J.L., Bahreini, R., Flagan, R.C., Seinfeld, J.H., Hämeri, K., Pirjola, L., Kulmala, M., Jennings, S.G., & Hoffmann, T., (2002). Marine aerosol formation from biogenic iodine emissions. *Nature*, 417(6889), 632–6. doi:10.1038/nature00775
- Oancea, S., & Drăghici, O., (2013). pH and thermal stability of anthocyanin-based optimised extracts of romanian red onion cultivars. *Czech Journal of Food Sciences*, 31(3), 283–291. doi:10.17221/302/2012-CJFS
- Okamoto, Y., Kubota, T., Gotoh, H., Ohto, Y., Aritani, H., Tanaka, T., & Yoshida, S., (1998). XAFS study of zirconia-supported copper catalysts for the NO-CO reaction: Deactivation, rejuvenation and stabilization of Cu species. *Journal of the*

- Chemical Society - Faraday Transactions*, 94(24), 3743–3752.  
doi:10.1039/a807152g
- Oladoja, N.A., Alliu, Y.B., Ofomaja, A.E., & Unuabonah, I.E., (2011). Synchronous attenuation of metal ions and colour in aqua stream using tannin-alum synergy. *Desalination*, 271(1–3), 34–40. doi:10.1016/j.desal.2010.12.008
- Pacini, F., Vorontsova, T., Demidchik, E., Molinaro, E., Agate, L., Romei, C., Shavrova, E., Cherstvoy, E., Ivashkevitch, Y., Kuchinskaya, E., Schlumberger, M., Ronga, G., Filesi, M., & Pinchera, A., (1997). Post-Chernobyl thyroid carcinoma in Belarus children and adolescents: Comparison with naturally occurring thyroid carcinoma in Italy and France. *Journal of Clinical Endocrinology and Metabolism*, 82, 3562–2569.
- Papageorgiou, S.K., Kouvelos, E.P., Favvas, E.P., Sapalidis, A.A., Romanos, G.E., & Katsaros, F.K., (2010). Metal-carboxylate interactions in metal-alginate complexes studied with FTIR spectroscopy. *Carbohydrate Research*, 345(4), 469–473. doi:10.1016/j.carres.2009.12.010
- Paredes, S.P., Fetter, G., Bosch, P., & Bulbulian, S., (2006). Iodine sorption by microwave irradiated hydrotalcites. *Journal of Nuclear Materials*, 359(3), 155–161. doi:10.1016/j.jnucmat.2006.07.022
- Park, S.D., Kim, J.S., Han, S.H., Ha, Y.K., Song, K.S., & Jee, K.Y., (2009). The measurement of <sup>129</sup>I for the cement and the paraffin solidified low and intermediate level wastes (LILWs), spent resin or evaporated bottom from the pressurized water reactor (PWR) nuclear power plants. *Applied Radiation and Isotopes*, 67(9), 1676–1682. doi:10.1016/j.apradiso.2009.01.086
- Parker, K.E., Golovich, E.C., & Wellman, D.M., (2014). Iodine adsorption on ion-exchange resins and activated carbons – batch testing. Richland, WA. doi:10.2172/1163822
- Pathak, P.D., Mandavgane, S.A., & Kulkarni, B.D., (2017). Fruit peel waste: characterization and its potential uses. *Current Science*, 113(3), 444–454. doi:10.18520/cs/v113/i03/444-454
- Perez-Granados, A.M., & Vaquero, M.P., (2002). Silicon, aluminium, arsenic and lithium: Essentiality and human health implications. *The journal of Nutrition Health and Aging*, 6(2), 154–162.

- Peterson, J., MacDonell, M., Haroun, L., & Monette, F., (2007). *Radiological and chemical fact sheets to support health risk analyses for contaminated areas*. Argonne: Argonne National Laboratory Environmental Science Division.
- Phanthuwongpakdee, J., Babel, S., Dwivedi, S., Takada, K., Hirayama, T., & Kaneko, T., (2020). Anion-scavenging biopolyamides from quaternized 4-aminocinnamic acid photodimers. *ACS Sustainable Chemistry & Engineering*, doi:10.1021/acssuschemeng.9b07003
- Plazinski, W., (2012). Sorption of metal cations by alginate-based biosorbents. On the correct determination of the thermodynamic parameters. *Journal of Colloid and Interface Science*, 368(1), 547–551. doi:10.1016/j.jcis.2011.11.025
- Plazinski, W., & Drachb, M., (2015). Binding of bivalent metal cations by  $\alpha$ -1-gulonate: insights from the DFT-MD simulations. *New Journal of Chemistry*, 39(5), 3987–3994. doi:10.1039/C4NJ02206H
- Pour, P.G., Takassi, M.A., & Hamoule, T., (2014). Removal of aluminum from water and industrial waste water. *Oriental Journal of Chemistry*, 30(3), 1365–1369. doi:10.13005/ojc/300356
- Prados-Roman, C., Cuevas, C.A., Fernandez, R.P., Kinnison, D.E., Lamarque, J.F., & Saiz-Lopez, A., (2015). A negative feedback between anthropogenic ozone pollution and enhanced ocean emissions of iodine. *Atmospheric Chemistry and Physics*, 15(4), 2215–2224. doi:10.5194/acp-15-2215-2015
- Raddum, G.G., & Fjellheim, A., (2002). Species composition of freshwater invertebrates in relation to chemical and physical factors in high mountains in Soutwestern Norway. *Water, Air and Soil Pollution: Focus*, 2(2), 311–328. doi:10.1023/A
- Ramana, M.V., (2009). Nuclear power: Economic, safety, health, and environmental issues of near-term technologies. *Annual Review of Environment and Resources*, 34, 127–152. doi:10.1146/annurev.environ.033108.092057
- Ravichandran, R., Binukumar, J.P., Sreeram, R., & Arunkumar, L.S., (2011). An overview of radioactive waste disposal procedures of a nuclear medicine department. *Journal of Medical Physics*, 36(2), 95–99. doi:10.4103/0971-6203.79692
- Ren, L., Qiu, H., Qin, W., Zhang, M., Li, Y., & Wei, P., (2018). Inhibition mechanism

- of  $\text{Ca}^{2+}$ ,  $\text{Mg}^{2+}$  and  $\text{Fe}^{3+}$  in fine cassiterite flotation using octanohydroxamic acid. *Royal Society Open Science*, 5(8). doi:10.1098/rsos.180158
- Rendleman, J.A., (2003). The reaction of starch with iodine vapor. Determination of iodide-ion content of starch-iodine complexes. *Carbohydrate Polymers*, 51(2), 191–202. doi:10.1016/S0144-8617(02)00053-X
- Riebe, B., Bors, J., & Dultz, S., (2001). Retardation capacity of organophilic bentonite for anionic fission products. *Journal of Contaminant Hydrology*, 47(2–4), 255–264. doi:10.1016/S0169-7722(00)00154-6
- Riebe, B., Dultz, S., & Bunnenberg, C., (2005). Temperature effects on iodine adsorption on organo-clay minerals - I. Influence of pretreatment and absorption temperature. *Applied Clay Science*, 28, 9–16. doi:10.1016/j.clay.2004.01.004
- Rodriguez, N.M., & Marsh, H., (1987). Surface Structure of Coals Studied by Iodine and Water Adsorption. *Fuel*, 66(12), 1727–1732.
- Rose, A.L., & Waite, T.D., (2003). Kinetics of hydrolysis and precipitation of ferric iron in seawater. *Environmental Science and Technology*, 37(17), 3897–3903. doi:10.1021/es034102b
- Saibene, D., & Seetharaman, K., (2006). Segmental mobility of polymers in starch granules at low moisture contents. *Carbohydrate Polymers*, 64(4), 539–547. doi:10.1016/j.carbpol.2005.11.025
- Sakuma, S.H., & Marzukee, N., (1995). Removal of iodine-125 from effluents by chemical and soil column methods. *Journal of Radioanalytical and Nuclear Chemistry*, 196(1), 77–87.
- Sánchez-Polo, M., Rivera-Utrilla, J., Salhi, E., & Gunten, U., (2006). Removal of bromide and iodide anions from drinking water by silver-activated carbon aerogels. *Journal of Colloid and Interface Science*, 300(1), 437–441. doi:10.1016/j.jcis.2006.03.037
- Sancho, M., Arnal, J.M., Verdú, G., Lora, J., & Villaescusa, J.I., (2006). Ultrafiltration and reverse osmosis performance in the treatment of radioimmunoassay liquid wastes. *Desalination*, 201(1–3), 207–215. doi:10.1016/j.desal.2006.02.015
- Sato, I., Kudo, H., & Tsuda, S., (2011). Removal efficiency of water purifier and adsorbent for iodine, cesium, strontium, barium and zirconium in drinking water. *The Journal of Toxicological Sciences*, 36(6), 829–834. doi:10.2131/jts.36.829



- Sazarashi, M., Ikeda, Y., Seki, R., & Youshikawa, H., (1994). Adsorption of I<sup>-</sup> Ions on Minerals for <sup>129</sup>I Waste Management. *Journal of Nuclear Science and Technology*, 31(6), 620–622. doi:10.1080/18811248.1994.9735198
- Schmidt, A., Schnabel, C., Handl, J., Jakob, D., Michel, R., Synal, H.A., Lopez, J.M., & Suter, M., (1998). On the analysis of iodine-129 and iodine-127 in environmental materials by accelerator mass spectrometry and ion chromatography. *Science of the Total Environment*, 223(2–3), 131–156. doi:10.1016/S0048-9697(98)00309-X
- Schwarzenbach, R.P., Gschwend, P.M., & Imboden, D.M., (2002). Thermodynamics and kinetics of transformation reactions. *Environmental Organic Chemistry*, (pp 461–488). Hoboken, NJ: Wiley-Interscience. doi:10.1002/0471649643.ch12
- Sedman, A.B., Alfrey, A.C., Miller, N.L., & Goodman, W.G., (1987). Tissue and cellular basis for impaired bone formation in aluminum-related osteomalacia in the pig. *Journal of Clinical Investigation*, 79(1), 86–92. doi:10.1172/JCI112813
- Serrano-Aroca, Á., Ruiz-Pividal, J.F., & Llorens-Gámez, M., (2017). Enhancement of water diffusion and compression performance of crosslinked alginate films with a minuscule amount of graphene oxide. *Scientific Reports*, 7(1), 1–8. doi:10.1038/s41598-017-10260-x
- Shaw, G., Bailey, E., Crout, N., Field, L., Freeman, S., Gaschak, S., Hou, X., Izquierdo, M., Wells, C., Xu, S., & Young, S., (2019). Analysis of <sup>129</sup>I and <sup>127</sup>I in soils of the Chernobyl Exclusion Zone, 29 years after the deposition of <sup>129</sup>I. *Science of the Total Environment*, 692, 966–974. doi:10.1016/j.scitotenv.2019.07.319
- Shimamoto, Y.S., & Takahashi, Y., (2008). Superiority of K-edge XANES over L<sub>III</sub>-edge XANES in the speciation of iodine in natural soils. *Analytical Sciences*, 24(3), 405–409. doi:10.2116/analsci.24.405
- Shimura, H., Itoh, K., Sugiyama, A., Ichijo, S., Ichijo, M., Furuya, F., Nakamura, Y., Kitahara, K., Kobayashi, K., Yukawa, Y., & Kobayashi, T., (2012). Absorption of radionuclides from the Fukushima Nuclear accident by a novel algal strain. *PLoS ONE*, 7(9), 1–9. doi:10.1371/journal.pone.0044200
- Simonin, J.P., (2016). On the comparison of pseudo-first order and pseudo-second order rate laws in the modeling of adsorption kinetics. *Chemical Engineering Journal*, 300, 254–263. doi:10.1016/j.cej.2016.04.079

- Smith, D.K., Finnegan, D.L., & Bowen, S.M., (2003). An inventory of long-lived radionuclides residual from underground nuclear testing at the Nevada test site, 1951-1992. *Journal of Environmental Radioactivity*, 67(1), 35–51. doi:10.1016/S0265-931X(02)00146-7
- Sposito, G., (1998). On points of zero charge. *Environmental Science and Technology*, 32(19), 2815–2819. doi:10.1021/es9802347
- Sugioka, M., (2009). UV Talk Letter. Tokyo.
- Sun, H., La, P., Yang, R., Zhu, Z., Liang, W., Yang, B., Li, A., & Deng, W., (2017). Innovative nanoporous carbons with ultrahigh uptakes for capture and reversible storage of CO<sub>2</sub> and volatile iodine. *Journal of Hazardous Materials*, 321, 210–217. doi:10.1016/j.jhazmat.2016.09.015
- Sussman, S., & Mooretown, N.J., (1948). *Anion exchange resins*. New York: The Permutit Company.
- Sutton, A., Harrison, G.E., Carr, T.E.F., & Barltrop, D., (1971). Reduction in the Absorption of Dietary Strontium in Children by an Alginate Derivative. *International Journal of Radiation Biology and Related Studies in Physics, Chemistry and Medicine*, 19(1), 79–85. doi:10.1080/09553007114550091
- Suzuki, T., Banba, S., Kitamura, T., Kabuto, S., Isogai, K., & Amano, H., (2007). Determination of <sup>129</sup>I in environmental samples by AMS and NAA using an anion exchange resin disk. *Nuclear Instruments and Methods in Physics Research, Section B: Beam Interactions with Materials and Atoms*, 259(1), 370–373. doi:10.1016/j.nimb.2007.01.181
- Syukri, D., Darwis, D., & Santoni, A., (2013). Simple characterization of anthocyanin from *Ficus padana* Burm.f. *Journal of Chemical and Pharmaceutical Research*, 5(12), 1276–1282.
- Szente, L., Fenyvesi, É., & Szejtli, J., (1999). Entrapment of iodine with cyclodextrins: Potential application of cyclodextrins in nuclear waste management. *Environmental Science and Technology*, 33(24), 4495–4498. doi:10.1021/es981287r
- Tachibana, Y., Nogami, M., Nomura, M., & Suzuki, T., (2015). Simultaneous removal of various iodine species in aqueous solutions of high salt concentrations using novel functional adsorbents. *Journal of Radioanalytical and Nuclear Chemistry*,

- 307(3), 1911–1918. doi:10.1007/s10967-015-4441-6
- Takahashi, Y., (1987). Binding properties of alginic acid and chitin. *Journal of Inclusion Phenomena*, 5(4), 525–534. doi:10.1007/BF00664112
- Takayanagi, K., & Wong, G.T.F., (1986). The oxidation of iodide to iodate for the polarographic determination of total iodine in natural waters. *Talanta*, 33(5), 451–454. doi:10.1016/0039-9140(86)80115-1
- Talipov, S.A., Ibragimov, B.T., Tadjimukhamedov, F.K., Tiljakov, Z.G., Blake, A.J., Hertzsch, T., & Hulliger, J., (2007). Inclusion of molecular iodine into channels of the organic zeolite-like gossypol. *Journal of Inclusion Phenomena and Macrocyclic Chemistry*, 59, 287–292. doi:10.1007/s10847-007-9325-0
- Tay, T., Ucar, S., & Karagöz, S., (2009). Preparation and characterization of activated carbon from waste biomass. *Journal of Hazardous Materials*, 165(1–3), 481–485. doi:10.1016/j.jhazmat.2008.10.011
- Thommes, M., & Cychosz, K.A., (2014). Physical adsorption characterization of nanoporous materials: Progress and challenges. *Adsorption*, 20(2–3), 233–250. doi:10.1007/s10450-014-9606-z
- Tien, C.-J., (2002). Biosorption of metal ions by freshwater algae with different surface characteristics. *Process Biochemistry*, 38, 605–613. doi:10.1016/S0032-9592(02)00183-8
- Tits, J., Geipel, G., Macé, N., Eilzer, M., & Wieland, E., (2011). Determination of uranium(VI) sorbed species in calcium silicate hydrate phases: A laser-induced luminescence spectroscopy and batch sorption study. *Journal of Colloid and Interface Science*, 359(1), 248–256. doi:10.1016/j.jcis.2011.03.046
- Tits, J., Wieland, E., Müller, C.J., Landesman, C., & Bradbury, M.H., (2006). Strontium binding by calcium silicate hydrates. *Journal of Colloid and Interface Science*, 300(1), 78–87. doi:10.1016/j.jcis.2006.03.043
- Tournassat, C., Gaucher, E.C., Fattahi, M., & Grambow, B., (2007). On the mobility and potential retention of iodine in the Callovian-Oxfordian formation. *Physics and Chemistry of the Earth*, 32(8–14), 539–551. doi:10.1016/j.pce.2005.12.004
- Toyohara, M., Kaneko, M., Mitsutsuka, N., Fujihara, H., Saito, N., & Murase, T., (2012). Contribution to understanding iodine sorption mechanism onto mixed solid alumina cement and calcium compounds. *Journal of Nuclear Science and*

- Technology*, 39(9), 950–956. doi:10.1080/18811248.2000.9714980
- Tsunogai, S., & Henmi, T., (1971). Iodine in the surface water of the ocean. *Journal of the Oceanographical Society of Japan*, 27(2), 67–72. doi:10.1007/BF02109332
- United Nations Scientific Committee on the Effects of Atomic Radiation, (2000). *Exposures and effects of the Chernobyl accident*. New York: United Nations.
- US Environmental Protection Agency, (2008). *Copper Facts*. Washington, D.C: US Environmental Protection Agency.
- Van Der Bruggen, B., Vandecasteele, C., Van Gestel, T., Doyen, W., & Leysen, R., (2003). A review of pressure-driven membrane processes in wastewater treatment and drinking water production. *Environmental Progress*, 22(1), 46–56. doi:10.1002/ep.670220116
- Vitt, J.E., & Johnson, D.C., (1994). Oxidation of iodide to iodate concurrently with evolution of oxygen at Kelgraf composite electrodes. *Journal of Applied Electrochemistry*, 24(2), 107–113. doi:10.1007/BF00247780
- Wang, S., Xu, Y., Norbu, N., & Wang, Z., (2018). Remediation of biochar on heavy metal polluted soils. *IOP Conference Series: Earth and Environmental Science*, 108(4). doi:10.1088/1755-1315/108/4/042113
- Ward, J.F., (1988). DNA damage produced by ionizing radiation in mammalian cells: identities, mechanisms of formation, and reparability. *Progress in nucleic acid research and molecular biology*,. doi:10.1016/S0079-6603(08)60611-X
- Watanabe, Y., Ikoma, T., Yamada, H., Suetsugu, Y., Komatsu, Y., Stevens, G.W., Moriyoshi, Y., & Tanaka, J., (2009). Novel long-term immobilization method for radioactive iodine-129 using a zeolite/apatite composite sintered body. *Applied Materials and Interfaces*, 1(7), 1579–1584. doi:10.1021/am900251m
- Wheaton, R.M., & Lefevre, L.J., (2000). *Dowex ion exchange resins: Fundamentals of ion exchange*. Amsterdam: The Dow Chemical Company.
- Whitehead, D.C., (1984). The distribution and transformations of iodine in the environment. *Environment International*, 10(4), 321–339. doi:10.1016/0160-4120(84)90139-9
- Whitehead, D.C., (1978). Iodine in soil profiles in relation to iron and aluminium oxides and organic matter. *Journal of Soil Science*, 29, 88–94.
- Whitehead, D.C., (1974). The sorption of iodide by soil components. *Journal of the*

- Science of Food and Agriculture*, 25, 73–79.
- Williams, E., & Tronko, N., (1996). *Molecular, cellular, and biological characterization of childhood thyroid cancer*. Luxembourg: European Commission.
- Wittman, G., (1981). *Metal Pollution in Aquatic Environment.*, Springer. ed. Berlin: Springer.
- Wolniak, M., & Wawer, I.Å., (2008). <sup>13</sup>C CPMAS NMR and DFT calculations of anthocyanidins. *Solid State Nuclear Magnetic Resonance*, 34, 44–51. doi:10.1016/j.ssnmr.2008.06.003
- Xu, W., Zhang, W., Kang, J., & Li, B., (2019). Facile synthesis of mesoporous Fe-based MOFs loading bismuth with high speed adsorption of iodide from solution. *Journal of Solid State Chemistry*, 269(July 2018), 558–565. doi:10.1016/j.jssc.2018.10.028
- Yamani, J.S., Lounsbury, A.W., & Zimmerman, J.B., (2014). Adsorption of selenite and selenate by nanocrystalline aluminum oxide, neat and impregnated in chitosan beads. *Water Research*, 50, 373–381. doi:10.1016/j.watres.2013.10.054
- Yan, C., & Mu, T., (2014). Investigation of ionic liquids for efficient removal and reliable storage of radioactive iodine: a halogen-bonding case. *Physical chemistry chemical physics : PCCP*, 16(11), 5071–5. doi:10.1039/c4cp00279b
- Yang, D., Sarina, S., Zhu, H., Liu, H., Zheng, Z., Xie, M., Smith, S. V., & Komarneni, S., (2011). Capture of radioactive cesium and iodide ions from water by using titanate nanofibers and nanotubes. *Angewandte Chemie - International Edition*, 50(45), 10594–10598. doi:10.1002/anie.201103286
- Yang, O.B., Kim, J.C., Lee, J.S., & Kim, Y.G., (1993). Use of activated carbon fiber for direct removal of iodine from acetic acid solution. *Industrial and Engineering Chemistry Research*, 32(8), 1692–1697. doi:10.1021/ie00020a023
- Yang, Y., He, Z., Lin, Y., Philips, E.J., Stoffella, P.J., & Powell, C.A., (2009). Temporal and spatial variations of copper, cadmium, lead, and zinc in Ten Mile Creek in South Florida, USA. *Water Environment Research*, 81(1), 40–50. doi:10.2175/106143008x296479
- Yao, M., Zhang, Q., Hand, D.W., Perram, D., & Taylor, R., (2009). Adsorption and regeneration on activated carbon fiber cloth for volatile organic compounds at

- indoor concentration levels. *Journal of the Air and Waste Management Association*, 59(1), 31–36. doi:10.3155/1047-3289.59.1.31
- Ye, Z., Chen, L., Liu, C., Ning, S., Wang, X., & Wei, Y., (2019). The rapid removal of iodide from aqueous solutions using a silica-based ion-exchange resin. *Reactive and Functional Polymers*, 135, 52–57. doi:10.1016/j.reactfunctpolym.2018.12.002
- Yoon, J., Ha, J., Hwang, J., Hwang, B.-H., & Brown, G.E.B.J., (2009). Study of iodide adsorption on organobentonite using X-ray absorption spectroscopy. *Journal of the Mineralogical Society of Korea*, 22(1), 23–34.
- Zaafarany, I., (2010). Non-isothermal decomposition of Al, Cr and Fe cross-linked trivalent metal-alginate complexes. *Journal of King Abdulaziz University-Science*, 22(1), 193–202. doi:10.4197/sci.22-1.13
- Zhang, H., Gao, X., Guo, T., Li, Q., Liu, H., Ye, X., Guo, M., & Wu, Z., (2011). Adsorption of iodide ions on a calcium alginate-silver chloride composite adsorbent. *Colloids and Surfaces A: Physicochemical and Engineering Aspects*, 386(1–3), 166–171. doi:10.1016/j.colsurfa.2011.07.014
- Zhang, H., Hu, Y., Ye, X., Liu, H., Li, Q., Guo, M., & Wu, Z., (2013). Iodide adsorption from aqueous solutions by bis(trimethoxysilylpropyl)amine polycondensate/silver chloride composites. *Desalination and Water Treatment*, 51(19–21), 3930–3937. doi:10.1080/19443994.2013.795006
- Zhang, K., & Chen, T., (2018a). Sorption and removal of iodate from aqueous solution using dried duckweed (*Landoltia punctata*) powder. *Journal of Radioanalytical and Nuclear Chemistry*, 316(2), 543–551. doi:10.1007/s10967-018-5807-3
- Zhang, K., & Chen, T., (2018b). Dried powder of corn stalk as a potential biosorbent for the removal of iodate from aqueous solution. *Journal of Environmental Radioactivity*, 190–191(February), 73–80. doi:10.1016/j.jenvrad.2018.05.008
- Zhang, P., Chen, Y.P., Wang, W., Shen, Y., & Guo, J.S., (2016). Surface plasmon resonance for water pollutant detection and water process analysis. *Trends in Analytical Chemistry*, 85, 153–165. doi:10.1016/j.trac.2016.09.003
- Zhang, S., Xu, C., Creeley, D., Ho, Y.F., Li, H.P., Grandbois, R., Schwehr, K.A., Kaplan, D.I., Yeager, C.M., Wellman, D., & Santschi, P.H., (2013). Iodine-129 and iodine-127 speciation in groundwater at the Hanford site, U.S.: Iodate

incorporation into calcite. *Environmental Science and Technology*, 47(17), 9635–9642. doi:10.1021/es401816e

Zhang, X., Gu, P., Li, X., & Zhang, G., (2017). Efficient adsorption of radioactive iodide ion from simulated wastewater by nano Cu<sub>2</sub>O/Cu modified activated carbon. *Chemical Engineering Journal*, 322, 129–139. doi:10.1016/j.cej.2017.03.102

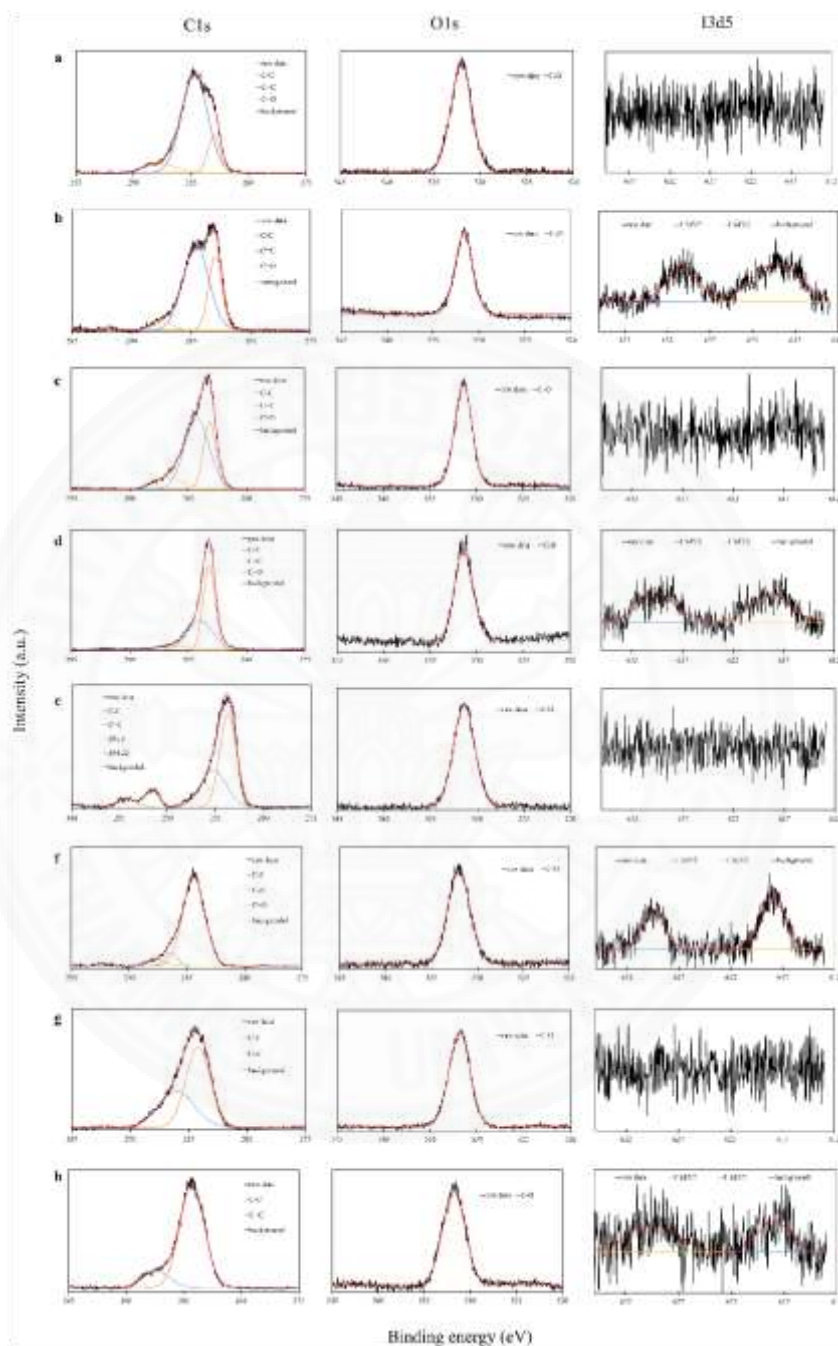
Zhou, J., Hao, S., Gao, L., & Zhang, Y., (2014). Study on adsorption performance of coal based activated carbon to radioactive iodine and stable iodine. *Annals of Nuclear Energy*, 72, 237–241. doi:10.1016/j.anucene.2014.05.028



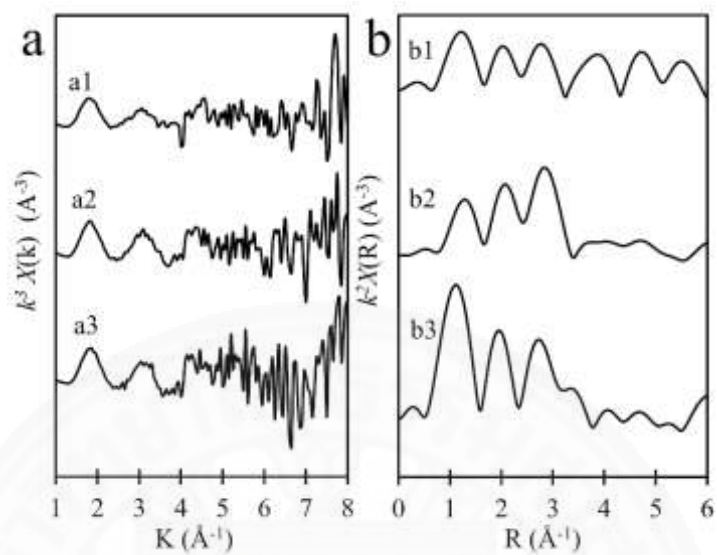




**APPENDIX A**  
**XPS SPECTRA OF C1s, O1s AND I3d5**



(a) virgin mangosteen pericarps, (b) mangosteen pericarps after  $\Gamma^-$  adsorption, (c) virgin red onion peels, (d) red onion peels after  $\Gamma^-$  adsorption, (e) virgin red dragon fruit peels, (f) red dragon fruit peels after  $\Gamma^-$  adsorption, (g) virgin passion fruit rinds, (h) passion fruit rinds after  $\Gamma^-$  adsorption

**APPENDIX B****EXAFS SPECTRA AT IODINE L<sub>III</sub>-EDGE**

(a) graph of transformed K-space, (b) graph of transformed R-space [1. mangosteen pericarps 2. red onions peels 3. cyanidin solution]

## BIOGRAPHY

Name	Mr. Jakkapon Phanthuwongpakdee
Date of Birth	December 22, 1990
Education	2020: Doctor of Philosophy (Material Science) Japan Advanced Institute of Science and Technology 2012: Master of Science (Urban Water Engineering and Management) The University of Sheffield 2011: Bachelor of Science (Environmental Science) University of Oregon

### Publications

Phanthuwongpakdee, J., Harimoto, T., Babel S., Dwevidi S., Takada K., & Kaneko T. (2021). Flame retardant transparent films of thermostable biopolyimide metal hybrids. *Polymer Degradation and Stability*. 188, 109571. doi: 10.1016/j.polymdegradstab.2021.109571

Phanthuwongpakdee, J., Babel, S., & Kaneko T. (2021). Screening of New bio-based materials for radioactive iodide adsorption from water environment. *Journal of Water Process Engineering*, 40, 101955. doi: 10.1016/j.jwpe.2021.101955

Phanthuwongpakdee, J., Babel, S., Laohhasurayotin, K., Sattayaporn, S. & Kaneko, T. (2020). Anthocyanin Based Agricultural Wastes as Bio-Adsorbents for Scavenging Radioactive Iodide from Aqueous Environment. *Journal of Environmental Chemical Engineering*. 8(5). 104147. doi: 10.1016/j.jece.2020.104147

Phanthuwongpakdee, J., Babel, S., Dwivedi, S., Takada, K., Hirayama, T. & Kaneko, T. (2020) Anion-Scavenging Biopolyamides from Quaternized 4-Aminocinnamic Acid Photodimers. *ACS Sustainable Chemistry & Engineering*. 8(9). 3786–3795. doi: doi.org/10.1021/acssuschemeng.9b07003

Phanthuwongpakdee, J., Babel, S. & Kaneko, T. (2020). Natural Adsorbents for Removal of Different Iodine Species from Aqueous Environment: A Review. In *Recent Trends in Waste Water Treatment and Water Resource Management* (pp 171–198). Singapore: Springer Singapore.

Phanthuwongpakdee, J., Babel, S. & Kaneko, T. (2018). Adsorption of Iodide in the Water by Natural Products and Waste Biomass for the Application of Radioactive Iodide Remediation. Proceedings of *8th International Conference on Sustainable Waste Management* (pp 1006–1013). Guntur: Swachh Andhra Corporation.

